AD 427751

64-7

ARL 63-223

THE ARL THIRTY-INCH HYPERSONIC WIND TUNNEL INITIAL CALIBRATON AND PERFORMANCE

N. E. SCAGGS
W. BURGGRAF
M. GREGOREK

THE OHIO STATE UNIVERSITY
COLUMBUS, OHIO

DECEMBER 1963

AEROSPACE RESEARCH LABORATORIES
OFFICE OF AEROSPACE RESEARCH
UNITED STATES AIR FORCE

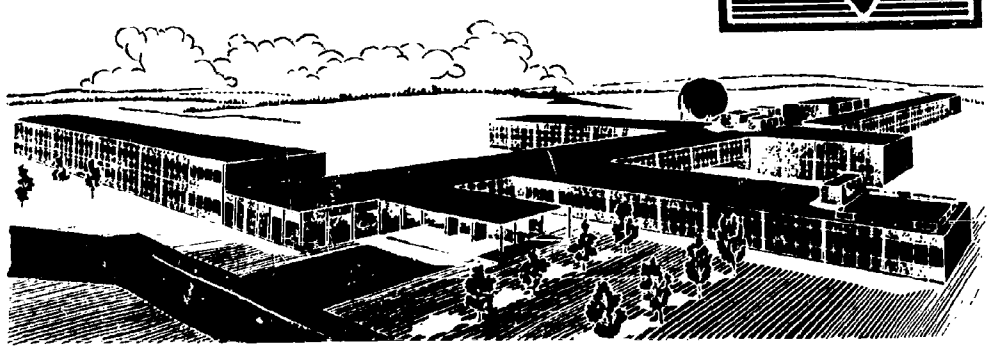

NOTICES

When Government drawings, specifications, or other data are used for any purpose other than in connection with a definitely related Government procurement operation, the United States Government thereby incurs no responsibility nor any obligation whatsoever; and the fact that the Government may have formulated, furnished, or in any way, supplied the said drawings, specifications, or other data, is not to be regarded by implication or otherwise as in any manner licensing the holder or any other person or corporation, or conveying any rights or permission to manufacture, use, or sell any patented invention that may in any way be related thereto.

- - - - - - - - - -

Qualified requesters may obtain copies of this report from the Defense Documentation Center, (DDC), Cameron Station, Alexandria, Virginia.

- - - - - - - - - -

This report has been released to the Office of Technical Services, U. S. Department of Commerce, Washington 25, D. C. for sale to the general public.

- - - - - - - - - -

Copies of ARL Technical Documentary Reports should not be returned to Aerospace Research Laboratories unless return is required by security considerations, contractual obligations or notices on a specified document.

300 - January 1964 - 162-23-433

ARL 63-223

THE ARL THIRTY-INCH HYPERSONIC WIND TUNNEL INITIAL CALIBRATON AND PERFORMANCE

N. E. SCAGGS
W. BURGGRAF
G. M. GREGOREK

THE OHIO STATE UNIVERSITY
COLUMBUS, OHIO

DECEMBER 1963

Contract AF 33(657)-8106
Project 7065
Task 706501

AEROSPACE RESEARCH LABORATORIES
OFFICE OF AEROSPACE RESEARCH
UNITED STATES AIR FORCE
WRIGHT-PATTERSON AIR FORCE BASE, OHIO

FOREWORD

This interim technical report was prepared by the Aerodynamic Laboratory of The Ohio State University, Columbus, Ohio, for the Aerospace Research Laboratories, Office of Aerospace Research, United States Air Force, under Contract AF 33(657)-8106. The work reported herein was performed under Task 706501 entitled "Fluid Dynamics Facilities Research" of Project 7065 entitled "Aerospace Simulation Techniques Research". Technical monitor for the contractual period January 15, 1962 to March 15, 1964, was Mr. Emil Walk of the Hypersonic Facilities Laboratory of ARL.

ABSTRACT

The ARL 30" Hypersonic Wind Tunnel is a large blow-down facility that uses a methane-oxygen fired zirconia pebble bed to heat the air prior to expansion to flow Mach numbers ranging from 16 to 22 at free stream Reynolds numbers approaching 10^6/ft. This report describes the components of the facility, discusses the operation of the tunnel, and presents calibrations of two conical nozzles, developing approximately M = 16.5 and M = 18.5. The performances of the heater, diffuser and vacuum system are evaluated and the operational experiences gained during the initial operating period are reviewed.

To aid in planning test programs for the facility, an appendix is included that details the performance of the facility, including the wind tunnel performance with a planned expansion of the vacuum station.

TABLE OF CONTENTS

LIST OF ILLUSTRATIONS

LIST OF ILLUSTRATIONS (CONTINUED)

LIST OF ILLUSTRATIONS (CONTINUED)

LIST OF SYMBOLS

c_p	Specific heat at constant pressure
c_v	Specific heat at constant volume
$\Delta c_{p_{v,l}}$	Difference of specific heats of vapor and liquid
h	Enthalpy
m	Mass
$\dot{m}$	Mass flow rate
n_1	Number of first stage vacuum pumps
n_2	Number of second stage
n_3	Number of third stage
t	Time
v	Volume of vacuum sphere
A*	Area of nozzle throat
B	Vacuum pump constant, Eq. (B-7)
C	Vacuum Pump constant, Eq. (B-6)
E	Energy
ΔH_{vap}	Heat of vaporization
M	Mach number
P	Pressure
P_{t_2}	Total pressure behind normal shock
R	Gas constant
R_e	Reynolds number
T	Temperature
V	Volume flow rate
V_{vap}	Specific volume of vapor phase

V_{liq}	Specific volume of liquid phase
W	Work
γ	Ratio of specific heats
μ	Viscosity
η	Pressure recovery factor
ρ	Density

Subscripts

a	Conditions based on standard atmosphere
i	Conditions at the initiation of process
o	Conditions in the stagnation region
H	Conditions downstream of aftercooler

I. INTRODUCTION

At the Aerospace Research Laboratories of the Office of Aerospace Research, USAF, experimental facilities are being developed to explore the fluid dynamic phenomena of very high speed flight. The hypersonic wind tunnel facilities of this laboratory have received considerable attention during the past several years. A three-inch continuous flow wind tunnel has been operational for more than four years[1]; recently it has delivered flows with a Mach number of 17. A twenty-inch, intermittent operating facility, has been in use since late 1961,[2,3] delivering flows in the range of Mach numbers from 12 to 14. Both facilities operate at moderate free stream Reynolds numbers -- on the order of 10^6/ft -- and use an electric resistance type of heater capable of maximum wire temperatures of 2900°R.

The most recent hypersonic installation at the Aerospace Research Laboratory is the Thirty-Inch Hypersonic Wind Tunnel (30" HWT), shown in Figure 1. This facility is designed to deliver flows with Mach numbers from 16 to 22 and with Reynolds numbers from 10^4/ft to 10^6/ft at air stagnation temperatures near 4400°R. To accomplish this task, and to overcome the problems ~~which hamper~~ development of high Mach number flow requires a highly sophisticated installation. A 3000 psia high pressure air station and a 35000 ft3 vacuum sphere coupled to a 3-stage vacuum pumping station provide the pressure ratio necessary to establish isentropic flow. A gas fired zirconia pebble bed storage heater increases the stagnation temperature of the air to values sufficient to avoid liquefaction effects. Axisymmetric nozzles of 30" exit diameter are fitted to the tunnel to allow models of relatively large size to be tested, even after a sizable boundary layer growth. These basic components provide a wide test capability, and the 30" HWT should prove a valuable addition to the experimental hypersonic research equipment of the laboratory.

It is the purpose of this report to describe the ARL 30" HWT, to discuss its operation, and to present the results of the initial calibration program. The operational experience gained in this shakedown period is also set down. In order that the report may be used to plan test programs in the facility, pertinent parameters, e.g. run times, evacuation rates, heating rates, etc., are included in an Appendix.

A general description and discussion of the operation of the facility follow these introductory remarks. The performance of the individual components of the tunnel are then examined and the experiences of the first year of operation are reviewed.

Manuscript released October 1963 by authors for publication as an ARL Technical Document.

II. DESCRIPTION AND OPERATION

GENERAL DESCRIPTION

Classification and Simulation Capability

The ARL 30" HWT, shown schematically in Figure 2 is a free-jet facility that is operated in a blow-down fashion, using 30" exit diameter, axisymmetric nozzles to generate very high Mach number air flows. As indicated in the schematic, many components are required to develop this hypersonic stream; this section will describe these components and discuss the operation of the facility.

Before considering the individual components in detail, it is desirable to note the simulation capability of the complete installation. Figure 3 presents the Mach number and Reynolds number range covered by the ARL 30" HWT. The maximum Reynolds number, at a given Mach number, is determined by the highest available stagnation pressure and the lowest temperature which will avoid the adverse effects of air condensation. The dotted line designated "saturation, P_o = 3000 psia" is a limit imposed by the equilibrium vapor pressure of a nitrogen-oxygen mixture at very low static pressures and temperatures. Because the properties of air are not well known under these extreme conditions, a semi-empirical method, the details of which will be treated in a later section, was used to approximate the saturation conditions of the air. The solid upper bound is an empirical limit based on the observed onset of condensation phenomena in several hypersonic wind tunnels about the country[4].

The lowest possible Reynolds number, again at a given Mach number, is established by the minimum allowable stagnation pressure and the maximum obtainable stagnation temperature. A conservative estimate of these two parameters is a stagnation pressure corresponding to an impact pressure of 10 mm Hg and a stagnation temperature of 4000°R; these conditions provide the lower bound shown.

High Pressure Air Station

The high pressure system of the facility consists of three components: an air compressor, a drying system and a bottle storage farm. Air is inducted from the atmosphere by a Chicago-Pneumatic pump rated at 400 scfm with a maximum pressure of 3000 psig, processed by Kemp silica-gel dryers which lower the dew-point to below -60°F, and then stored in high pressure bottles of 1400 ft^3 volume at pressures up to 3000 psig for use as needed.

Air Heater

The heater for the 30" HWT is a gas fired, pebble bed, regenerative type storage heater. A schematic of the heater is shown in Figure 4; the burner and igniter assemblies are shown in Figure 5. As shown in the drawing, the steel pressure vessel, rated at 3500 psia, is lined with several layers and types of insulation. The pebble bed, made up of 7/8" diameter pebbles of several varieties of refractory materials is 12 1/2 foot deep. It is supported by a stainless steel grate. In operation, the bed is heated from the top by a burner which uses methane, oxygen and air combustion.

As the different levels of the bed are exposed to a wide range of temperature and mechanical stresses, the proper selection of ceramics for the different levels is quite important. In the upper portion of the heater two types of zirconia are used -- partially stabilized zirconia and cubic zirconia. The partially stabilized form contains a small percentage of lime (CaO) which tends to reduce the inversion in the thermal expansion coefficient experienced by unstabilized zirconia at temperatures between 2000°R and 2700°R. Cubic zirconia has a crystal structure which does not exhibit this inversion characteristic of the expansion coefficient; however, it is more sensitive to thermal shock than the partially stabilized zirconia as it possesses a larger coefficient of expansion. Because of these characteristics, partially stabilized zirconia is used at the very top of the bed and in the surrounding insulation, where extreme thermal shock is encountered. At a lower level in the bed, where the refractories are not subjected to severe thermal shock, cubic zirconia is used.

In the lowest portions of the bed, the pebbles and insulation are of alumina; this material has a greater load carrying ability and is more economical than zirconia. As alumina and zirconia are not compatible above 2500°R, a buffer layer of magnesia separates the alumina from the zirconia. Experience has shown that zirconia and magnesia do not react at temperatures near 3000°R - the design temperature of the bed at this level.

On the side of the heater vessel near the top of the bed, as shown in Figure 4, a viewport is built into the vessel so that it is possible to see the top of the bed at all times. This viewport allows the temperature of the top of the bed to be monitored with an optical pyrometer.

Nozzles

The facility is presently equipped with a conical nozzle of dimensions shown in Figure 6. Beryllium copper and Zirconia-copper nozzle throat sections are fitted to a steel nozzle; the throats may be changed as desired, providing a

range of Mach numbers between 16 and 22. Three nozzle throats have been fabricated and a fourth is to be built. The diameters of the throat sections and the nominal Mach number delivered (based on an estimated boundary layer growth) are:

Dia. in inches	Nominal Mach No.
0.293	16
0.195	18
0.145	20
0.100	22

The 0.195 nozzle throat was the first installed in the wind tunnel and will henceforth be termed Throat No. 1; the 0.293 throat was next installed and will be designated Throat No. 2.

The somewhat novel features of Throats No. 1 and 2 are indicated by the detailed drawings of Figure 7. The thin wall of the beryllium copper liner is required to dissipate the high heat fluxes to the back side water coolant. This thin wall is subjected to high pressure stresses during tunnel operation, and it is necessary to provide a high cooling water pressure (1000 psia) to maintain the structural integrity of the nozzle liner.

A conical nozzle, rather than a contoured design, was chosen as the initial nozzle configuration as uncertainties in calculating boundary layer growth exist in theories at these extreme Mach numbers. Once the behavior of the boundary layer in the conical nozzles is ascertained, a contoured nozzle will be designed.

Test Cabin

The test cabin is a 5 foot steel box that forms the plenum chamber for the free jet of the nozzle. Dimensions of the test cabin allow adequate provision for model and instrumentation storage outside the jet. The test cabin is arranged as in Figure 6, with a free jet equal to the nozzle exit diameter. The side walls are hinged for accessibility and contain 14" diameter windows for flow visualization apparatus.

Installed in the test cabin and mounted on the left wall (looking upstream) is the model support system. This mechanism inserts sting-mounted models into the nozzle centerline after flow has been established and then pitches and rolls the model according to pre-programmed instructions. The capability of the system is an angle of attack of -60° to $+20^{\circ}$ and a pitch

rate of 2°/sec; a full 360° of roll is possible at a rate of 6°/sec. A remotely controlled traversing mechanism for mounting impact pressure, angularity, and total temperature probes is fastened to the top surface of the cabin, and may be used as required.

Diffuser and Aftercooler

The diffuser used in the ARL 30" HWT is of the converging-constant area-diverging, axisymmetric configuration used successfully in several hypersonic facilities[5,6]. Pertinent dimensions of the diffuser are shown in Figure 6. A water jacket surrounds the entire diffuser to maintain the diffuser at low temperatures.

As the diffuser performance critically influences the hypersonic tunnel operation, e.g., minimum stagnation pressure allowable for running and duration of tect runs, its performance must be evaluated closely. For this purpose the diffuser is equipped with fourteen static pressure taps.

The aftercooler uses axially-aligned finned tubes to reduce the stream temperatures to the order of 100°F, reducing the volume flow rate to the vacuum station and protecting the vacuum pumps. The axial flow arrangement is a special low drag design which is used to increase the overall pressure recovery efficiency.

The Vacuum Pumping Station

The station consists of thirteen sliding vane vacuum pumps and a 35,000 ft^3 vacuum sphere. The vacuum pumps, shown in Figure 8, are installed in a three stage system -- ten pumps pumping into two pumps which, in turn, exhaust into a single vacuum pump. Pumps of the first two stages are Allis Chalmers type 27D pumps while the third stage pump is a smaller type 12S. Volume flow pumping capability rises from zero at 0.1 mm Hg and levels at 24000 ft^3/min at 2.0 mm Hg. The pumps are used to evacuate the sphere and to extend the running time of the tunnel by accepting a portion of the delivered mass while the facility is operating.

OPERATION OF THE FACILITY

Heater Operation

Two distinct modes of operation are used with the pebble bed heater. The first mode, called the idle mode, provides the energy necessary to maintain the top of the bed near 2800°R at all times, including non-working hours. The second

mode provides the energy to heat the bed to the desired temperature, just prior to a test. Energy addition for the two modes of heater operation is adjusted from the burner control panels shown in Figure 9. The combustion reactants for the burner are natural gas from a city gas line, air supplied by a two stage rotary blower, and oxygen. The natural gas and the air or a combination of air and oxygen are pre-mixed outside the heater and then ignited at the end of the burner that protrudes into the heater.

A pre-mix burner is preferred as the reactants are thoroughly mixed; hence, the combustion of the mixture is practically completed before the burning gases come in contact with the heater insulation or the pebbles. In order to ensure complete burning of the gas before it reaches the heater insulation or pebbles, a stoichiometric mixture plus twenty percent excess oxygen is always regulated into the burner. Care must be used with a pre-mix burner to eliminate the possibility of combustion occurring in the mixing chamber outside of the heater. This premature combustion has not been a problem with the present configuration.

Another type of burner that has been used with some success is the type in which the mixing takes place inside the heater in the flame area. This type doesn't provide as complete combustion and consequently, the insulation is subjected to a slow reducing process.

The ignition of the flame is accomplished by two different methods depending on the temperature of the top of the bed. If the temperature is below 2000°R, a 5000 volt DC spark plug is inserted through the burner into the heater and when the combustive mixture is properly set up, the plug is energized and the flame is ignited by the open spark. If the top of the bed is above 2000°R, automatic ignition occurs when the combustive mixture is introduced into the heater.

In the idle mode, the top of the bed is kept above 2800°R at all times except for heater and auxiliary equipment repairs. This procedure reduces the number of temperature inversions experienced by the bed -- the inversion temperature range of partially stabilized zirconia is between 2000°R and 2700°R. The burner is kept on idle settings during off duty hours and does not have to be checked by an operator. An alarm system is built into the control circuits for the burner and heater. When a malfunction occurs, the system shuts down the burner and sets off a signal in a control center that is manned 24 hours a day.

Prior to a tunnel run, the bed temperature is increased

gradually by adding energy to the bed according to the schedule presented in Table I. This table shows the burner settings, the duration of each setting and the BTU/hr input for each setting.

TABLE I

Burner Settings Used for Charging Pebble Bed

Heating Step	Input of ~~Air~~ (SCFM)	Input of Natural Gas (SCFM)	Input of Oxygen (SCFM)	Energy Input Rate (BTU/HR)	Flame Temperature (°R)	Duration of Each Step (Minutes)
Idle	36.7	3.20	0	172,000	3680	----
1	41.25	4.46	2.25	240,000	4040	40
2	70.5	7.81	4.02	360,000	4040	40
3	53.6	9.50	11.75	480,000	4420	40
4	64	11.15	14.00	600,000	4420	120

The heating rate of the bed is controlled by four factors: the energy input, the flame temperature, the position of the exhaust valve and the position of the stilling chamber by-pass valve. With the nozzle throat plugged from the test cabin side, the combustion gases exit through the exhaust valve and the stilling chamber by-pass valve; by throttling the combustion gases with these two valves, the flow of gases and consequently the heating rate of the bed and the stilling chamber can be controlled. Normally, the stilling chamber by-pass valve is left open during the complete heatup cycle so that the stilling chamber will also heat up to minimize the heat loss of the air passing through the stilling chamber during a run. The exhaust valve is kept closed during the early stages of the heatup cycle (and during idling) to protect the stainless steel grate. It is opened during the late stages so that a large amount of energy can be driven into the bed just prior to a tunnel run. The two other factors controlling heating rate are self-explanatory; i.e., the higher the energy input to the bed, the higher the storage rate; the higher the flame temperature, the higher the temperature of the top portion of the bed.

The temperature of the flame is controlled by varying the mass flow through the burner for a given natural gas flow. Since the amount of oxygen needed for stoichiometric plus twenty per cent excess oxygen for any natural gas setting can be obtained from either air or pure O_2, it is possible to vary the mass flow and still maintain the proper ratio of oxygen to natural gas. Of course, the higher the mass flow, the lower the flame temperature, and conversely.

The temperature of the bed is measured by an optical pyrometer. The bed is observed through the quartz viewport, and hence an error in bed temperature may be induced by the quartz window. Calibration of the pyrometer readings indicates measurements taken through the viewport are approximately three per cent lower than the actual bed temperature. It is also important for accurate temperature determination that the inside surface of the viewport be kept clean. To aid in this respect, cold air is blown across the inside surface of the quartz and down the channel to the bed. This keeps the combustion gases from the quartz surface and prevents the viewport from steaming up.

Tunnel Operation

The preparation for a tunnel run begins with the storage of energy in the pebble bed as described above. Once the bed has been heated to the desired temperature the heater is made ready for pressurization. The burner is shut down, removed and replaced with a water cooled plug. The water is started to all the tunnel components that require cooling during the run. The nozzle plug is removed from the nozzle and the test cabin checked and sealed. All of the openings in the heater vessel and the stilling chamber are closed. While these jobs are being performed, the sphere is pumped down to 0.5 mm Hg and isolated from the vacuum pumps and the tunnel by closing the sphere valve. The vacuum pumps are then shut down until pressurization of the heater begins. The tunnel is then ready for pressurization.

As soon as pressurization is begun ($p_o \simeq$ 100 psig), cold air injection is started into the air flowing down the tunnel. The cold air mixes with the hot air issuing from the heater and keeps the temperature in the test cabin below 400°F until the tunnel is brought into flow. The cold air injection system is basically a parallel air system with the pebble bed acting as the resistance in one line and the friction of the piping acting as the resistance in the other line. No attempt has been made to estimate the air flow through the two systems from the pressure loss through each, but since the temperature of the air coming out of each line is known approximately (about 500°R and

2500°R from the cold line and heater respectively) and the resultant mixture temperature is known (about 860°R), it is possible to estimate the ratio of cold air to hot air to be about three to one in terms of mass flow. This ratio can be varied by changing the resistance in the cold air line.

The cold air injection method of running the tunnel permits the operation of the tunnel without any type of shut-off valve between the pressure vessel and the nozzle throat. Since at the present time a shut-off valve is not available that will operate satisfactorily at 3000 psia pressure and at temperatures up to 4400°R, the cold air injection method is the most efficient way of running the tunnel. The tunnel could be operated without injecting cold air, but the test cabin components would be subjected to high temperatures and the heater would have to be pressurized more rapidly to protect the test cabin components from a prolonged exposure to the high temperatures.

A rapid heater pressurization risks lifting or floating the pebbles in the bed. Obviously, this is to be avoided as the pebbles may be blown down the stilling chamber and the nozzle and/or the pebbles and the insulation may be damaged when the bed drops back into place. The 30" HWT has a pressure differential indicator that is interlocked to the stagnation pressure controller to guard against lifting the bed. When the pressure difference from the bottom to the top of the bed exceeds a preset value, 4 psid, the stagnation pressure control valve is closed automatically, eliminating the possibility of floating the bed from too rapid pressurization.

With cold air injection in operation, and the stagnation pressure increasing, the tunnel valve is opened and the vacuum pumps restarted. The static pressure in the test cabin is maintained below one psia during the pressurization by the vacuum pumps, greatly reducing the heat input to the tunnel components. As the desired pressure level is approached to within 100 psia of the run condition, the cold air injection is stopped. The pressure is then brought up the last increment to the run condition and allowed to become steady. The time required for this pressurization process is about 5 minutes.

Everything is now ready for the run. The tunnel is brought into flow by opening the sphere valve which lowers the downstream pressure of the pressure recovery system to the sphere pressure. The tunnel stays in flow until the sphere pressure rises to a level insufficient to support isentropic flow in the nozzle. The inflow time of the tunnel is of the order of 30 seconds. A model is injected into the stream as soon as the tunnel goes into flow and, if possible, ejected before the tunnel drops out of flow. This procedure protects the model

from the large loads imposed by the starting and unstarting shocks and from the high static temperature of the subsonic flow when the tunnel is not in flow.

As soon as the tunnel drops out of flow, the heater is depressurized through the exhaust valve, care being taken not to overload the pebble bed in the downward direction by depressurizing too fast. The tunnel valve is then closed and the sphere is pumped down again in preparation for the next run. While the sphere is being pumped down, changes in the test cabin can be made and any instrumentation changes can be accomplished. About fifteen minutes are required to pump the sphere down to 0.5 mm Hg and then another tunnel run can be made. Three consecutive runs can usually be made in this fashion, with no recharging of the heater the limiting factors being the wall temperature of the stilling chamber and the temperature level of the bed. The maximum temperature limit of the stilling chamber wall is 500°F; the minimum bed temperature is 2800°R, since the temperature of the partially stabilized zirconia pebbles and insulation might decrease to the inversion range of 2000°R to 2700°R, if another run were attempted.

The test section flow conditions at a model are determined by the stagnation conditions and the nozzle throat size. The stagnation pressure is controlled and monitored by a set of Ashcroft transmitters and a Taylor recorder and controller. The accuracy of the pressure system is 1% of full scale. The stagnation temperature of the stream is difficult to measure as the temperature is quite high. The bed temperature is measured before and after each run with an optical pyrometer as noted previously; the temperature of the air as it exits from the bed should be very close to the bed temperature. However, the air must pass through the 14 ft. long, 3/4" diameter tube in the stilling chamber and the cold air injection flange before it reaches the nozzle throat, causing energy losses. In order to determine the temperature loss through the stilling chamber, a platinum - platinum, 13% rhodium bare wire thermocouple is inserted into the air stream at the end of the stilling chamber close to the nozzle throat. Measurements from this thermocouple are used to determine the stagnation temperature of the air. As the air passes through the cold air injection flange, a temperature loss of about 40°F was estimated by noting the temperature rise of the cooling water as it passes through the cold air injection flange. The stagnation conditions can be measured accurately with the above technique as long as the total temperature at the end of the stilling chamber does not exceed 3500°R - the highest temperature at which a platinum-platinum 13% rhodium thermocouple can be used. Above 3500°R, a measurement of the mass flow rate and stagnation pressure can be used to calculate the stagnation temperature, although this method has not been used in this

test sequence.

The Mach number delivered to the test section is determined by the diameter of the nozzle throat. Calibrations of the nozzle with two different throats have been performed; following these descriptive remarks of tunnel operation, these calibrations are presented in the following section.

III. PERFORMANCE

HEATER PERFORMANCE

Charge Cycle

Operation of the regenerative heater is relatively complex, many variations in the rates of charge (and discharge) are possible. The object of the charging process is to store the maximum amount of energy in the bed at the desired temperature. Ideally, the temperature should be constant in the top sections of the bed. With no initial temperature variation, the heater, upon discharge, would deliver a constant outlet air temperature until the most downstream portion of the bed has been cooled by the tunnel air. In practice, temperature gradients cannot be eliminated in the bed and hence some small temperature drop may be anticipated during a test run.

An indication of the gradients observed in the heater bed is given in Figure 10. The steps refer to the charge schedule set up in Table 1; the effect of the schedule may be readily observed. The idle temperature distribution represents an energy of 4.75×10^5 BTU stored in the bed, the maximum temperature distribution is equivalent to 9.69×10^5 BTU. Maximum bed temperature of 4200°R is reached after 200 minutes of charging; flame temperature at maximum conditions is 4420°R.

It is observed that the stainless steel grate supporting the pebble bed experiences a rise in temperature from 1100°R to 1700°R during the charge cycle. The latter temperature is near the maximum allowable for this component. Also of interest is the maximum temperatures of the magnesia buffer layer and of the alumina bottom layer, 2600°R and 2450°R, respectively.

Discharge Cycle

The rate of discharge of the energy stored in the bed is determined by the tunnel mass flow rate, a function of throat diameter, stagnation pressure and stagnation temperature. Of concern during the discharging process is the temperature drop that occurs during the test portion of the tunnel run. Figure 11 shows the temperature variation of the air leaving the stilling chamber during tunnel tests at several mass flow rates. The maximum temperature drop was less than 20°R and is not significant as far as most tunnel testing is concerned.

Through conservative operation and proper choice of test conditions, it is possible to obtain several runs for each charge cycle of the heater. Figure 12 presents the heater distributions at the end of a typical heat up period and after three consecutive tunnel runs. Each run requires approximately 100 lbm of air flow through the bed; this includes the flow during the pressurization, tunnel run, and depressurization processes. Assuming the air reaches the temperature of the top of the bed, 75,000 BTU's are extracted from the bed during each run.

NOZZLE PERFORMANCE

Throat Performance

Two different throat sections have been used in the 30" HWT. The first was made of Beryllium copper, with initially 0.040 inch thick wall and 0.195 inch dia. at the throat. This nozzle throat section failed after 83 runs. The failure allowed cooling water to pass through the wall into the air stream. Inspection of the section after the failure showed severe pitting and general erosion.

The erosion was caused by "dust" picked up by the air when passing through the heater and carried downstream through the nozzle throat. This "dust" can erode the nozzle throat and, over a period of time, reduce the tunnel Mach number, and finally cause nozzle throat failure.

After the 83 runs, the nozzle throat was 0.243 inch diameter with a corresponding change in Mach number of 4.86%.

The second throat section tested was made of nickel plated zirconium copper alloy with initially 0.060 inch thick wall and 0.293 inch dia. at the throat. This throat section is still in operation; after 62 runs, the throat diameter is 0.297 inches with a negligible Mach number variation. This second throat has a slower erosion rate, but it is not possible to tell at this time whether this slow rate is due to the different materials used for the throat or to the difference in throat dimensions and test conditions.

For this facility, the interchangeable throat sections serve two purposes: 1) a convenient method with which to vary the Mach number delivered by the conical nozzle, and 2) an economical way to handle the erosion problem characteristic of pebble bed facilities.

Nozzle Mach Number Calibration

A transversing impact pressure probe was used to obtain nozzle calibration data and a block diagram of the set-up is shown in Figure 13. A variable reluctance differential pressure transducer was used as a pressure pick-up and a slide wire voltage divider as a position pick-up. Both outputs were recorded on an X-Y plotter to give a continuous trace. A typical impact pressure trace transversing the stream at nozzle exit is shown in Figure 14. All of the data taken had the demonstrated small variation in impact pressure and thus a small variation of Mach number. The data presented in Figures 15 through 20 indicate the Mach number calibrations at three Reynolds numbers obtained in both the transverse and axial directions for both throat sections. The maximum Mach number gradients are summarized in Table II. The gradients are expressed in percent change of Mach number from centerline value over an inch distance.

TABLE II

Mach Number Gradients at Nozzle Exit

Nozzle	Mach No.	Transverse	Axial
No. 2	17	0.6%/in.	0.5%/in.
No. 1	19	0.3%/in.	0.5%/in.

From Table II and from the calibration plots, the quality of the flow delivered by both nozzle throats may be observed to be good; certainly the nozzles may be used for meaningful aerodynamic tests.

The size of the isentropic core can also be estimated from the calibration. Although the usable test core is a function of Reynolds number and can be expected to vary somewhat, the core size of Throat No. 1 is approximately 19" in diameter; the isentropic core of Throat No. 2 is slightly greater than 20" in diameter. These large regions of isentropic flow allow relatively large size models to be tested in the very high Mach number flows delivered by the 30 inch exit diameter conical nozzles.

Angularity

Flow angularity can be an important parameter in test programs conducted in the ARL 30" HWT. Consequently an angularity model, Figure 21, was tested with the no. 2 throat to determine flow angularity. This model was a 45° half angle cone with pressure orifices opposite each other on the cone surface. A variable reluctance differential pressure transducer was used to determine the pressure difference across the cone orifices as a function of angle of attack. Preliminary data indicates the angularity relative to a horizontal plane at the centerline is $0.10^{\circ} \pm 0.03^{\circ}$. Additional angularity data are to be obtained.

Blockage

When planning test programs it is important to know what size models can be used and keep the wind tunnel in flow. In order to determine how much the flow could be blocked and maintain flow, two models were tested at varying angles of attack with the No. 1 throat. One model was a blunt flat plate and the other was a delta wing; dimensions of the models are given in Figure 22. With the flat plate installed on the sting support, the tunnel dropped out of flow at angles of attack of $\pm 16^{\circ}$. With the delta wing mounted the tunnel dropped out of flow at -30°. Both models were injected after flow was established in the tunnel.

Stream Properties

Due to the stagnation temperatures obtained in hypersonic wind tunnels, caloric imperfections become important in the determination of the free stream static state of the gas. This imperfection is due to the excited vibrational energy states at temperatures above $1000^{\circ}R$. Corrections to the perfect gas relations for caloric imperfections are given in Reference 7 and these corrections were applied, where applicable, to all calculations presented in this report.

The high expansion experienced in hypersonic wind tunnel nozzles causes the free stream static temperature to become quite low. When calculating flow parameters such as Reynolds number, it is necessary to know the viscosity of the gas, and at these temperatures, the well verified Sutherland's formula no longer is applicable. Recently, data has been taken in the temperature range of interest[8], and this data was used in all calculations involving viscosity.

Another result of the extremely low stream static temperatures is the possibility of liquefying components of the air.

In the temperature and pressure ranges of interest, there is no data on the saturation conditions of air and accurate evaluation of this condensation phenomena is difficult. Because of this absence of information, it has been the practice of many experimenters to extrapolate the data which exists for air at higher temperatures and pressures to the lower temperature and pressure ranges (see Appendix C). While this technique undoubtedly has questionable accuracy and does not specify the points of phase transitions, it is a simple method which appears to be in good agreement with the data taken on pure oxygen and pure nitrogen at low temperature. It is evident that before an adequate theory on the condensation of air in hypersonic wind tunnels can be formulated and the degree of supersaturation predicted, the saturation condition of the gas mixture, air, in the appropriate temperature and pressure range must be determined.

Due to the short run times, experimental data of condensation effects in the ARL 30" HWT is still incomplete. To estimate these effects, condensation data of other investigators, taken from similar hypersonic facilities and summarized in Reference 4, is presented in Figure 23. The range of operating static temperatures and pressures for Nozzle No. 1 and No. 2 is indicated on the plot. The data reveals that the ARL 30" HWT can be operated at levels of "apparent" supersaturation in excess of 30°R, based on an extrapolation of the air saturation curve; hence, the information gathered in this initial test program should be free of the adverse influence of condensation.

It should be noted, however, that the pebble bed air heater has unique characteristics which might induce condensation prior to what would be expected using other types of air heater. The presence of "dust" can act as a nucleus upon which condensation might occur. Consequently, further testing is mandatory before a precise determination of the amount of "apparent" supersaturation tolerable in the ARL 30" HWT is obtained.

DIFFUSER AND AFTERCOOLER PERFORMANCE

Because of the close link between the performance of the diffuser and of the aftercooler, the pressure recovery of these two components are normally treated together. An efficient diffuser has a low stream exit velocity and therefore a low entrance velocity for the aftercooler. This low velocity minimizes the pressure losses across the aftercooler and improves the pressure recovery. High recovery, of course, increases the run time of a blow down facility and extends the operating Reynolds number envelope.

Because of their importance, diffuser pressures at the drop-out are monitored and the pressure drop across the aftercooler

measured whenever the facility is operated at new test conditions. Typical of the pressure distributions obtained in the diffuser is that shown in Figure 24. Most of the pressure recovery may be observed to occur in the constant area section of the diffuser; a moderate pressure increase follows in the subsonic, diverging portion of the diffuser. The diffuser recovery consistently approaches 100% of the total pressure behind a normal shock based on the nozzle exit Mach number. This high efficiency obviously contributes to the low pressure drops noted across the aftercooler in Figure 25. The 1 mm Hg pressure differential is quite low for a heat exchanger of this capacity.

The overall pressure recovery, η , defined as

$$\eta = \frac{\text{total pressure downstream of the aftercooler}}{\text{total pressure behind the normal shock at diffuser entrance}}$$

has been measured at 0.90, $\pm$ 0.05, for both nozzles tested when an impact probe is in the stream. When models are placed in the stream (for example, the blockage models discussed previously) and are not retracted prior to flow breakdown, η drops to 0.80, $\pm$ 0.05.

A quantitative evaluation of the effect of on run times is made in Appendix B. Also presented in this Appendix is the rise in sphere pressure during tunnel operation with vacuum pumps operating and with no vacuum pumps on the line. Vacuum pump operation can greatly extend the run time if the flow rates are low; however, as may be noted in Figure 26, at high flow rates only a few seconds can be gained. The pressures measured during this test were just downstream of the aftercooler, hence the pressures are subject to line losses and pressure drops across two butterfly valves. A drop of 1 mm Hg between the aftercooler and the sphere would bring the theory in excellent agreement with experiment.

VACUUM SYSTEM PERFORMANCE

During the initial period of operation of the ARL 30" HWT, the three-stage vacuum pumping station has performed flawlessly. Although operated continuously for several hours at pressures below 10 mm Hg, there have been no overheating or other operational type problems experienced.

As a single vacuum pump was examined to establish the

empirical pumping rate expression, it is of interest to note the performance of the entire thirteen pumps. The evacuation rate of the 35,000 ft^3 sphere is shown in Figure 27; the excellent agreement with the formulations of Appendix B is gratifying. Also of concern is the minimum sphere pressure that can be obtained in a three-stage configuration. Theoretically, this minimum pressure is 0.09 mm Hg; experimentally, pressures just above 0.10 mm Hg have been measured.

These observations and those made in the previous section lend confidence to the analyses made on the run times, the sphere pressure rise times, and the sphere evacuation rates that are presented in Appendix B. The predictions of the tunnel performance with an increased vacuum system can also be accepted as realistic.

IV. OPERATIONAL EXPERIENCES

The 30" HWT has been in operation for approximately nine months. During this period many problems have developed and many special procedures have been set up to cope with these situations. These special problems and their solutions are discussed in this section.

One of the most demanding characteristics of the 30" HWT is the fact that the pebble bed heater must be kept in continuous (idle) operation every hour of the day, day after day. This, of course, is required to keep certain portions of the bed and insulation above the inversion temperature and thus lengthen the life of the pebble bed. To keep the heater in continuous operation means trouble-free service from water pumps, air blowers, and power control systems, as well as an elaborate alarm system to monitor the heater during off-duty hours. In an effort to reduce the possibility of component failures, a thorough inspection of these items is performed daily and several items are replaced periodically. Two major items that are replaced periodically are the 150 psig water pump and the burner. The water pump is replaced about every six months, the removed one being reworked while the other is installed. The burner is replaced about once each month, as the water passages in the burner tend to clog with lime when in use for an extended period. Without adequate water cooling, the tip of the burner burns through to the water passage with subsequent water leakage into the heater. Two identical burners are available, so that when one is installed the other can be cleaned and delimed. Since the water cooling is so important to the safe operation of the heater, an emergency water system takes over if the normal water system pressure drops below 65 psig.

A phenomenon that is not, as yet, fully understood is the slowly decreasing height of the pebble bed. The top of the balls can be observed through the viewport, so a ready reference is available to measure the height of the pebbles. Over a period of nine months, the top of the bed has dropped a total of 18 inches (or about two inches per month of continuous operation). Fourteen inches of pebbles have been added during this period in order to keep the bed high enough to view through the viewport. The balls were poured on top of the bed, and are the partially stabilized zirconia type. There are several possible explanations for the apparent disappearance of the pebbles. Among them are: vaporization (although the boiling point of the various materials is never reached as far as can be determined from the measured bed temperature distribution); dusting of the pebbles, with the dust being blown down the tunnel or being packed more closely, thereby taking less volume; erosion of the insulation surrounding the bed, thus providing a larger volume for the bed; and possible reactions of ceramics with one another. There is some dusting of the ceramics since dust particles have been found in the test cabin and small pit marks have been found on models that were injected into the air flow. Additional evidence of dusting and packing is the gradually increasing pressure differential across the pebble bed that has been noted for the same pressurization rates. The complete explanation of the decrease in bed height will not be known until the ceramics are removed from the heater and studied carefully.

An undesirable product of the combustion process is the formation of large amounts of water, and if allowed to condense, the water will soak into the insulation and reduce the life of the ceramics. This is also a possible source of water vapor that will mix with the desired dry air required for a tunnel test. Figure 40 of Appendix A shows the production of water for various initial mixtures. In an effort to prevent any water condensation in the heater, all parts of the heater are kept above 212°F. This keeps the water in vapor form and most of it is blown out of the heater.

In order to determine the most effective recharging schedule for the heater, it is desirable to have thermocouples located directly in the bed at as many different levels as possible. Since 3500°R is about the maximum temperature that thermocouples will operate continuously in an oxidizing atmosphere, the maximum allowable temperature distribution in the bed will determine the highest level that the thermocouples can be placed. In the 30" HWT heater, thermocouples were installed at the grate, the two and a half foot high level, and the five foot high level. The grate and 2-1/2 ft high level thermocouples are chromel-alumel type and are still operational. Two thermocouples at the five foot high level were platinum-platinum 13% rhodium

thermocouples; they both became inoperative after approximately four months of continuous operation. Platinum-platinum 13% rhodium thermocouples are known to deteriorate with use, so it is imperative that they be installed in such a manner that they can be easily removed and replaced. All thermocouples in the bed should be designed for rapid replacement, as the shifting of the bed and continuous use can cause frequent failures. The five foot level thermocouples in the 30" HWT could not be removed when they failed so the heater has been operated without them, relying on the experience gained on the heater while they were in operation.

The grate in the bottom of the heater presents a special problem. It is made of stainless steel and supports the bed of pebbles; it therefore can not be heated to the point where it begins to lose its strength or else the weight of the pebbles will cause deformation and eventual failure of the grate. The temperature limit - 1200°F - on the grate is the major limiting factor in adding energy to the bed. It is evident that a water cooled grate is necessary for a highly successful pebble bed heater and this modification is planned for the 30" HWT heater when the ceramics have to be replaced.

It appears that it is possible to operate the heater for as much as a year before replacing the ceramics. In some pebble bed heaters, it has been necessary to replace the ceramics about every six months, but these heaters were allowed to cool down to ambient conditions frequently and this probably hastened the failure of the ceramics. With nine months of operation completed, a year of operation is within reach.

The stilling chamber has some unique problems associated with it, an important one being the temperature loss of the air flowing through the stilling chamber from the heater to the nozzle throat. By preheating the stilling chamber, the temperature loss can be kept between 400°F to 600°F. Another problem associated with the stilling chamber is the inability to keep the inner liner (made of partially stabilized zirconia) above 3000°R at all times. The portion end near the nozzle throat cycles through the inversion temperature range every day and this damages it. It has not been necessary to replace this liner yet, but it surely will be one of the first components requiring replacement.

The tunnel was originally designed to operate with a shut-off valve between the stilling chamber and the nozzle throat where the cold air injection system is now installed. The tunnel operates very satisfactorily with the cold air injection method, but an operational shut-off valve would allow the heater to be pressurized without hot air blowing down the tunnel during the pressurization process, and would allow the heater

vessel to remain pressurized between runs. These changes in procedure would conserve energy stored in the bed and thus, hotter runs could be made with the same charge in the bed. At the present time, a shut-off valve is not available that will operate at 3000 psia and 4000°R, although there is a hot valve installed on the 20" HWT of ARF that is operating successfully up to 2000 psia and 2000°R.

As there is no shut-off valve installed between the heater and the nozzle throat, some method was required to plug the nozzle during heat up of the bed to keep the combustion gases out of the test cabin. A copper plug with an O-ring seal on it was designed to seal the nozzle just downstream of nozzle throat. The plug is held in place by a long rod fastened to the end of the nozzle. The plug is removed just before a tunnel run when the test cabin is checked. A schematic of the plug is shown in Figure 28. The plug is not water cooled itself, but the nozzle wall is water cooled in the plug area. No difficulties have been encountered with the plug, but the seal must be complete to keep the hot gases from burning the O-ring.

The first nozzle throat installed in the tunnel was affected a great deal by the flow of high temperature, high pressure air and possibly by the zirconia dust that blew through it. The inside diameter of the throat grew as a function of accumulated run time as shown in Figure 29. It failed after 83 runs, the failure being detected by leakage of water into the nozzle. Upon examination, the inside of the throat appeared to be pitted in several places, as well as enlarged from its original dimension, 0.195 to 0.242 inches. Unfortunately the throat section was twisted into two pieces during disassembly, so it was not possible to measure the outside diameter of the throat section to determine if the whole throat section had expanded rather than eroded. It appeared, however, that most of the enlargement was due to erosion. The present throat section has enlarged from 0.293 to 0.297 inches after approximately 60 tunnel tests. The present nozzle is made of zirconium copper and coated with nickel with a ceramic coating on the converging portion of the throat section. The first nozzle was made of beryllium copper with no coatings. It appears that the second type throat section is superior to the first, but more test time is required before concrete conclusions can be drawn. One important factor that must be taken into consideration is the fact that most of the tunnel tests on the second throat were made at approximately 1200 psia and the tunnel tests on the first throat were made at approximately 2000 psia. The present nozzle will be run at pressures up to 2000 psia, so the comparison will be at similar conditions.

The problem of zirconia dust blowing down the tunnel during

a test is not as severe as might be expected. The most dusting occurs immediately after the heater has cooled down completely and then reheated. The first three to five runs following a cycle such as this produce a large amount of dust and a model should not be injected into the air flow until the major dusting subsides, as these dust particles can pit steel models.

In all of the various types of heaters for hypersonic wind tunnels, there are good and bad features of each. This section was included in the report so that a more accurate comparison of a typical pebble bed heater could be made to other type heaters. It is also felt that some of the same problems and phenomena encountered in the operation of the 30" HWT will appear in similar facilities, and perhaps this presentation will be helpful to the operations of such facilities in some way.

V. SUMMARY

In the preceding sections, the overall performance of the ARL 30" HWT has been considered at two Mach numbers. The important results of this preliminary operation are summarized below:

(1) The storage heater operation is now routine. Temperatures at the top of the bed are maintained continually above 2800°R to prolong the life of the bed by minimizing the number of temperature cycles through the inversion range of the refractory. Procedures for monitoring the heater and maintaining the associated equipment have been worked out.

(2) Maximum bed temperatures have been 4200°R, this limit established by the heating of the bed supporting grate to a temperature of 1700°R. A water cooled grate is contemplated to remove this limit. An excessive energy loss through the stilling chamber has prevented air temperatures above 3000°R from being delivered to the nozzle. This problem is being examined, corrections will be applied during the scheduled rebuilding of the heater after one year of operation.

(3) The nozzle has been calibrated using two of the interchangeable throats. Nominal Mach numbers of 16.5 and 18.5 have been obtained at three Reynolds numbers; small axial and transverse gradients have been noted and reported.

(4) Other nozzle characteristics, e.g. angularity and blockage effects have been examined for the nozzles. A small angularity of the flow (0.1°) has been found; relatively large models -- a flat plate and a delta wing with a 1 foot chord -- have been tested at moderate angles of attack $\pm 25^{\circ}$.

(5) Two problems concerning the character of the delivered flow are being evaluated at this time. The "dusting" of the pebbles has not been as severe as anticipated and appears to be significant only in the very first few seconds of the test run. Operation of the tunnel has been in a region where other facilities have not detected any liquefaction. Investigation of condensation of the components of air is continuing in the ARL 30" HWT.

(6) Diffuser performance has been excellent, recovery has been close to the total pressure behind a normal shock at the nozzle Mach number. Similarly, the aftercooler has shown a very small pressure drop.

(7) The vacuum system has experienced no problems, with measured minimum sphere pressures near 0.1 mm Hg. Rapid evacuation of the sphere following a tunnel run has been accomplished with ease.

These comments indicate the test program performed to date. Aerodynamic testing is being initiated and further evaluation of the problems peculiar to this type of facility are continuing. The appendices which follow deal with the theoretical performance of the installation for use as a test planning guide.

REFERENCES

1. Fiore, A. W., "Estimated Performance of the Three Inch Hypersonic Wind Tunnel".

2. Gregorek, G. M. and Lee, J. D., "Design Performance and Operational Characteristics of the ARL Twenty-Inch Hypersonic Wind Tunnel". ARL 62-392, August 1962.

3. Gregorek, G. M., "Initial Calibrations and Performance of the ARL Twenty-Inch Hypersonic Wind Tunnel", ARL 62-393, August 1962.

4. Daum, F. L., "Air Condensation in a Hypersonic Wind Tunnel", AIAA Journal, Vol I. No. 5, May 1963.

5. Thomas, R. E. and Lee, J. D., "Operational Experiences from the ALOSU 12 Inch Continuous Tunnel in the Mach Number Range from 6 to 14", TN ALOSU 559-2, The Ohio State University Research Foundation Tech. Report to WADC, 1959.

6. Petrie, S. L. and Scaggs, N. E., "Experimental Studies of Hypersonic Wind Tunnel Diffusers" TN ALOSU 561-1, Technical Report to Cornell Aeronautical Laboratory, Inc., 1961.

7. Ames Research Staff, "Equations, Tables, and Charts for Compressible Flow" NACA Report 1135, 1953.

8. Greiser, D. R. and Goldthwaite, W. H., "Experimental Determination of the Viscosity of Air in the Gaseous State at Low Temperatures and Pressures" AEDC-TDR-63-143, June 1963.

9. Johnson, V. J., "A Compendium of the Properties of Materials at Low Temperature (Phase 1)", WADD TR 60-56, Part 1, July 1960.

10. Bromley and Wilke, "Viscosity at Low Temperatures" TR HE-130-157, University of California.

APPENDIX A

HEATER CHARACTERISTICS

Recharging Considerations

Although the determination of the recharging rate of the heater is complex, some method of estimating the time required to bring the energy level of the bed up to test conditions is desirable to allow run schedules and available test time to be accurately planned. A semi-empirical method has been developed to estimate the time and energy required for recharging, using some of the experimental data taken during the operation of the heater. Although an approximate technique, the method does predict energy level and required time well enough to be useful in planning tunnel tests.

Since the bed is kept at idle conditions at all times, the recharging rate will be considered only from the idle condition to the full charged condition. Figure 30 shows the temperature distribution in the bed for both idle condition and the maximum design temperature distribution. The idle temperature distribution represents 4.75×10^5 BTU's stored in the bed and the maximum design temperature distribution represents 10.62×10^5 BTU's stored in the bed.

The recharging rate depends on two major items; the rate of energy input to the bed, and the rate of energy loss to the bed surroundings. In order to make an approximate analysis of the recharging rate, an assumption is made that the rate of energy loss from the bed is directly proportional to the energy stored in the bed. The rate of energy loss from the bed is known at idle conditions since all the heater temperatures come to an equilibrium level and when this occurs, the rate of energy loss is equal to the rate of energy input. At idle conditions the rate of energy input is 172,000 BTU/Hr and the rate of energy loss is the same. With this known value and the assumption that the rate of energy loss is proportional to the energy stored in the bed, the rate of energy loss for any temperature distribution can be determined. The rate of energy loss at the maximum design temperature distribution is equal to 3.84×10^5 BTU/Hr.

In general, any recharging cycle will be aimed at obtaining the maximum design temperature distribution so that the bed will see all the possible energy levels between the idle condition and the maximum temperature condition. Now, if the temperatures in the bed are increasing at an approximate linear rate during the heat up the average value of the energy loss at idle and

the maximum design temperature distribution should give a good approximation to the total energy loss during the heat up cycle if the average energy loss rate is multiplied by the total heat up time. The average energy loss rate calculated in this manner is 2.78×10^5 BTU/Hr.

For a given energy input schedule, then, it is possible to calculate the energy stored in the bed at any time, or, if the energy input rate is held constant, it is possible to calculate the time required to recharge the bed to a given energy level. Since a constant rate of energy input would place too much of a thermal shock on the bed initially - to reach high bed energy levels, the constant rate of energy input would be very high - a variable energy input schedule has been used in the 30" HWT and is listed in the table below.

TABLE A-I

Recharging Schedule

Heating Step	Energy Input Rate	Time	Flame Temp.
1	240,000 BTU/hr.	2/3 hr.	4040($^\circ$R)
2	420,000 BTU/hr.	2/3 hr.	4040($^\circ$R)
3	480,000 BTU/hr	2/3 hr.	4420($^\circ$R)
4	600,000 BTU/hr.	4/3 hr.	4420($^\circ$R)

The temperature distributions in the bed at various times during the heat up have been shown previously in Figure 10. The maximum temperature distribution reached for this heating schedule after 200 minutes is given in Figure 30 and represents 9.69×10^5 BTU stored in the bed. The analytical method can be used to calculate the energy level of the bed and a comparison made between the measured energy levels and the calculated energy level:

$$E_{calculated} = E_{idle} + \sum_{i=1}^{4} E_{input_i} \Delta t_i - 2.78 \times 10^5 \sum_{i=1}^{4} \Delta t_i \quad \text{A-1}$$

or $E_{calculated} = 11 \times 10^5$ BTU

where i is the heating step,
Δt_i is the heating time of ith step
E_{input_i} is the heating rate of ith step.

This represents a discrepancy of less than 15%, but it does give an estimate of time and energy levels for use in planning tests for the tunnel. It appears that the average heat loss rate should be weighted more toward the high energy levels. This is indicated from the temperature distributions shown in Figure 10. The rate of increase in energy level decreases as the maximum value is approached using the heating schedule given in the above table.

Combustion Analysis

In order to more fully understand the thermodynamics of the combustion process of the burner for the 30" HWT, an analysis was made in which eleven products of combustion were considered. This gives a solution to the combustion process as it occurs in the high temperature portion of the pebble bed. The following equation represents the reaction considered:

$$CH_4 + GO_2 + XN_2 = n_1H + n_2OH + n_3O + n_4O_2 + n_5N + n_6NO + n_7H_2 + n_8H_2O + n_9N_2 + n_{10}CO + n_{11}CO_2 \qquad A\text{-}2$$

where the special notation used in the study are listed at the end of this Appendix for convenience. The solution assumed chemical equilibrium, a pressure of one atmosphere, and an initial temperature of 520°R for the reactants.

For the general combustion process described by the relation

$$\sum_{j=1}^{n} a_j A_j \longrightarrow \sum_{k=1}^{m} b_k B_k \qquad A\text{-}3$$

the flame temperature can be found by equating

$$\sum_{k=1}^{m} b_k \left[\left(H_{Bk}^{T_c} - H_{Bk}^{0} \right) - \left(H_{Bk}^{520} - H_{Bk}^{0} \right) \right] = \qquad A\text{-}4$$

$$- \left[\sum_{k=1}^{m} b_k \left(\Delta H_{f_{Bk}}^{\circ} \right) - \sum_{j=1}^{n} a_j \left(\Delta H_{f_{Aj}}^{\circ} \right) \right]$$

An iterative solution is necessary, the iterations carried out until both sides of Eq. A-4 are equal.

The equation A-4 is such that if the assumed value of T_c is greater than the actual T_c, the right hand side of the equation will be greater than the left.

The Heats of Formation used for the various gases involved in the analysis are shown in the following table.

TABLE A-II

Heats of Formation

Gas	ΔH_f^o (kcal/mole)	Gas	ΔH_f^o (kcal/mole)
CH_4	-17.889	N	112.75
O_2	-	NO	21.60
N_2	-	H_2	-
H	52.089	H_2O	-57.7979
OH	10.06	CO	-26.416
O	59.159	CO_2	-94.052

The air model used for these calculations was argon free air, and its composition compared with actual air is:

Air		Air Model	
Component	Concentration (moles/mole of air)	Component	Concentration (moles/mole of air)
N_2	0.7809	N_2	0.7905
O_2	0.2095	O_2	0.2095
AR	0.0093		---
CO_2	0.0003		---
	1.0000		1.000
Molecular Wt =	28.966	Molecular Wt =	28.850

The assumption of argon free air should have no serious effect on the results, as the oxygen content is identical in both cases.

In addition to the flame temperature, the thermodynamics program tabulated the molecular weight of the initial mixture and the concentrations of the products of combustion. The concentrations are presented in terms of moles of the product per mole of methane initially entering the reaction, enabling comparison of the quantity of the product produced per unit heating rate. This is a more realistic parameter for heater operation than the conventional concentration in moles per mole of initial mixture.

The quantities of oxygen and nitrogen per mole of methane were used as input to the thermodynamic program. The various combinations of methane, oxygen, and nitrogen mixtures are shown in the following table.

TABLE A-III

Combinations of Oxygen and Nitrogen

G = 2	G = 2.1	G = 2.2	G = 2.3	G = 2.4	G = 2.5	G = 2.6	G = 2.7
X	X	X	X	X	X	X	X
7.5	7.9	8.2	8.6	9.0	10.5	12.0	13.5
7.0	7.5	7.5	8.0	8.5	9.0	10.0	12.0
6.5	7.0	7.0	7.5	8.0	8.0	8.0	10.0
6.0	6.5	6.5	7.0	7.0	7.0	7.0	8.0
5.5	6.0	6.0	6.0	6.0	6.0	6.0	6.0
5.0	5.0	5.0	5.0	5.0	5.0	5.0	5.0
4.0	4.0	4.0	4.0	4.0	4.0	4.0	4.0
3.0	3.0	3.0	3.0	3.0	3.0	3.0	3.0
2.0	2.0	2.0	2.0	2.0	2.0	2.0	2.0
1.0	1.0	1.0	1.0	1.0	1.0	1.0	1.0

The values of G range from a stoicmetric mixture to thirty five percent excess oxygen; the values of X range from an Air-Methane mixture at the maximum value of X to a one to one ratio of nitrogen to methane.

The results of the calculations are shown in Figures 31 to 43 with Flame Temperature, Molecular Weight, and SPFR(1) plotted versus the various combinations of initial reactants.

The thermodynamic program used in these calculations was originally set up by the Propulsion Laboratory, Aeronautical Systems Division, Wright-Patterson Air Force Base. The program was modified slightly to accommodate the air-oxygen-methane mixture utilized in the 30" HWT Heater System. The authors wish to express appreciation to the Computer Section of the Aeronautical Systems Division of Wright-Patterson Air Force Base in running this program.

Notations

a_j -moles jth substance in initial reactants

b_i -moles of ith substance in products of combustion

n_i -mole number of ith product

A_j -jth substance in initial reactants

B_i -ith product of combustion

G -moles of oxygen in initial reactants per mole of fuel in the initial reactants

ΔH_f^o -heat of formation

$H^{T_i}-H^o$ -enthalpy difference from absolute zero to T_i

T_f -flame temperature

X -moles of nitrogen in initial reactants per mole of fuel in the initial reactants

SPFR(i)-specific fuel ratio - moles of ith product of combustion per mole of fuel (methane) in initial reactants

Subscripts

1 Atomic Hydrogen (H)

2 Hydroxyl Radical (OH)

3 Atomic Oxygen (O)

4 Molecular Oxygen (O_2)

5 Atomic Nitrogen (N)

6	Nitric Oxide (NO)
7	Molecular Hydrogen (H_2)
8	Water (H_2O)
9	Molecular Nitrogen N_2
10	Carbon Monoxide (CO)
11	Carbon Dioxide (CO_2)

APPENDIX B

WIND TUNNEL OPERATING CHARACTERISTICS

Mass Flow Rate

Of prime importance in the design and operation of a wind tunnel is the mass flow rate. This parameter determines the energy required to heat the air, the volume flow rate that must be accepted by the vacuum pumping system, and the time required to fill a vacuum sphere to the flow drop-out pressure. The mass flow rate, in slugs/sec and in terms of stagnation conditions and nozzle throat area is given below:

$$\dot{m} = \frac{P_o A^*}{60.5\sqrt{T_o}} \qquad \text{B-1}$$

In Figure (44), the mass flow rate divided by the throat area, is presented for the stagnation conditions in the range of interest of the ARL 30" HWT.

The mass flow rates may be noted to range from about 0.003 to 0.067 slugs/sec.

Vacuum System

The vacuum pumping capability of a hypersonic installation is also of concern. The volume flow which may be handled by the available pumps determines whether operation of the wind tunnel will be continuous or blow down; the flow rate will also establish the rate of evacuation of the vacuum sphere. Minimum sphere pressure is likewise a function of the pumping system.

In order to conduct an analytic evaluation of the several possible pumping combinations, the pumping characteristics of each pump must be known. The ARL facility uses Allis-Chalmers, sliding vane pumps of two sizes, types 27D and 12S. Empirical relations which fits the pumping curves of these two types of pumps are

$$\text{type 27D} \quad V = 3150 - 157 \frac{P_2}{P_1} \frac{ft^3}{min} \qquad \text{B-2}$$

$$\text{type 12S} \quad V = 1044 - 52.2 \frac{P_2}{P_1} \frac{ft^3}{min} \qquad \text{B-3}$$

With these characteristics it is possible to set up general expressions for the pumping station in any particular configuration i.e., all pumps in one state; n_1 pumps in the first stage and n_2 pumps in the second; n_1 pumps in the first stage, n_2 in the second and n_3 in the third, etc. For example, a two stage vacuum pumping station of type 27D pumps would have a pumping characteristic given by

$$V = \frac{n_2 \left(63{,}200 - 157 \frac{P_a}{P_1}\right)}{1 + 20.05 \frac{n_2}{n_1}} \frac{ft^3}{min} \qquad \text{B-4}$$

where P_a is the atmospheric pressure and P_1 is the inlet pressure.

This expression has been obtained by assuming continuity of flow through the stages and an interstage heat exchanger to maintain a constant temperature into both stages. Similarly, although somewhat more algebraic manipulation is involved, the pumping characteristics of a three stage system may be determined.

$$V = C - \frac{B}{P_1} \qquad \text{B-5}$$

$$\text{where} \quad C = 3150 - \frac{494{,}600 n_1^2}{3150 n_2 + 157 n_1 - \frac{494{,}600 n_2^2}{3150 n_3 + 157 n_2}} \qquad \text{B-6}$$

$$\text{and} \quad B = \frac{157^3 \, n_1 \, n_2 \, P_A}{(3150 n_2 + 157 n_1)(157 n_2 + 3150 n_3) - 494{,}600 n_2^2} \qquad \text{B-7}$$

The original 12 type 27D pumps at ARL were arranged in a two-stage configuration and performed as anticipated from Eq. B-4. The minimum sphere pressure predicted where V = 0, 1.9 mm Hg, was verified by experiment. As lower sphere pressures were desired, a three stage system was assembled with one of the smaller type 12S pumps in the third stage. With the introduction of the smaller pump characteristic described by Eq. B-3, the volume flow rate, Eq. B-5 has slightly different values for the parameters B and C:

$$B = \frac{1{,}267{,}000\, n_1 n_2 PA}{(3150n_2 + 157n_1)\,(157n_2 + 1044n_3) - 494{,}600n_2^2} \qquad \text{B-7a}$$

$$C = 3150n_1 - \frac{494600n_1^2}{3150n_2 + 157n_1 - \dfrac{494{,}600n_2^2}{1044n_3 + 157n_2}} \qquad \text{B-6a}$$

Figure (45) presents the pumping rate of several combinations of pumps in various stagings. The nomenclature 10-2-1_S refers to a three stage operation with ten pumps in the first stage, two in the second and the small type 12S pump in the third. The advantages of staging are clearly shown in the figure by noting the minimum pressures theoretically obtainable, 38 mm Hg for the single stage, 1.9 mm Hg for the two stage, and 0.1 mm Hg for the three stage configuration. As the laboratory will soon obtain twelve additional Allis Chalmers type 27D pumps, several combinations of twenty-four of these pumps are shown.

Evacuation Rate of Spheres

Once the volume flow pumping capability of the vacuum system is known, the time to pump the sphere down to any desired pressure is obtained easily. The mass of air in the sphere at any time t is

$$m = \rho v \text{ slugs} \qquad \text{B-8}$$

Depending upon the pumping capability of the vacuum system, this mass may be reduced at the rate

$$\dot{m} = \rho V = \frac{P}{RT} V \quad \text{slugs/sec} \qquad \text{B-9}$$

where V is the pumping rate in ft^3/sec obtained from Eq. B-5. Assuming an isothermal evacuation, the time rate of change of mass in the sphere may be written

$$\dot{m} = \frac{v}{RT} \frac{dP}{dt} \quad \text{slugs/sec} \qquad \text{B-10}$$

where v is the volume of the sphere in question. Hence, equating equations B-9 and B-10 after introducing B-5 determines the differential equation which must be solved

$$P \frac{dP}{(C - \frac{B}{P})} = \frac{1}{v} dt \qquad \text{B-11}$$

Letting t = 0 when $P = P_i$, the initial pressure, one obtains

$$P = \frac{B}{C} + (P_i - \frac{B}{C}) e^{-\frac{Ct}{v}} \qquad \text{B-12}$$

This general expression has been used to find the evacuation rate of the 35,000 ft^3 sphere and of the combined 135,000 ft^3 volume of the two spheres for several arrangements of the available vacuum pumps, Figures (46), (47) and (48).

Run Times

In an intermittent facility such as the ARL 30" HWT, the duration of the test is determined by the time required for the sphere pressure to rise to a level which is not sufficient to maintain isentropic flow. The sphere pressure rise with time, subject to a constant mass flow input, must first be determined.

Assuming an adiabatic sphere filling process, the first law of thermodynamics may be written

$$\delta E = \delta W \qquad \text{B-13}$$

where δE is the internal energy change within the sphere δW is the work done by the added mass. The change in energy may be represented by

$$\delta E = E - E_1 = mc_vT - m_1c_vT_1 \qquad \text{B-14}$$

where a constant specific heat is assumed and the subscript 1 refers to the initial sphere conditions. Introducing the perfect gas relation into the expression for the mass in the sphere gives

$$E - E_1 = \frac{c_vV}{R}\left[P - P_1\right] \qquad \text{B-15}$$

The work done by the added mass may be expressed as

$$\delta W = h\dot{m}t = C_pT_H\,\dot{m}t \qquad \text{B-16}$$

where any changes in kinetic and potential energy have been neglected and the enthalpy, h, has been evaluated at the temperature of the flow entering the sphere, T_H, established by the aftercooler downstream of the wind tunnel diffuser.

Making the above substitutions into Eq. B-13, and rearranging, one obtains the time required for the sphere to reach any pressure, P, above P_1:

$$t = \frac{v}{\gamma \dot{m} R T_H} \left[P - P_1 \right] \text{ seconds} \qquad \text{B-17}$$

The run time of the facility will be a function of the diffuser recovery efficiency, η , as this component determines the required pressure to maintain isentropic nozzle flow. A convenient diffuser performance parameter is the normal shock pressure ratio, P_{t_2}/P_o, hence by defining the recovery efficiency as

$$\eta = \frac{\text{total pressure downstream of aftercooler}}{\text{total pressure at entrance to diffuser}} \qquad \text{B-18}$$

the pressure at drop out may be expressed as

$$P = \eta \frac{P_{t_2}}{P_o} P_o \qquad \text{B-19}$$

Inserting Eq. B-19 into B-17, the time to arrive at the terminating pressure is

$$t = \frac{v P_o}{\gamma \dot{m} R T_H} \left[\eta \frac{P_{t_2}}{P_o} - \frac{P_1}{P_o} \right] \qquad \text{B-20}$$

By introducing the mass flow rate, Eq. B-1, in terms of the stagnation conditions, a convenient run time expression is obtained:

$$t = \frac{60.5\ v\sqrt{T_o}}{\gamma A^* R T_H} \left[\eta \frac{P_{t_2}}{P_o} - \frac{P_1}{P_o}\right] \qquad \text{B-21}$$

The run time for a particular facility is therefore determined by the stagnation conditions, T_o and P_o, by the recovery efficiency η, and by the Mach number through the normal shock relation P_{t_2}/P_o. Figures (49) through (52) indicate the run times expected from four nozzle throats delivering Mach numbers of 16, 18, 20 and 22, as a function of stagnation temperature. The two sphere volumes are indicated and the recovery efficiency is used as a parameter. Of interest in these figures is the effect of excitation of the vibrational energy modes in the fluid, as indicated by the difference between the perfect gas run times and the thermally perfect gas times. Reduction in run times of about 25% are indicated for the thermally perfect analysis. This reduction is caused by the impact pressure, P_{t_2}, being reduced for a given M and P_o due to vibrational excitation; thereby decreasing the dropout pressure and shortening the time to reach this terminating pressure.

Extended Running

The possibility exists that the run time of the facility may be increased by operation of the vacuum pumps during the sphere filling process. By accepting an increasing portion of the mass delivered by the tunnel, the vacuum pumps reduce the rise time of the sphere pressure, extending the duration of the test. The formulation of the problem to determine the actual increase in time will now be made.

The mass entering the sphere, m, is the difference between the mass delivered by the tunnel m_o and the mass accepted by the pumps, m_p.

Hence $$\dot{m} = \dot{m}_o - \dot{m}_p \qquad \frac{\text{Slugs}}{\text{sec}} \qquad \text{B-22}$$

Equation B-5 may be put in terms of the mass flow rate by multiplying by the density of the fluid entering the pumps; making this substitution

$$\dot{m} = \dot{m}_o - \frac{CP - B}{RT} \qquad \text{B-23}$$

The time for the sphere to rise to a certain pressure is then determined as in the previous section:

$$t = \frac{V}{\gamma R T_H} \left[\frac{P - P_i}{\dot{m}_o + \frac{1}{RT} (B - CP)} \right] \qquad B\text{-}24$$

Here it is noted that the temperature T in the bracket is the sphere air temperature which will increase as the pressure increases according to the adiabatic relation:

$$T = \gamma T_H \left[\frac{P}{P - P_i \left(1 - \gamma \frac{T_H}{T_i}\right)} \right] \qquad B\text{-}25$$

Figures (53a) to (53d) present Eq. B-24 applied to the two different pumping systems and the two sphere volumes. Assuming sphere pressure when the tunnel drops out of flow is of the order of 15 mm Hg, it may be observed that the lower mass flow rates experience sizable extensions in the run time when the pumps are operated, while the high mass flow rates are not extended significantly. Therefore, for selected test conditions, pump operations during the test will produce desirable lengthening of test duration.

APPENDIX C

STREAM CHARACTERISTICS

Air Saturation Conditions

In a previous section on condensation, a technique was considered to predict saturation conditions for the gas mixture, air. This technique is complicated and requires that the saturation conditions for air in some temperature and pressure range plus the specific volume of both the vapor and liquid phases in the same temperature range be known. At this point it is interesting to note that there are two vapor pressure curves for air[9]. One is for the saturated liquid (bubble point), and the other is for the saturated vapor (dew point). The saturated vapor curve is the one of importance for the problem of onset of condensation of air in wind tunnels.

The data presented in Reference 9 for the vapor pressure curve of air must be extended to the temperature and pressure range which corresponds to the range of operation of the hypersonic wind tunnel in question. To do this the Clapeyron equation,

$$\frac{dP}{dT} = \frac{\Delta H_{vap}}{T(V_{vap} - V_{liq})} \qquad C\text{-}1$$

is used. This equation with the assumption that

$$V_{vap} - V_{liq} = V_{vap} \qquad C\text{-}2$$

and that the gas in question is a thermally perfect one, reduces to the Clausius - Clapeyron equation.

$$\frac{dP}{dT} = \frac{\Delta H_{vap}}{R} \quad \frac{P}{T^2} \qquad C\text{-}3$$

These two assumptions are reasonable for air in the temperature - pressure range which exists in hypersonic wind tunnels.

The Clausius-Clapeyron equation yields

$$\int_{P_{ref}}^{P} \frac{dP}{P} = \frac{1}{R} \int_{T_{ref}}^{T} \frac{\Delta H_{vap}}{T^2} \, dT \qquad \text{C-4}$$

If the temperature range is small, the assumption that the heat of vaporization, ΔH_{vap} = constant is justifiable and this is often used at this point. However, if the temperature range is large, as ~~in this~~ problem, the heat of vaporization must be considered a function of temperature if any degree of accuracy is to be obtained. This variation of ΔH_{vap} with temperature is given by

$$(\Delta H_{vap})_T = (\Delta H_{vap})_{T_{ref}} + \int_{T_{ref}}^{T} (c_{p_{vap}} - c_{p_{liq}}) \, dT$$

$$= (\Delta H_{vap})_{T_{ref}} + \int_{T_{ref}}^{T} \Delta C_{p_{v,l}} dT \qquad \text{C-5}$$

At this point another simplifying assumption is possible, i.e., $\Delta C_{p_{v,l}}$ = constant. This assumption is justifiable if the temperature range is sufficiently far away from the critical temperature.

From values of ΔH_{vap} for air given in Reference 9 it can be observed that at temperatures below 160°R ΔH_{vap} approaches a linear function of temperature. Again it should be noted that the values given are for the saturated liquid and thus should not be used in this analysis. However, if the ΔH_{vap} for air calculated along the saturated vapor curve using the Clapeyron equation and data in the same reference for V_{vap}, V_{liq}, P and T are used to graphically determine dP/dT, it is found that the

trend is similar and ΔH_{vap} becomes a linear function of temperature at temperatures below 150°R. Thus, if T and T_{ref} < 150°R,

$$(\Delta H_{vap})_T = (\Delta H_{vap})_{T_{ref}} + Ac_p \int_{T_{ref}}^{T} dT$$

$$= (\Delta H_{vap})_{T_{ref}} + \Delta c_{p_{v,l}}(T - T_{ref}) \qquad \text{C-6}$$

and from the Clausius - Clapeyron equation

$$\ln \frac{P}{P_{ref}} = \frac{(\Delta H_{vap})_{T_{ref}} - \Delta c_{p_{v,l}} T_{ref}}{R} \left[\frac{1}{T_{ref}} - \frac{1}{T}\right] + \frac{\Delta c_p}{R} \ln \frac{T}{T_{ref}} \qquad \text{C-7}$$

Figure 54 shows the saturation conditions predicted by the technique discussed above. No consideration of phase transition is attempted by this technique. The figure also shows an empirically derived expression for the amount of supersaturation which can be expected in hypersonic wind tunnels.

Viscosity of Air at Low Temperatures

Two of the important similarity parameters used in aerodynamic testing, Reynolds number and Prandtl number, require knowledge of the viscosity of the test fluid. In hypersonic facilities such as the ARL 30" HWT, the free stream temperature may be so low that experimental measurements of the viscosity (and, indeed most other gas properties) have not yet been performed for air in the appropriate temperature and pressure range. When this occurs, some analytic or empirical technique must be used to determine a quantitative value for the viscosity.

A viscosity-temperature relation applicable in the temperature range from 180°R to 3400°R is Sutherland's formula given in Reference 7.

$$\mu = 2.27 \times \frac{T^{3/2}}{T + 198.6} \times 10^{-8} \quad \frac{\text{slugs}}{\text{ft sec}} \qquad \text{C-8}$$

Some experimenters simply use a straight line extrapolation from this expression at 200°R to establish a viscosity curve. Other experimenters use the Bromley-Wilke[10] curve shown in Figure 55. The latest study[8] of air viscosity at low temperatures uses experimental data found in the temperature range of 93°R to 198°R to modify Eq. C-8 to have the form:

$$\mu = 2.211 \frac{T^{3/2}}{T + 178.6} \times 10^{-8} \frac{\text{Slugs}}{\text{ft sec}} \qquad \text{C-9}$$

This relation is also indicated in Figure 55. As this formula is based on experimental work near the range of interest, and as it uses the familiar Sutherland form, Eq. C-9 was used for all calculations in this report.

Free Stream Reynolds Number

The Reynolds number of the free stream is of interest in almost all aerodynamic tests; hence Figure 56 offers a convenient plot of the Reynolds number per foot for a stagnation pressure of 1 psia. Used in the calculations are the viscosity curve described in the preceding section, Eq. C-9, and the corrections required for a thermally perfect gas, as presented in Reference 7.

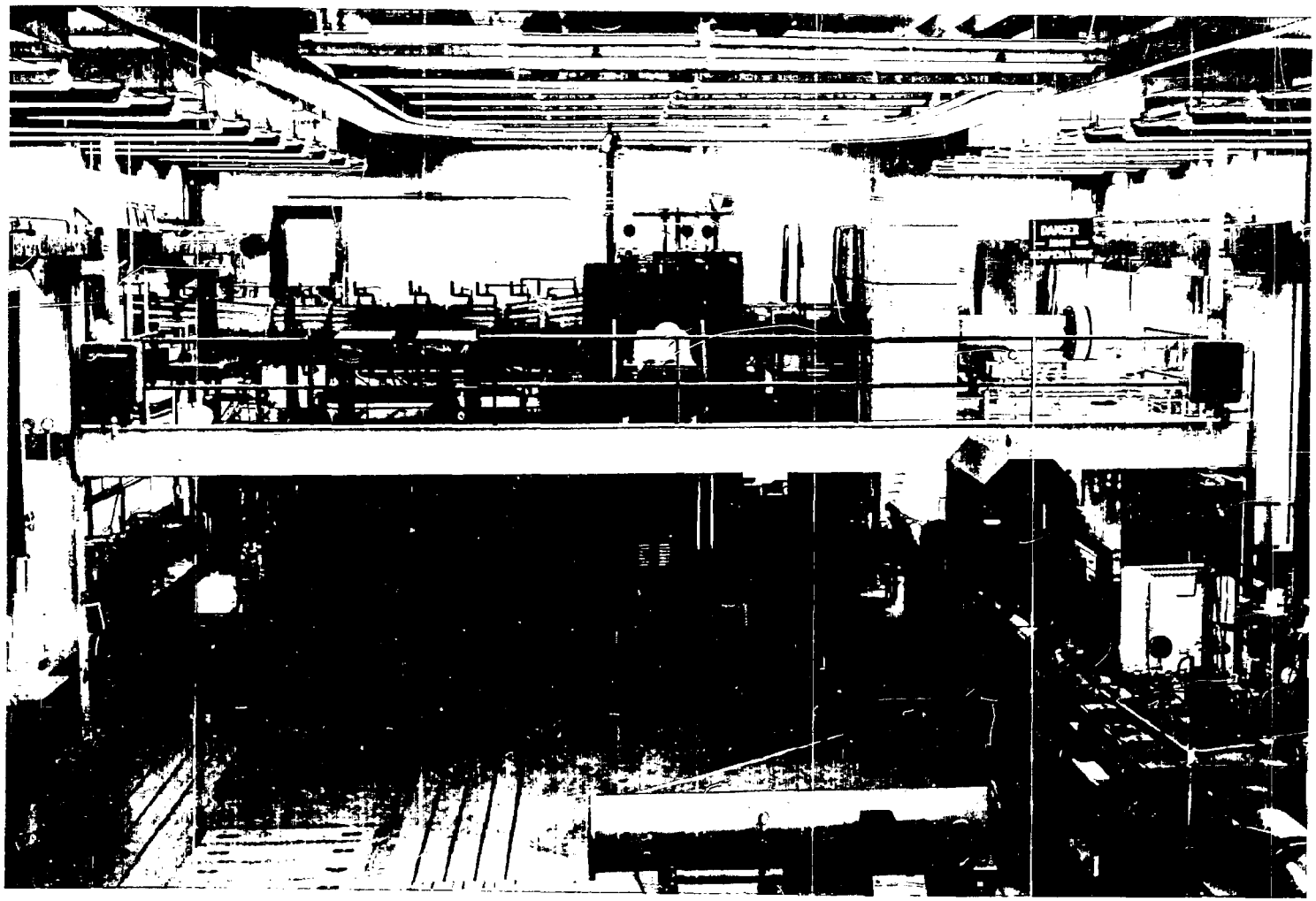

FIGURE 1—THE ARL 30" HYPERSONIC WIND TUNNEL

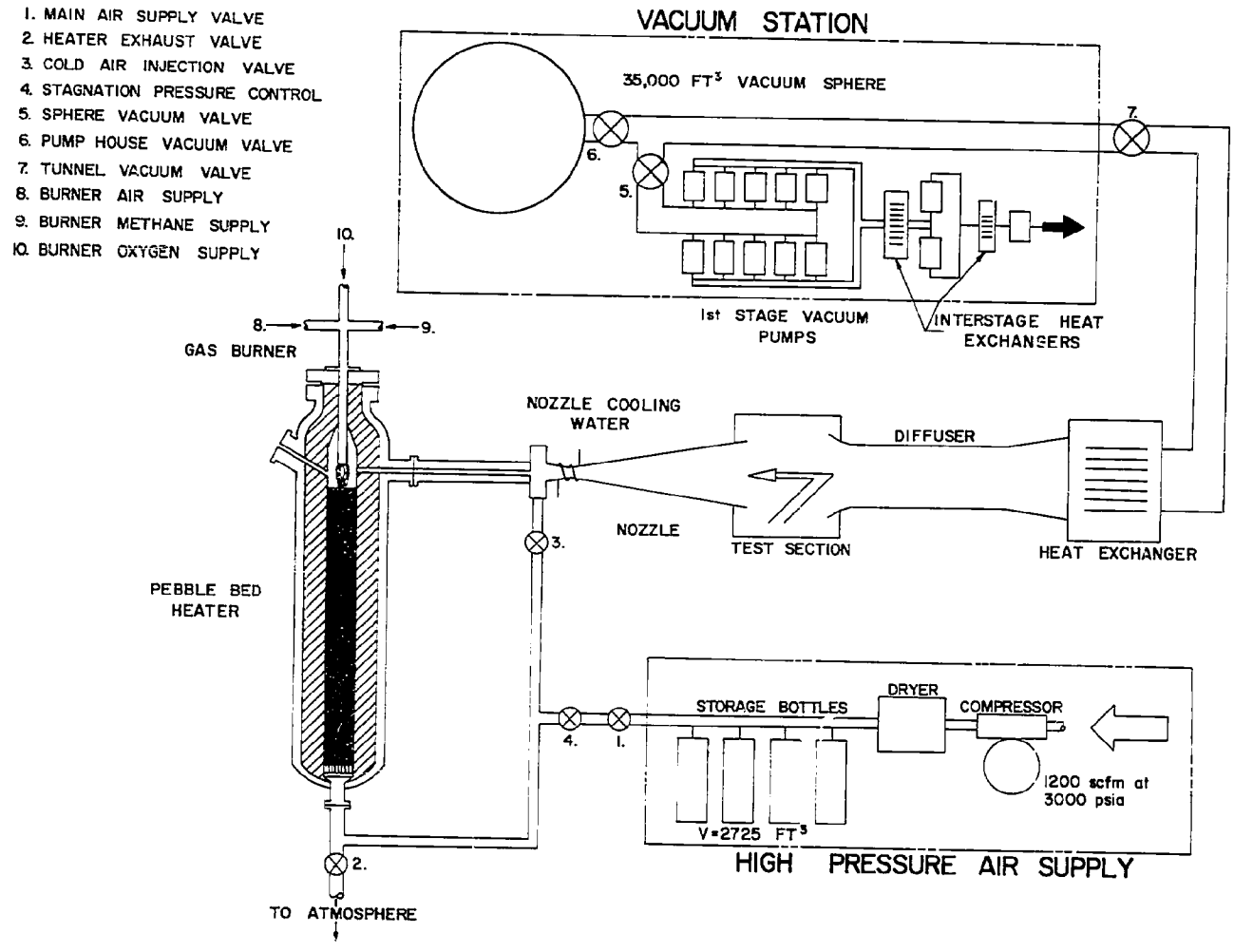

FIGURE 2 - THE ARL 30 INCH HYPERSONIC WIND TUNNEL
SCHEMATIC

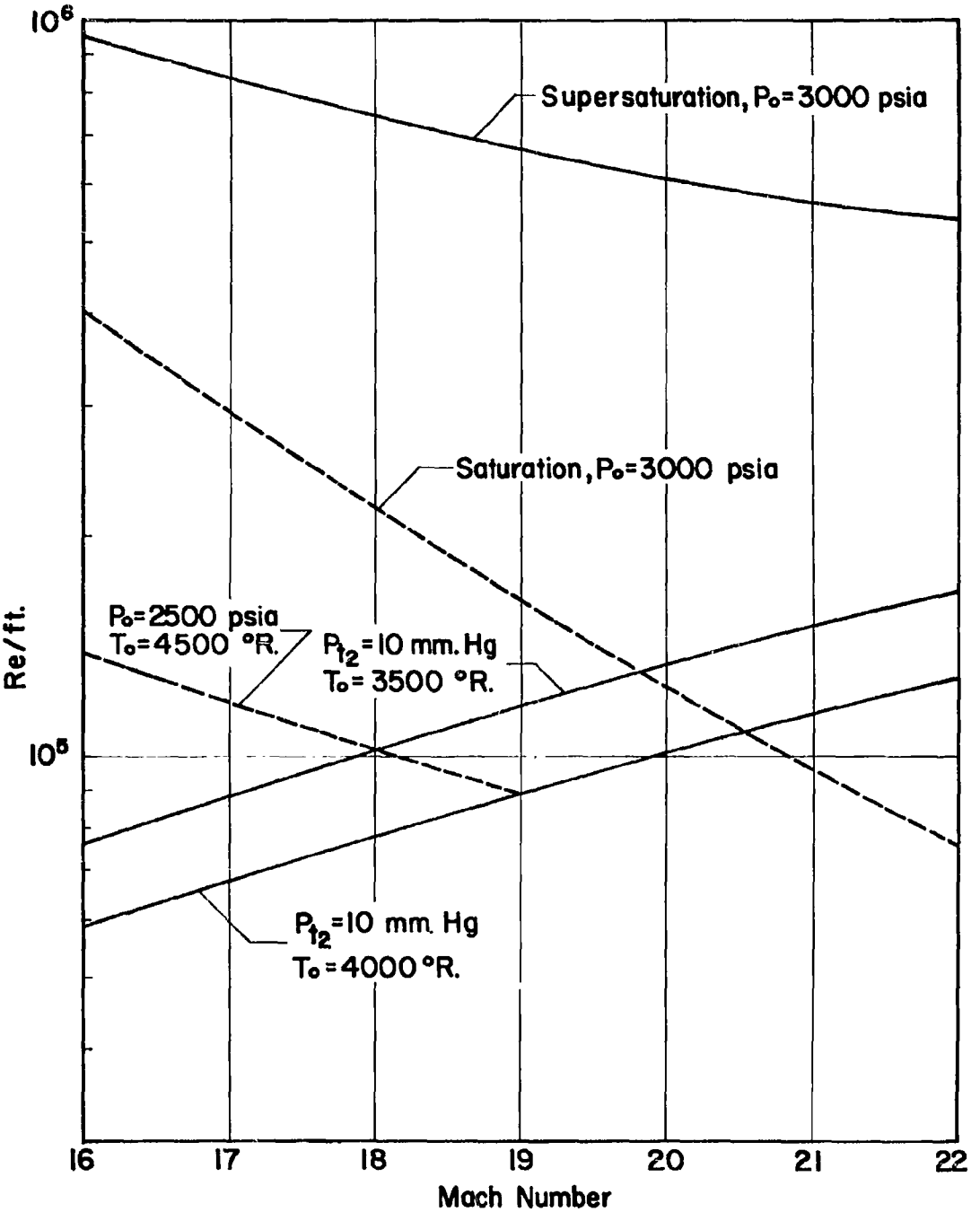

FIGURE 3 - MACH NUMBER AND REYNOLDS NUMBER SIMULATION OF THE ARL 30" HWT

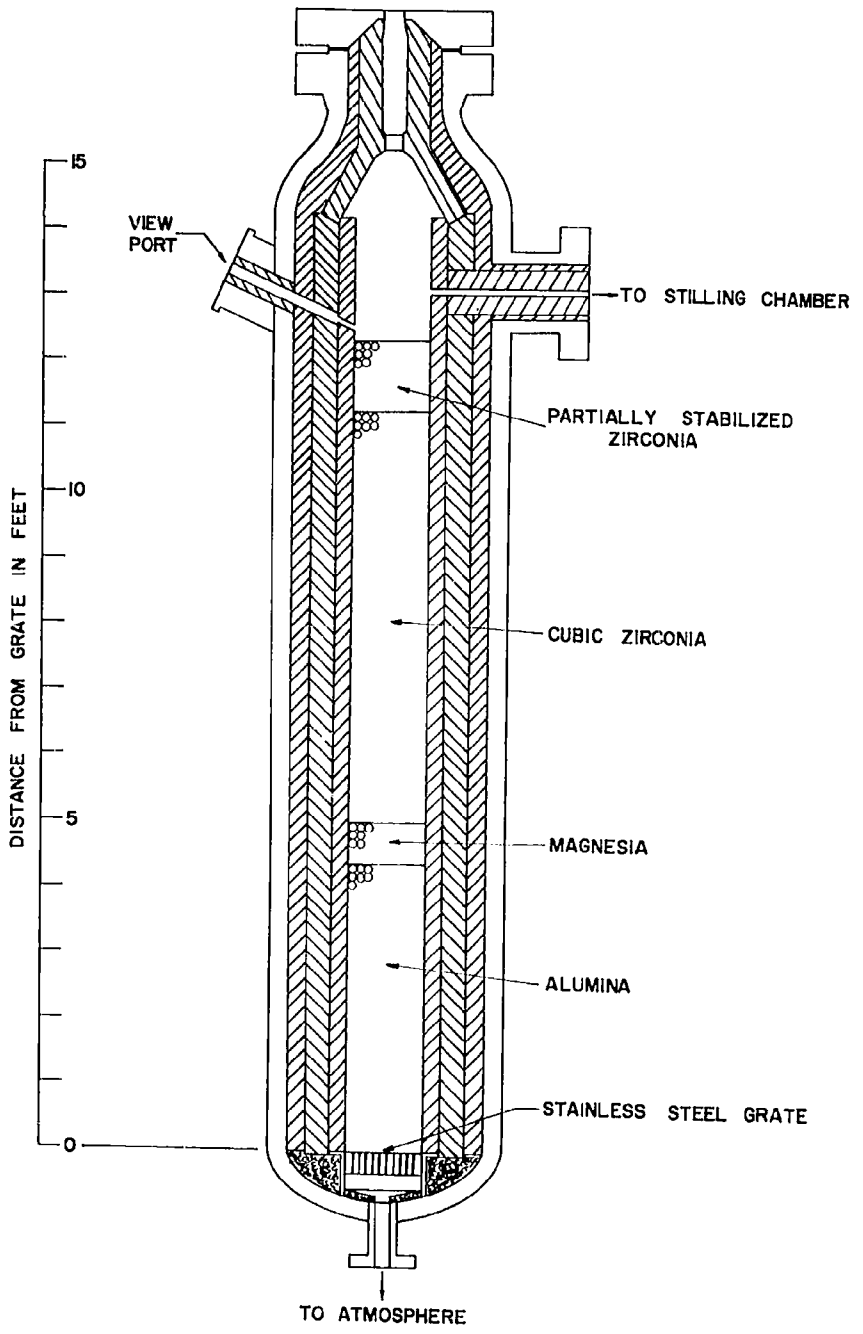

FIGURE 4 -PEBBLE BED HEATER

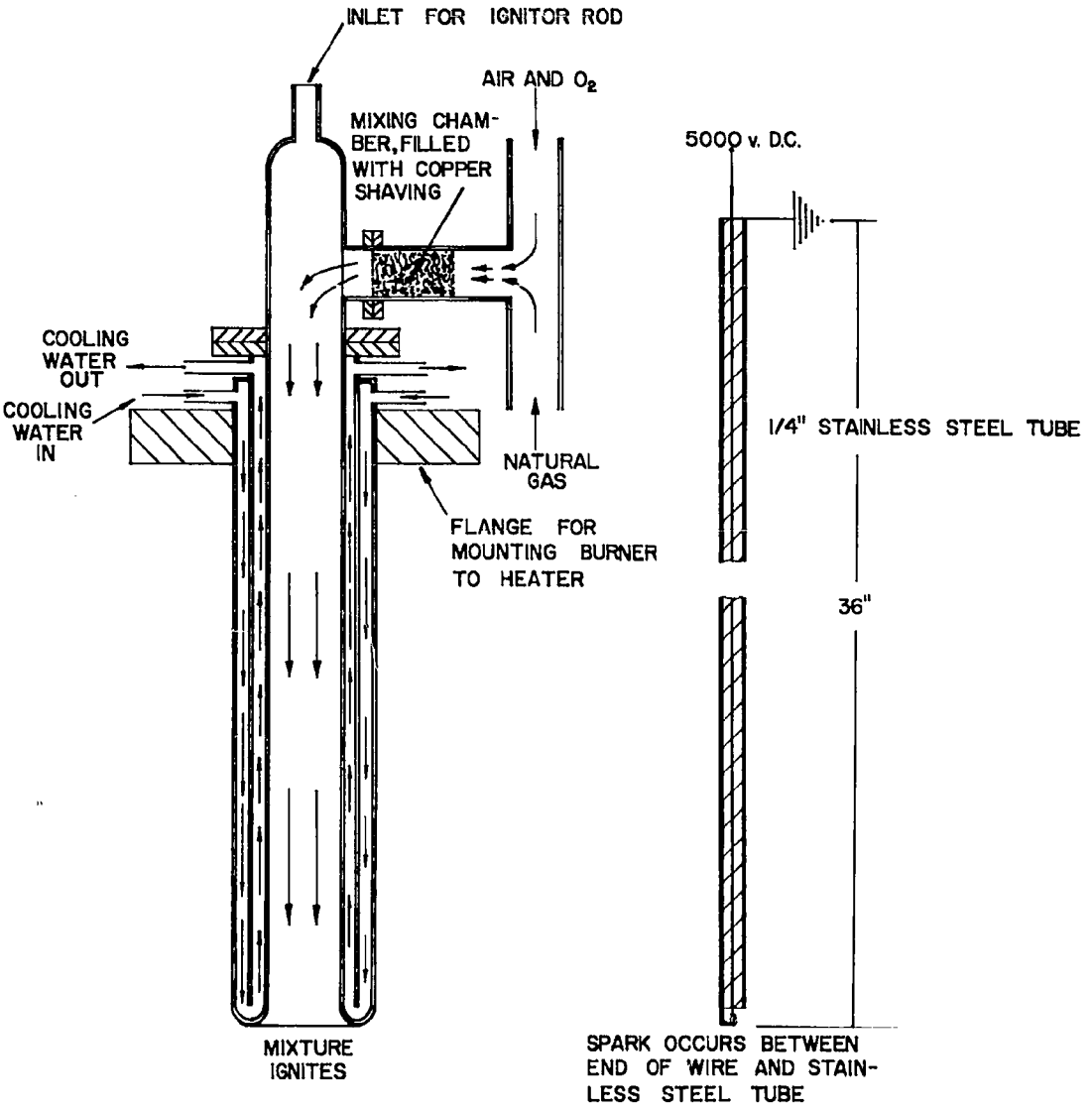

FIGURE 5 - BURNER AND IGNITER DETAILS

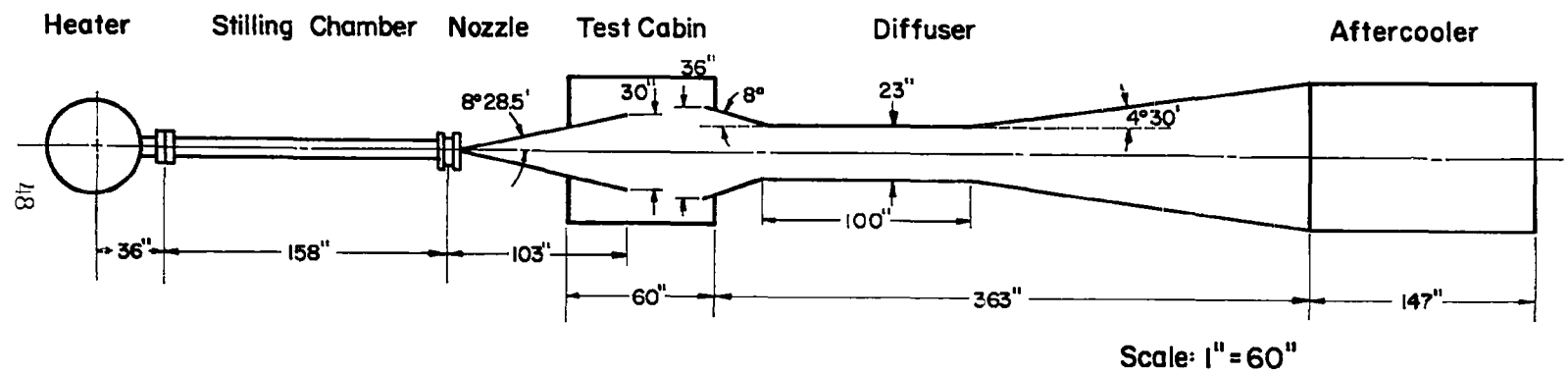

FIGURE 6-DIMENSIONS OF THE WIND TUNNEL COMPONENTS

Dimension	Throat No. 1	Throat No. 2
A	.195"	.293"
B	.275"	.413"
C	17°40'	12°20'

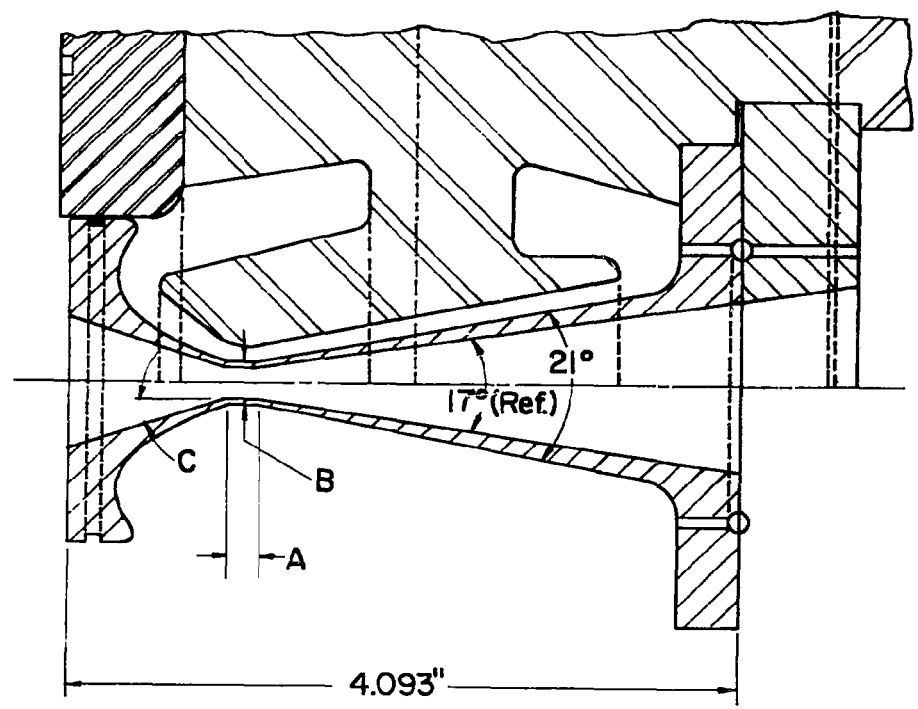

FIGURE 7 - DETAILS OF THE NOZZLE THROATS

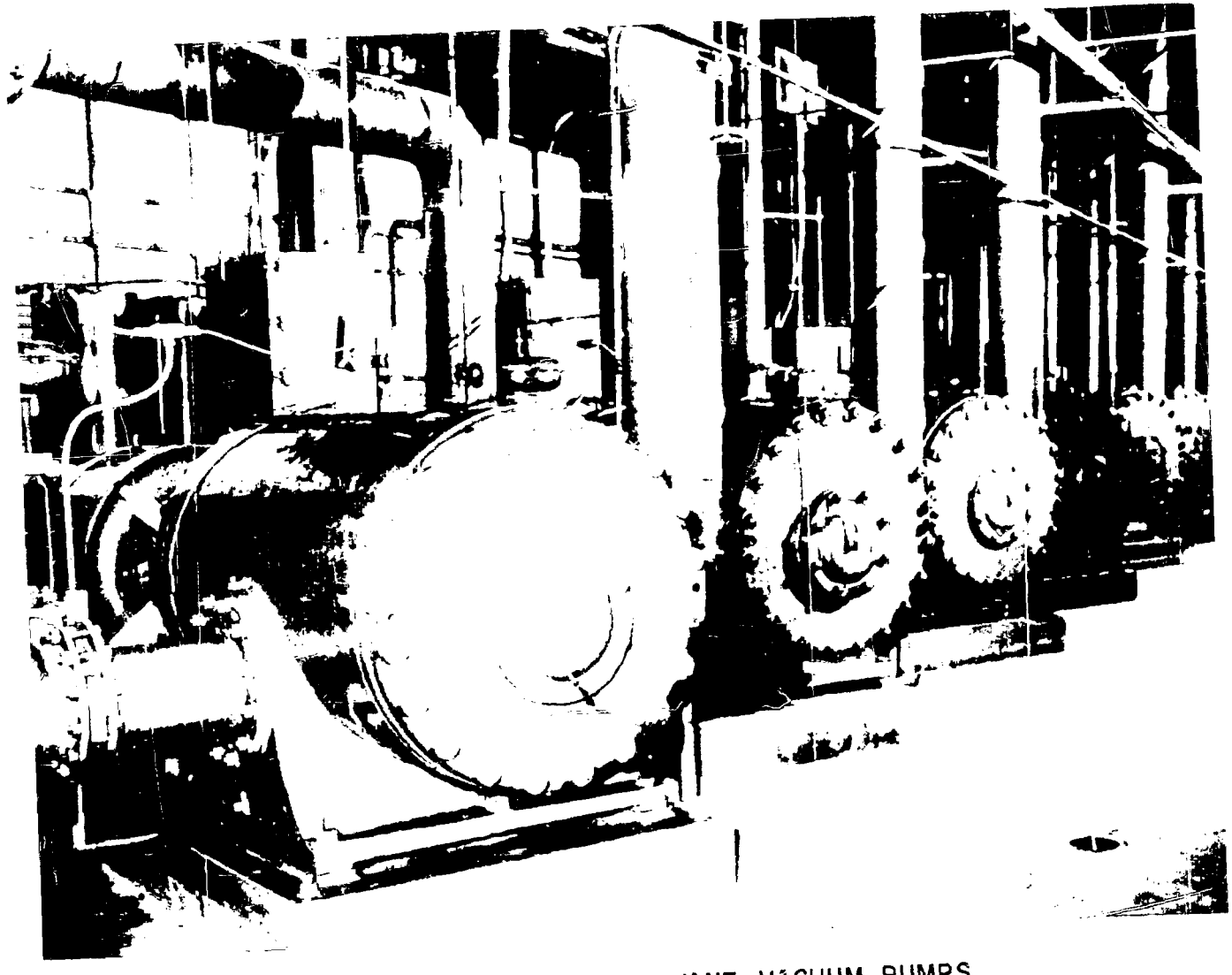

FIGURE 8 — AC 27D SLIDING VANE VACUUM PUMPS

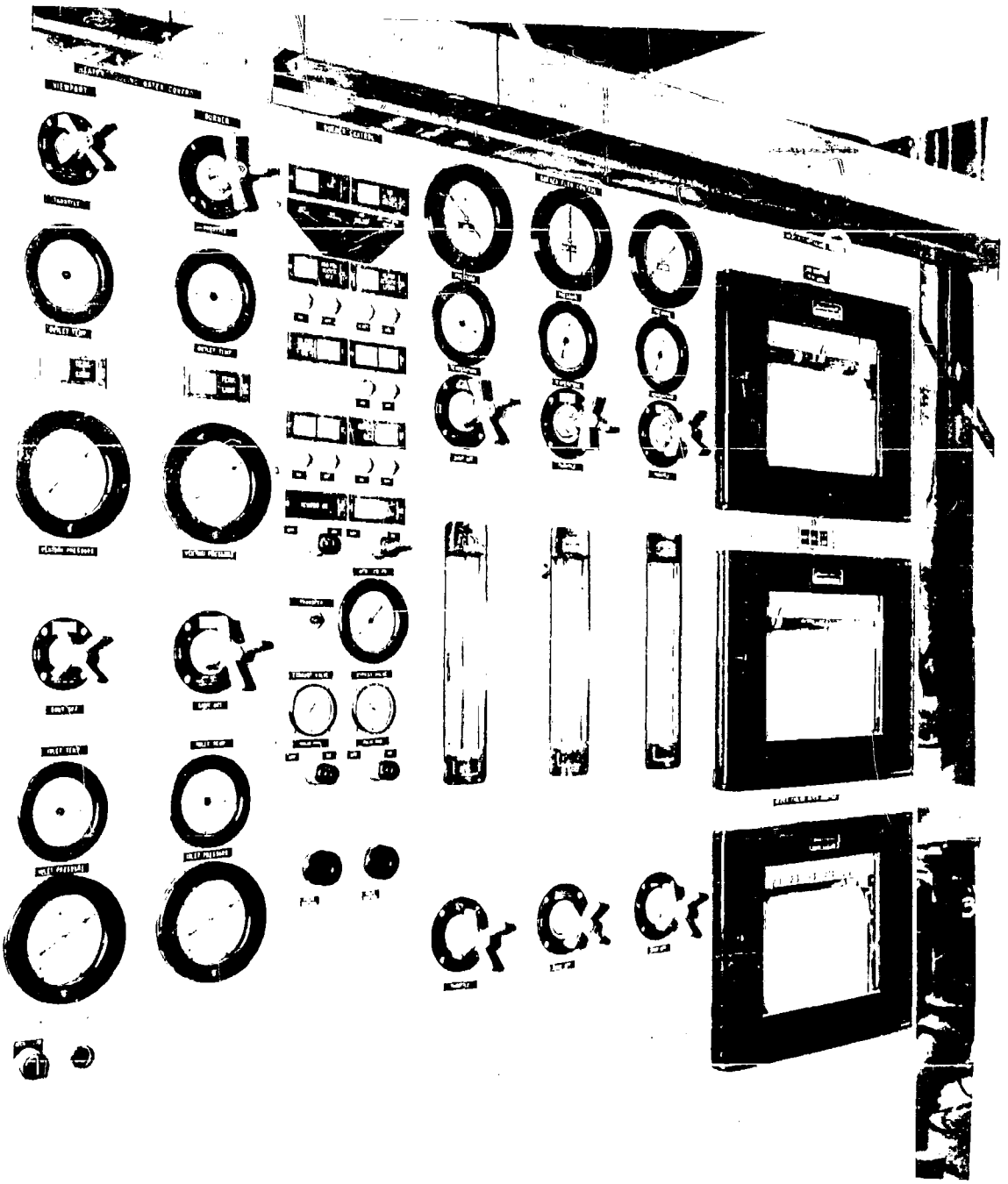

FIGURE 9 — THE BURNER CONTROL PANEL

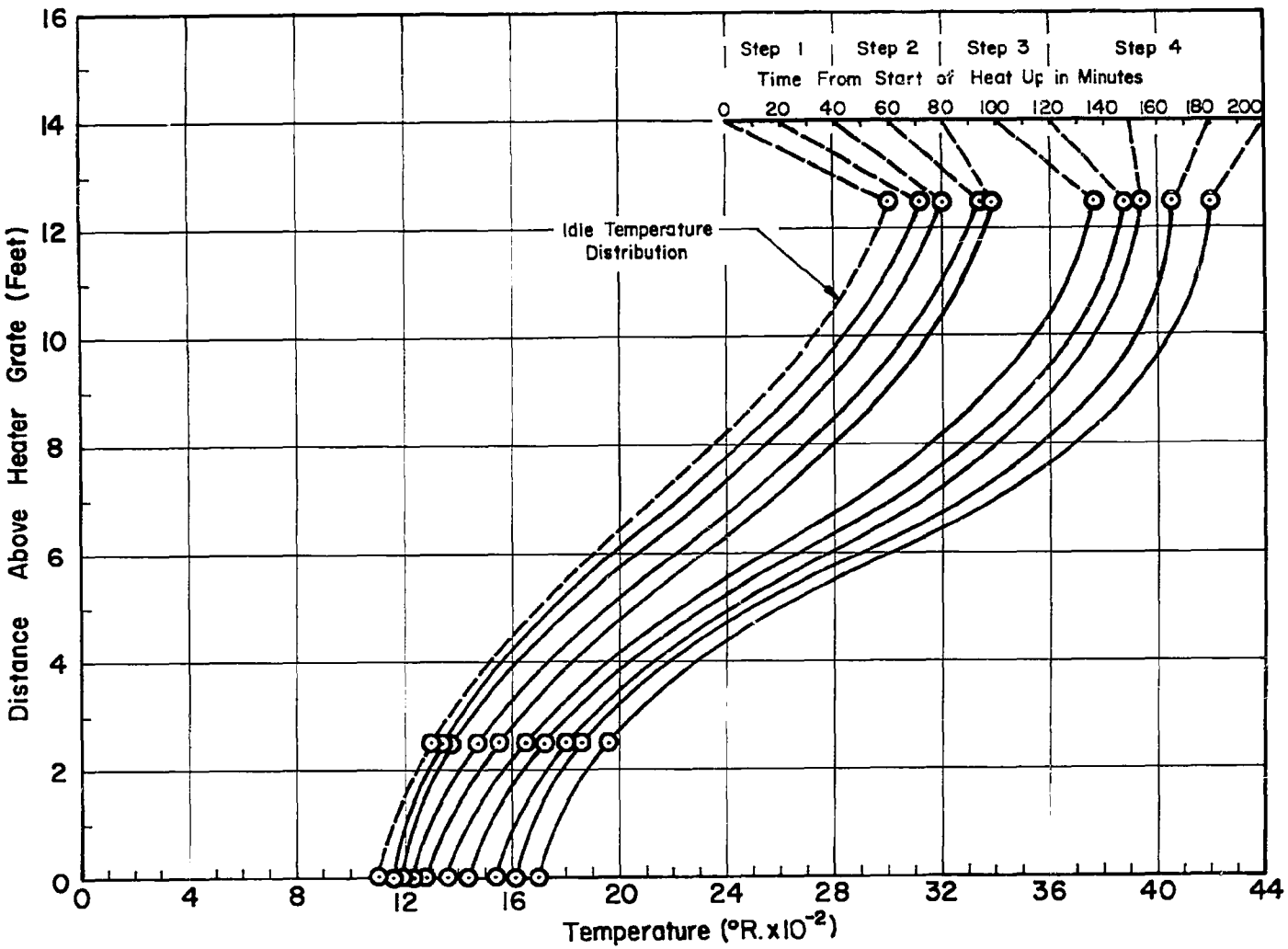

FIGURE 10 - TEMPERATURE DISTRIBUTIONS IN HEATER

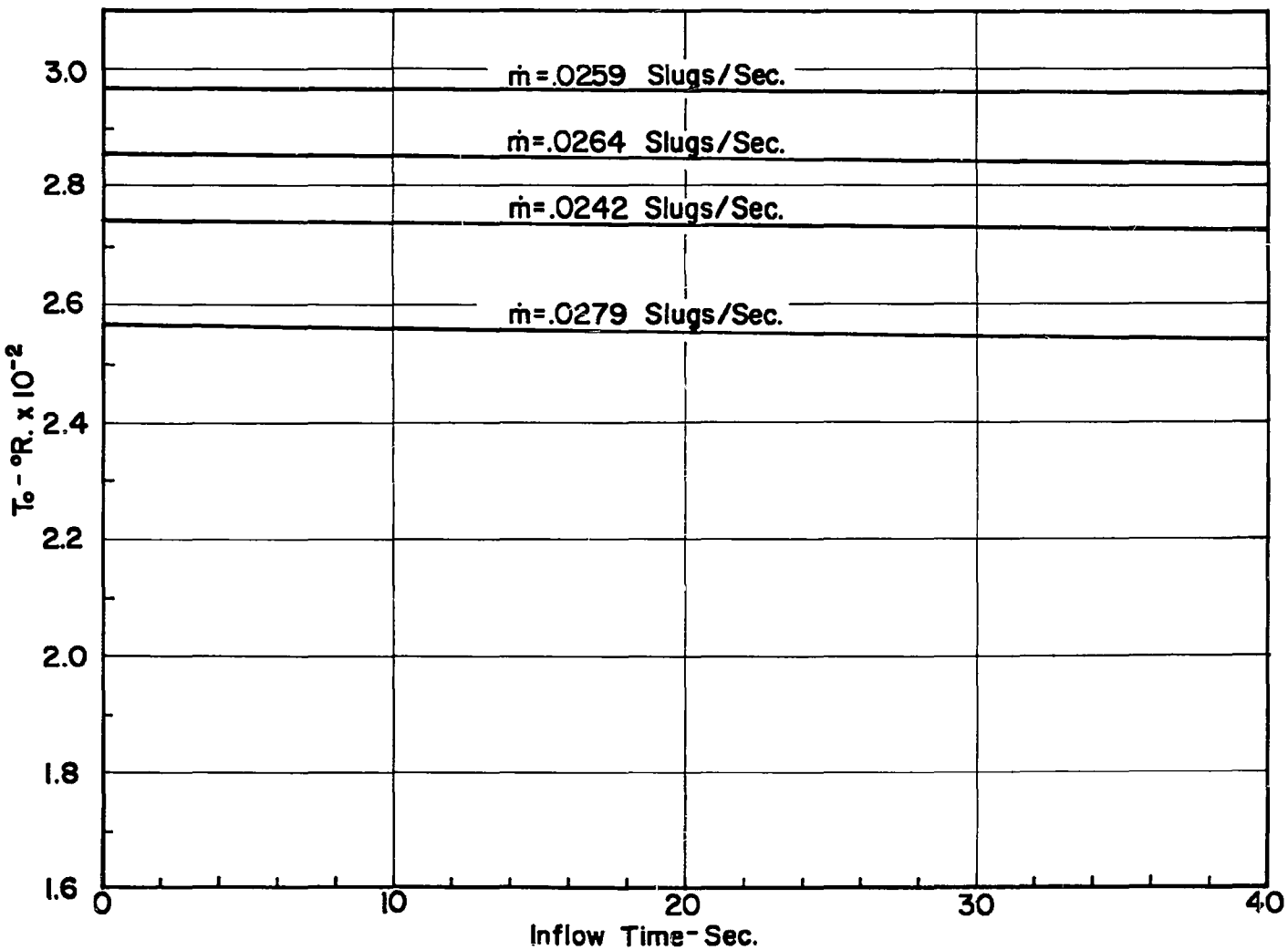

FIGURE II - AIR TEMPERATURE DURING IN-FLOW TIME

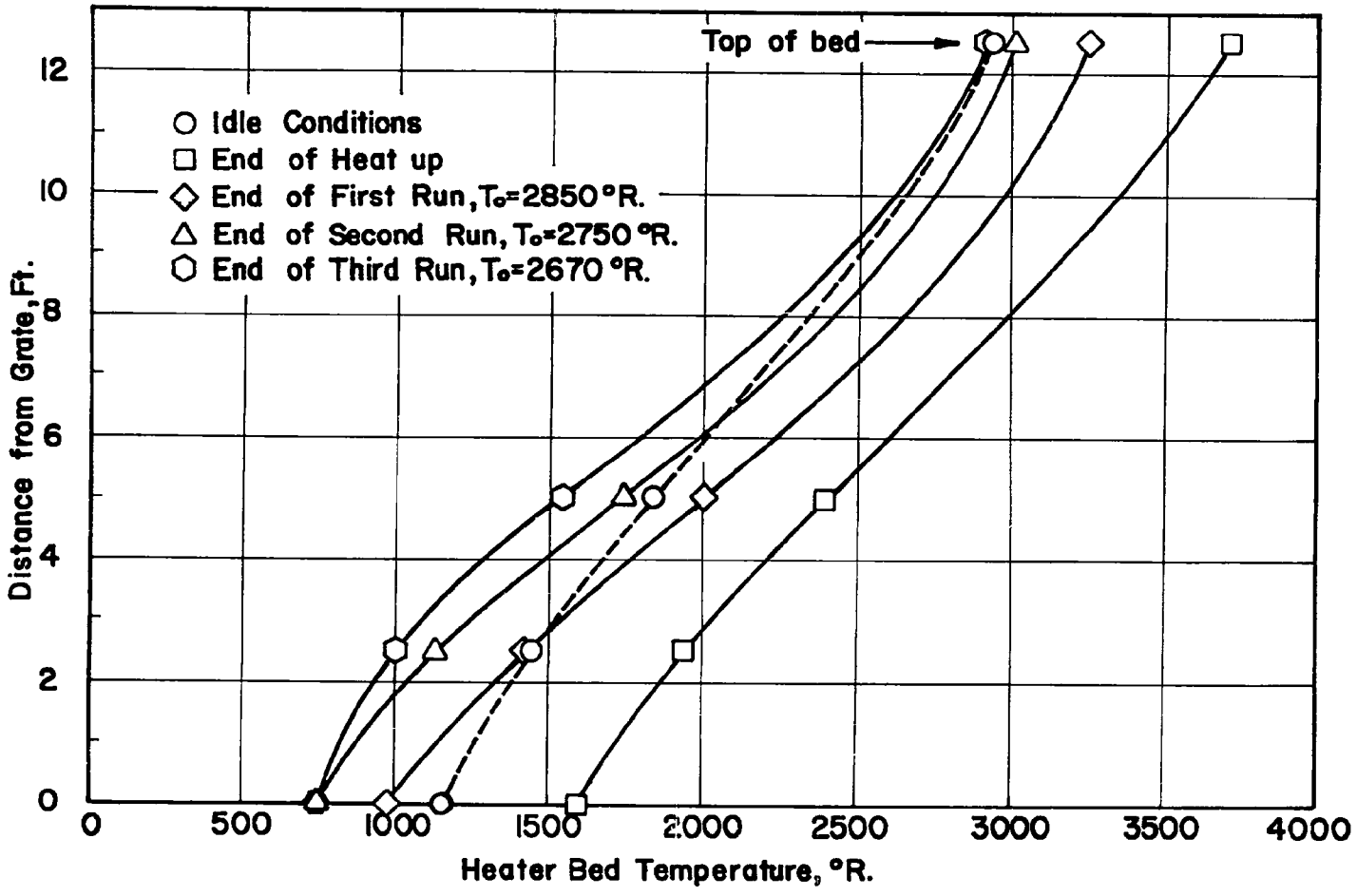

FIGURE 12 -TEMPERATURE DISTRIBUTION THROUGH BED AFTER TESTS

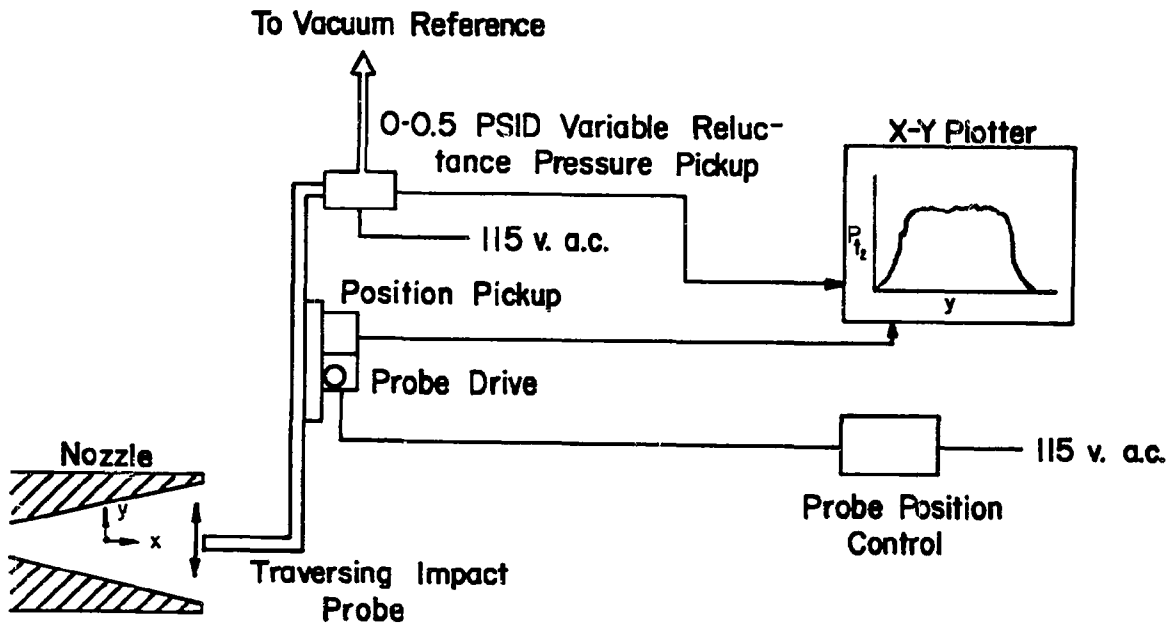

FIGURE 13-BLOCK DIAGRAM OF INSTRUMENTATION FOR NOZZLE IMPACT PRESSURE PROBE

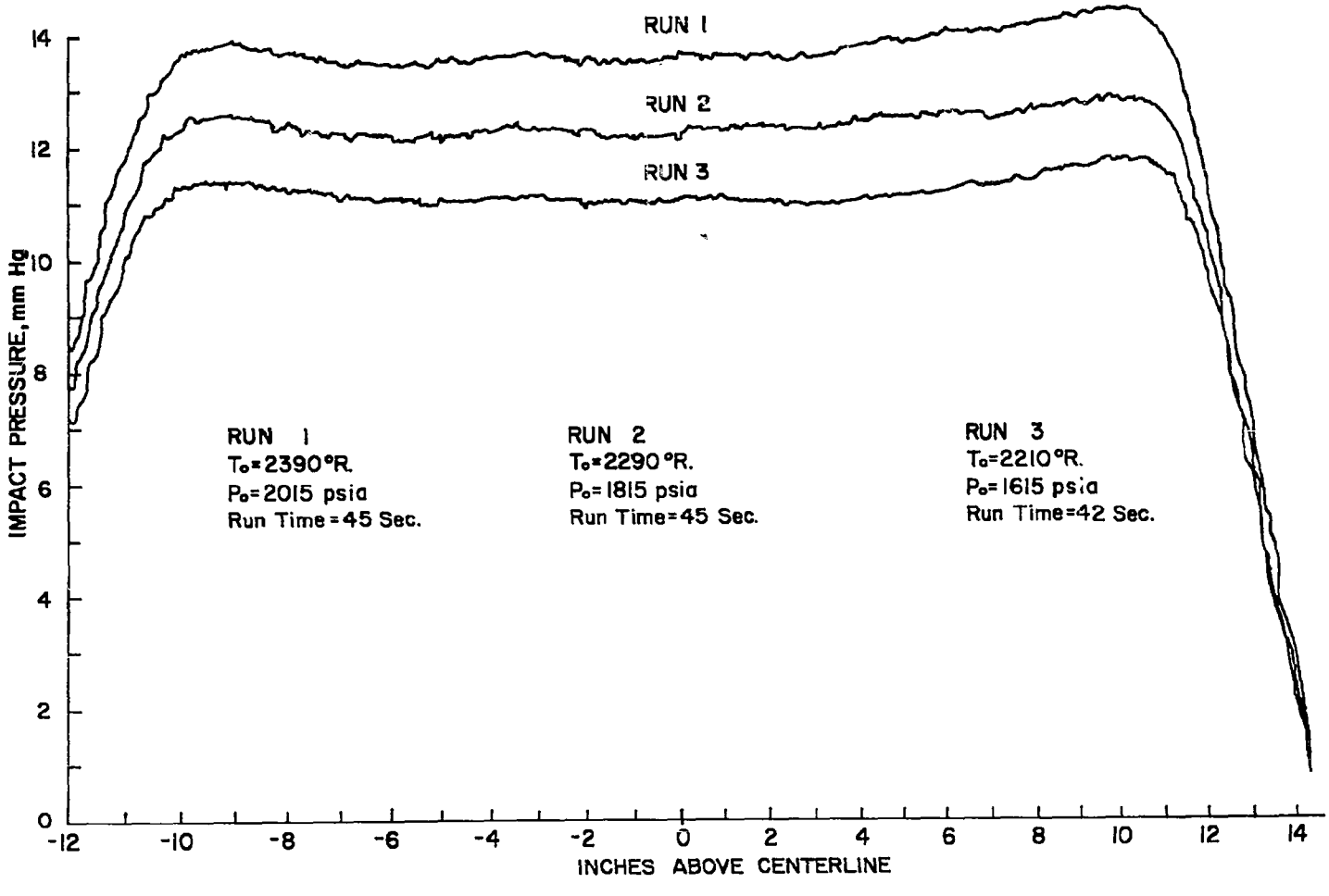

FIGURE 14 - TYPICAL DATA OUTPUT

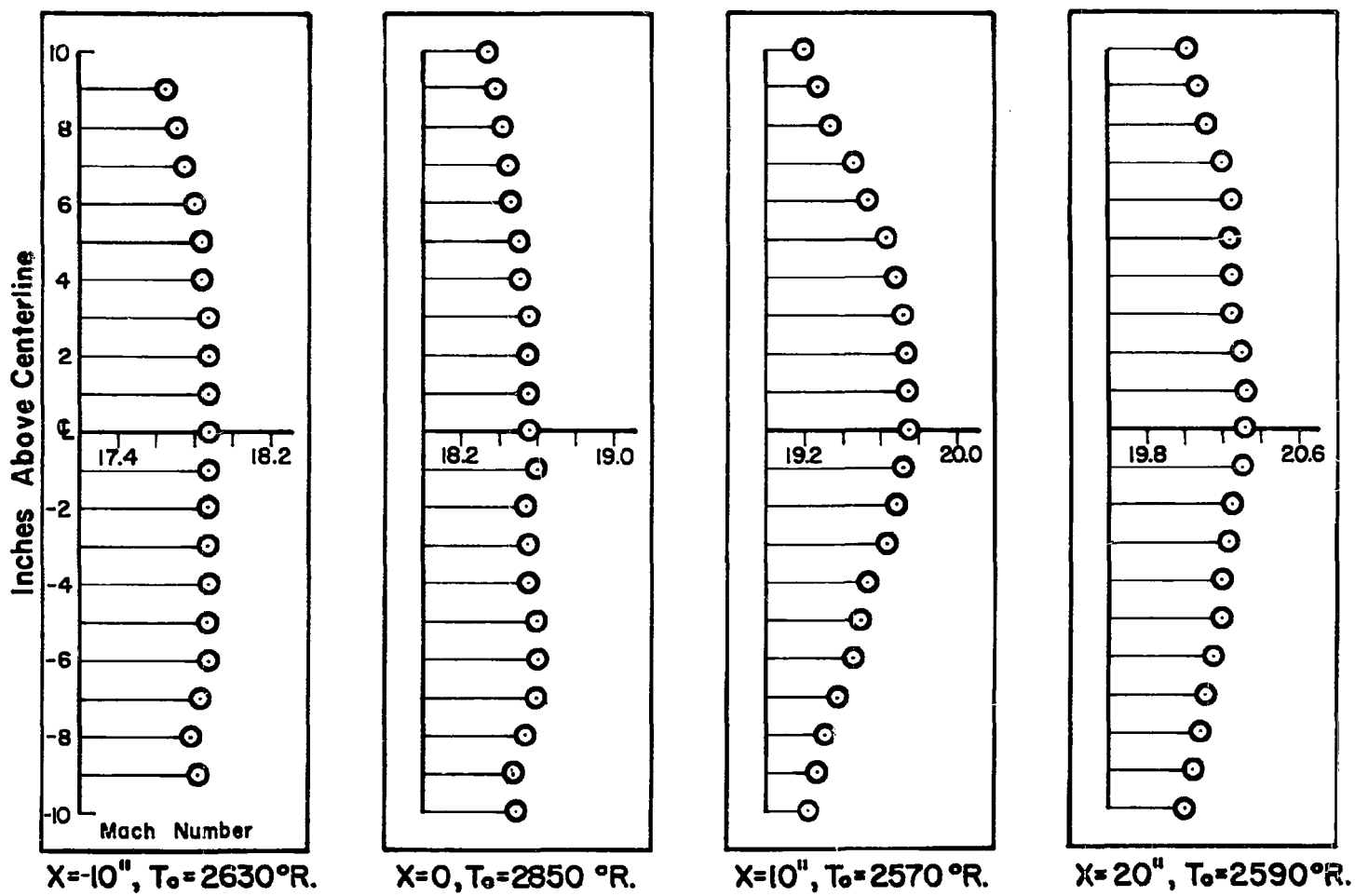

FIGURE 15 - MACH NUMBER CALIBRATION OF THROAT NO. 1 AT P_o=2015 psia

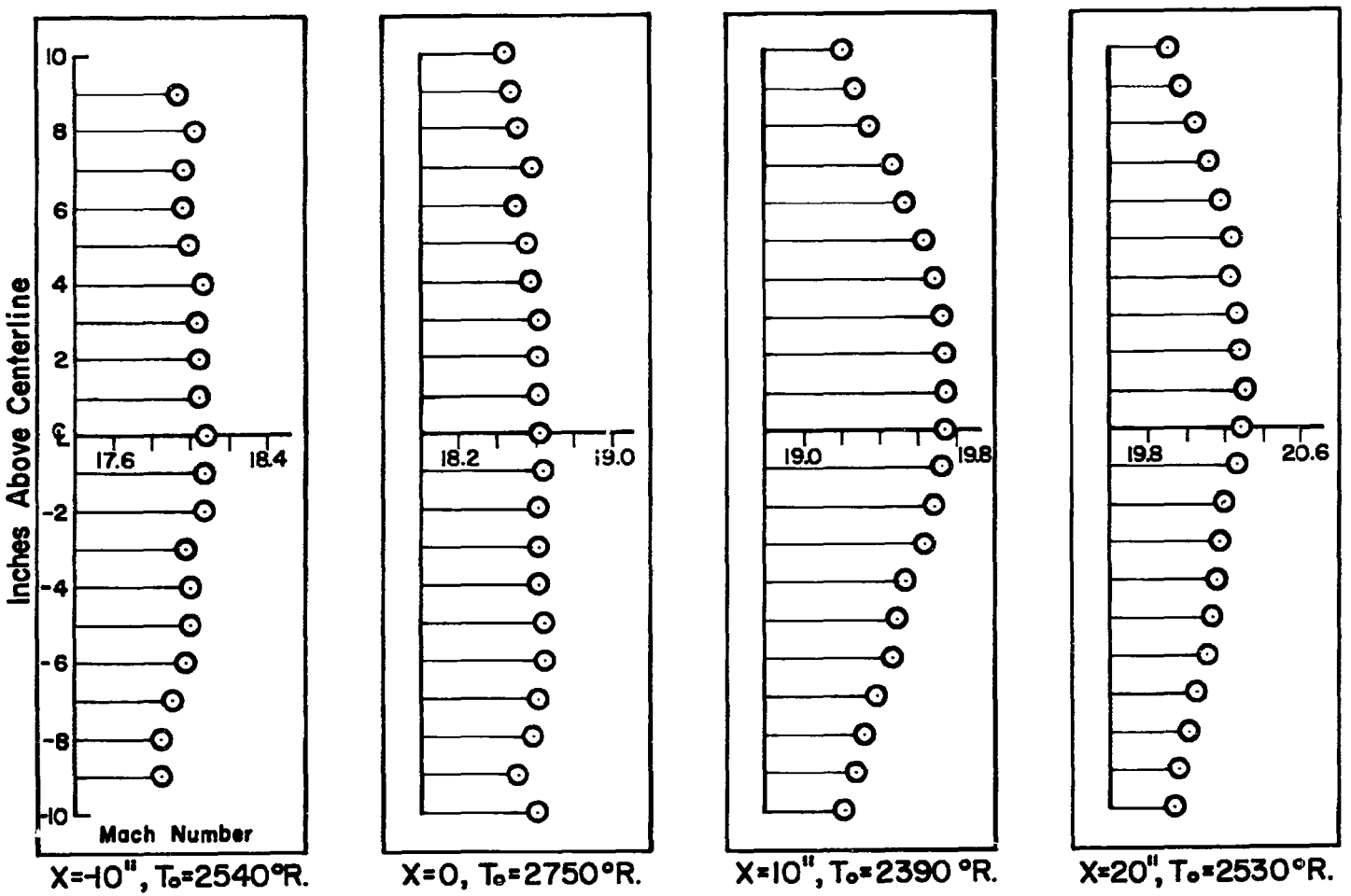

FIGURE 16 - MACH NUMBER CALIBRATION OF THROAT NO. 1 AT P_o=1815 psia

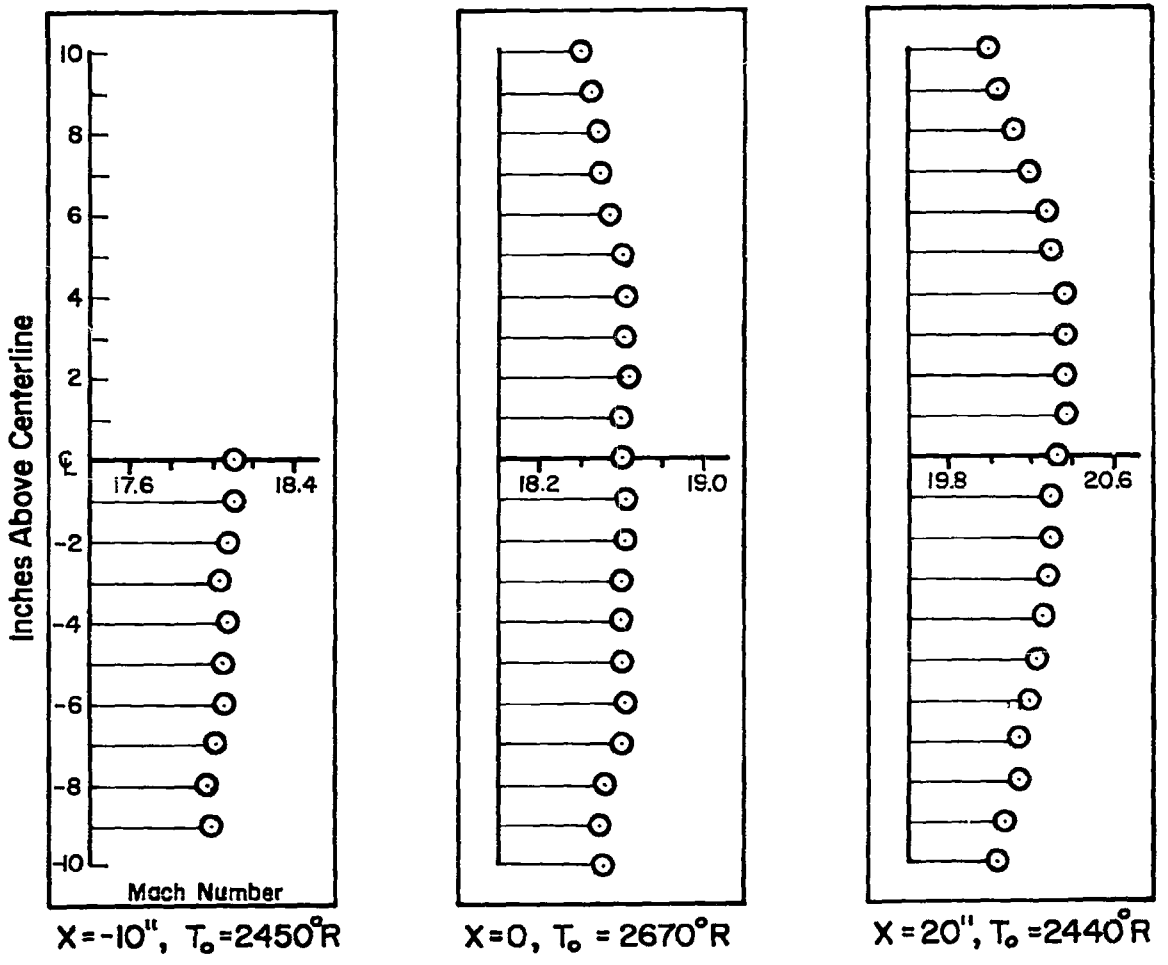

FIGURE 17 – MACH NUMBER CALIBRATION OF THROAT NO. 1 AT P_o = 1615 psia

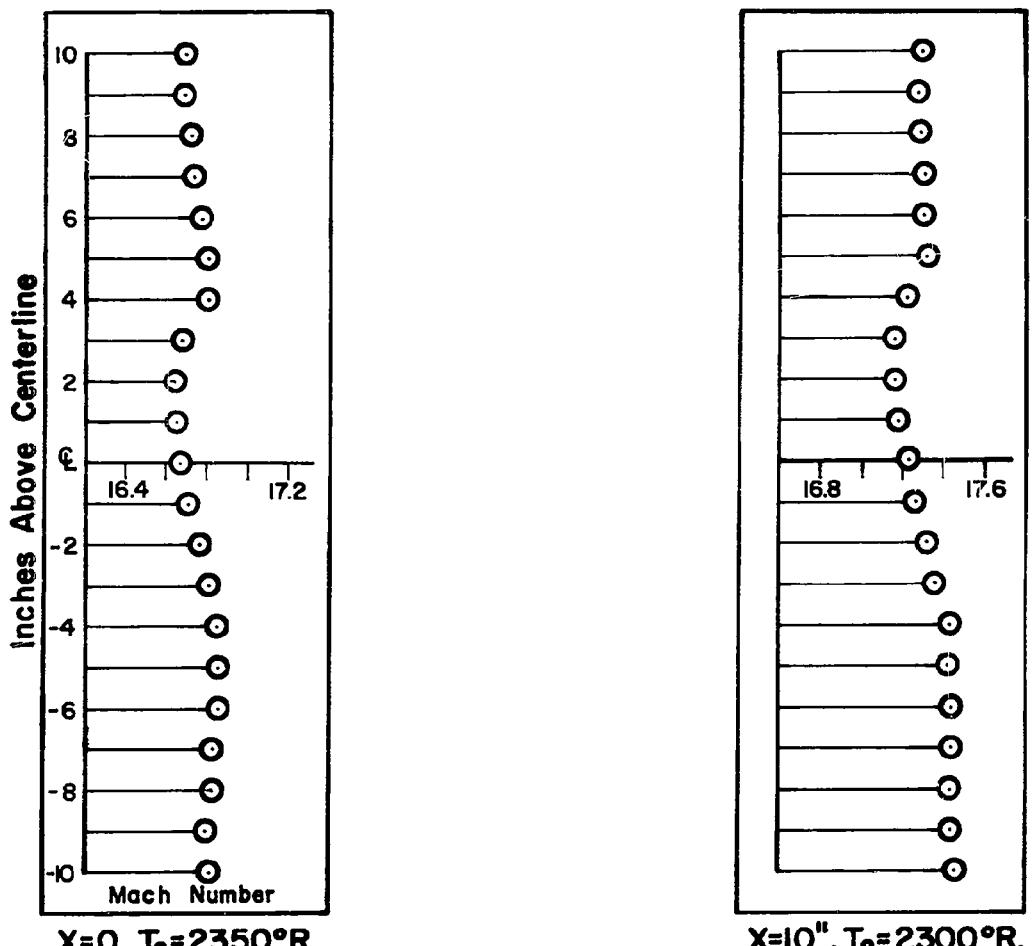

FIGURE 18-MACH NUMBER CALIBRATION OF THROAT NO. 2 AT P_o=1215 psia

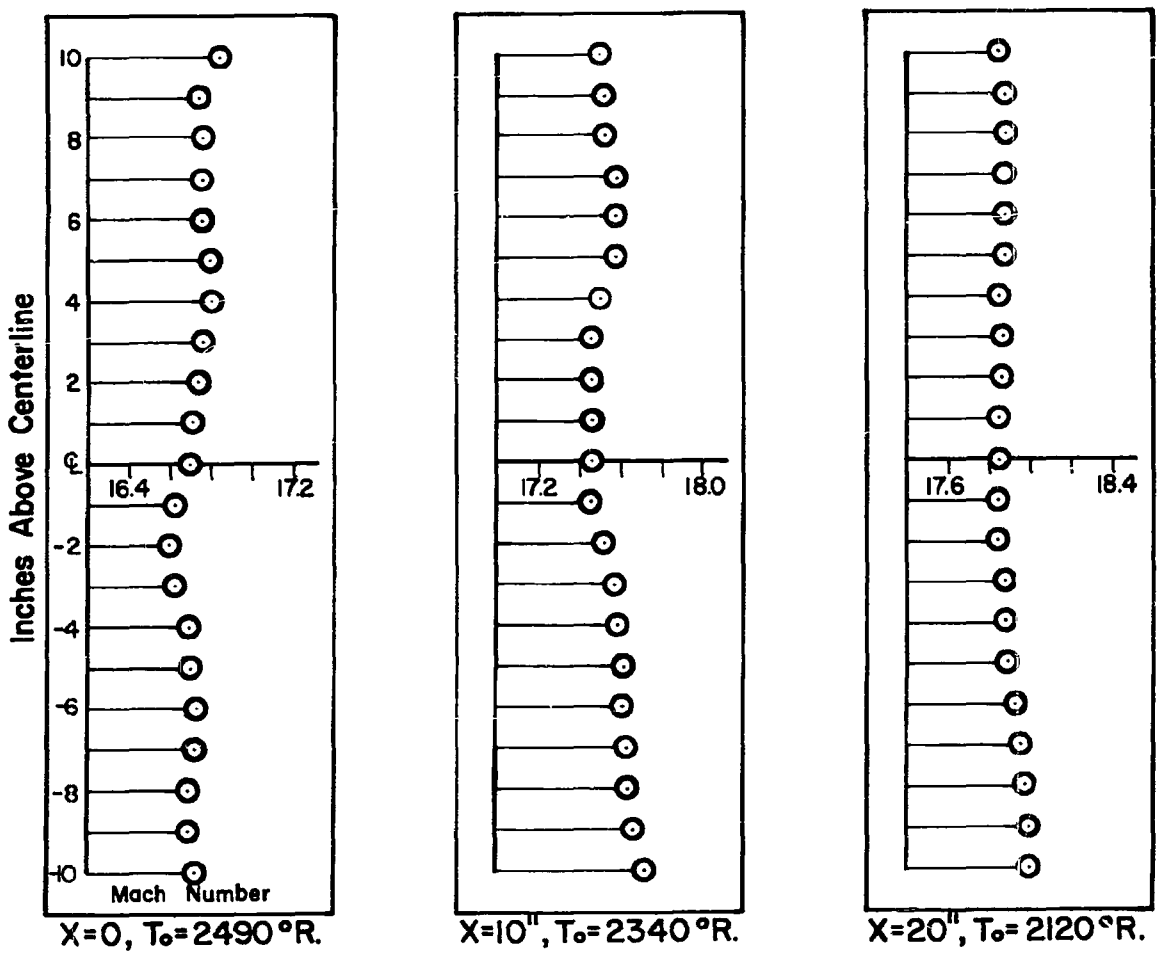

FIGURE 19- MACH NUMBER CALIBRATION OF THROAT NO.2 AT P_o=1015 psia

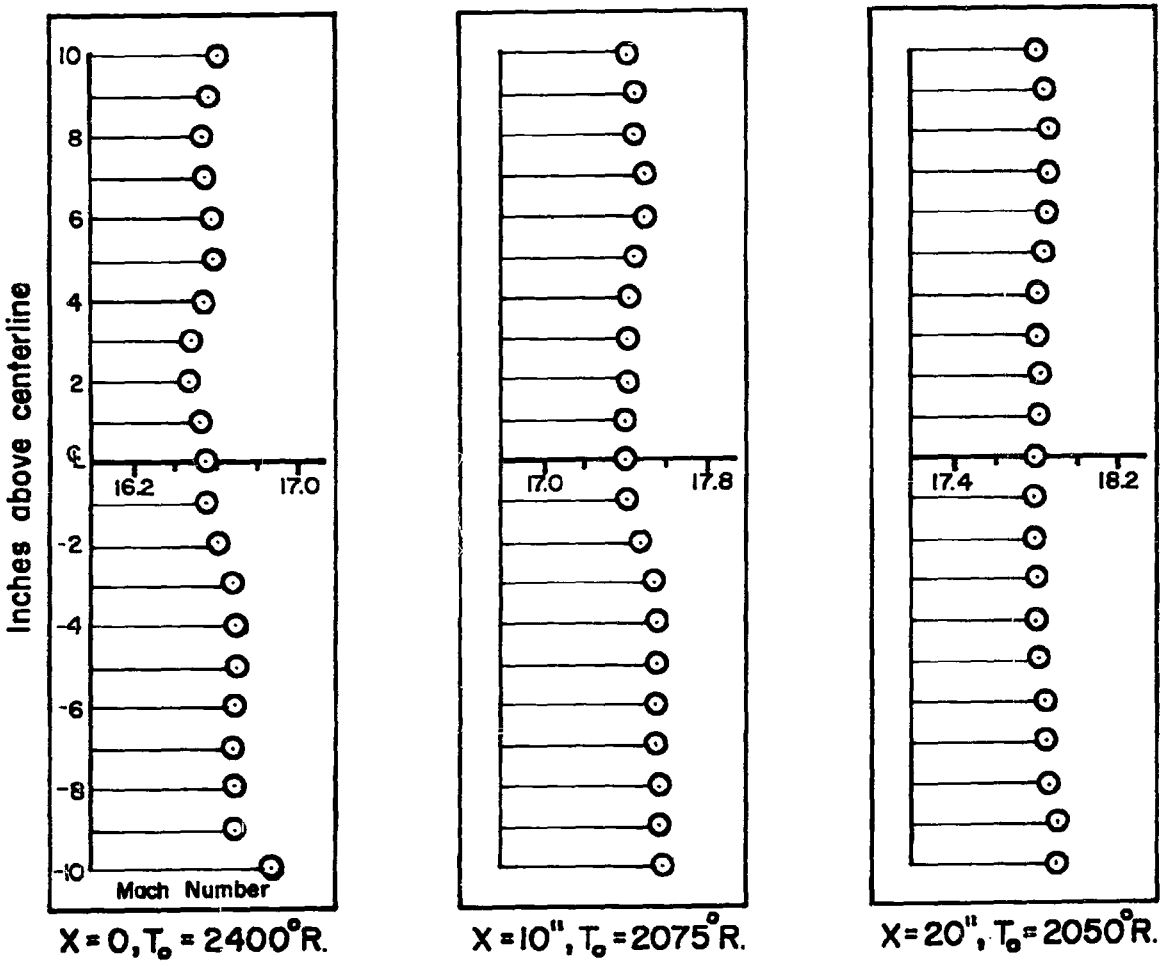

FIGURE 20–MACH NUMBER CALIBRATION OF THROAT NO. 2 AT P_o = 815 psia

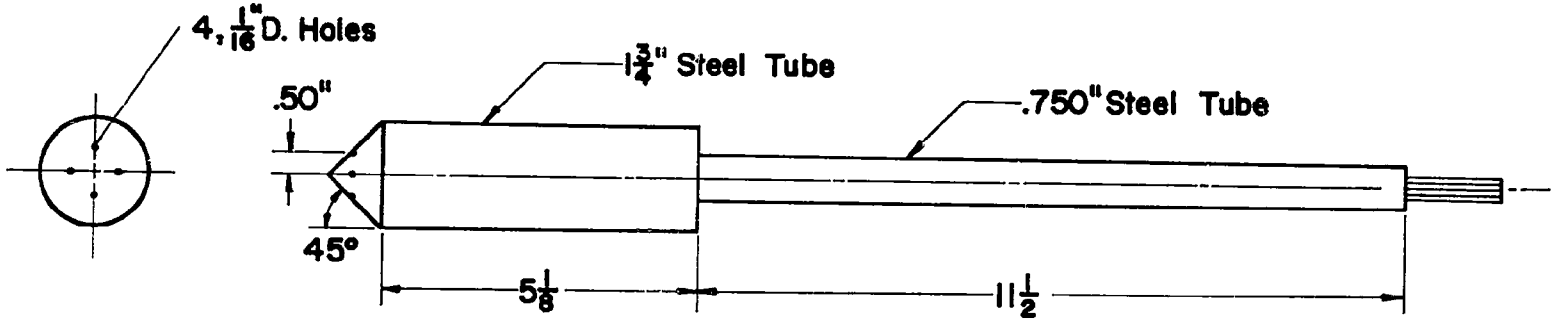

FIGURE 21 - ANGULARITY PROBE

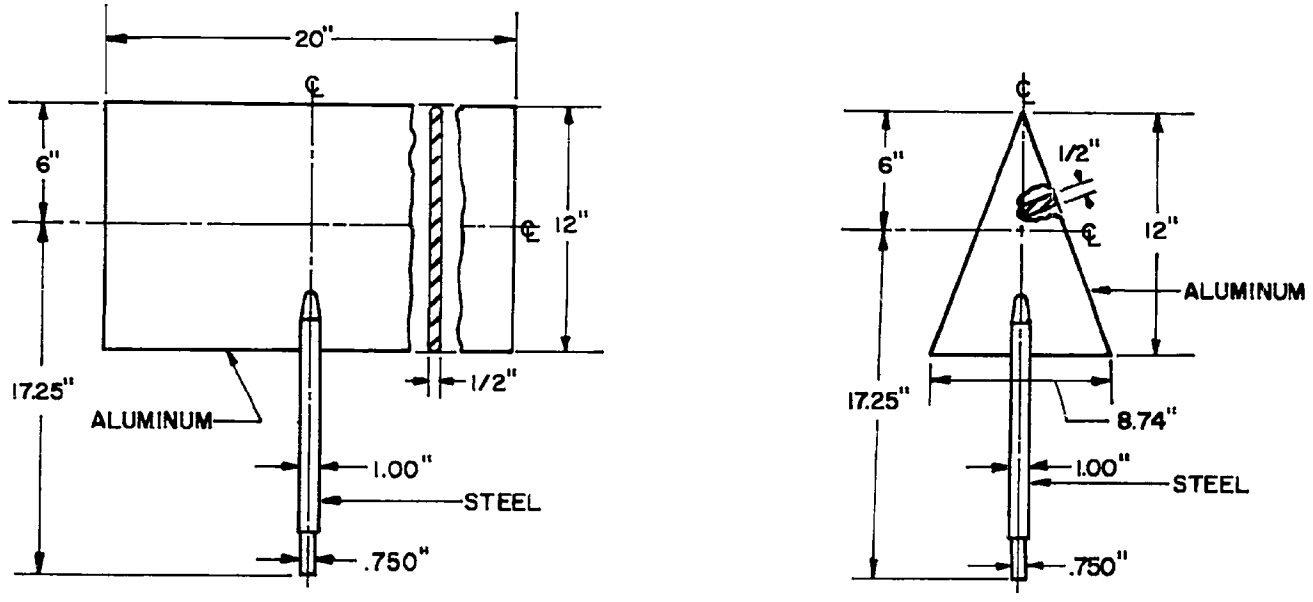

FIGURE 22-DIMENSIONS OF BLOCKAGE MODELS

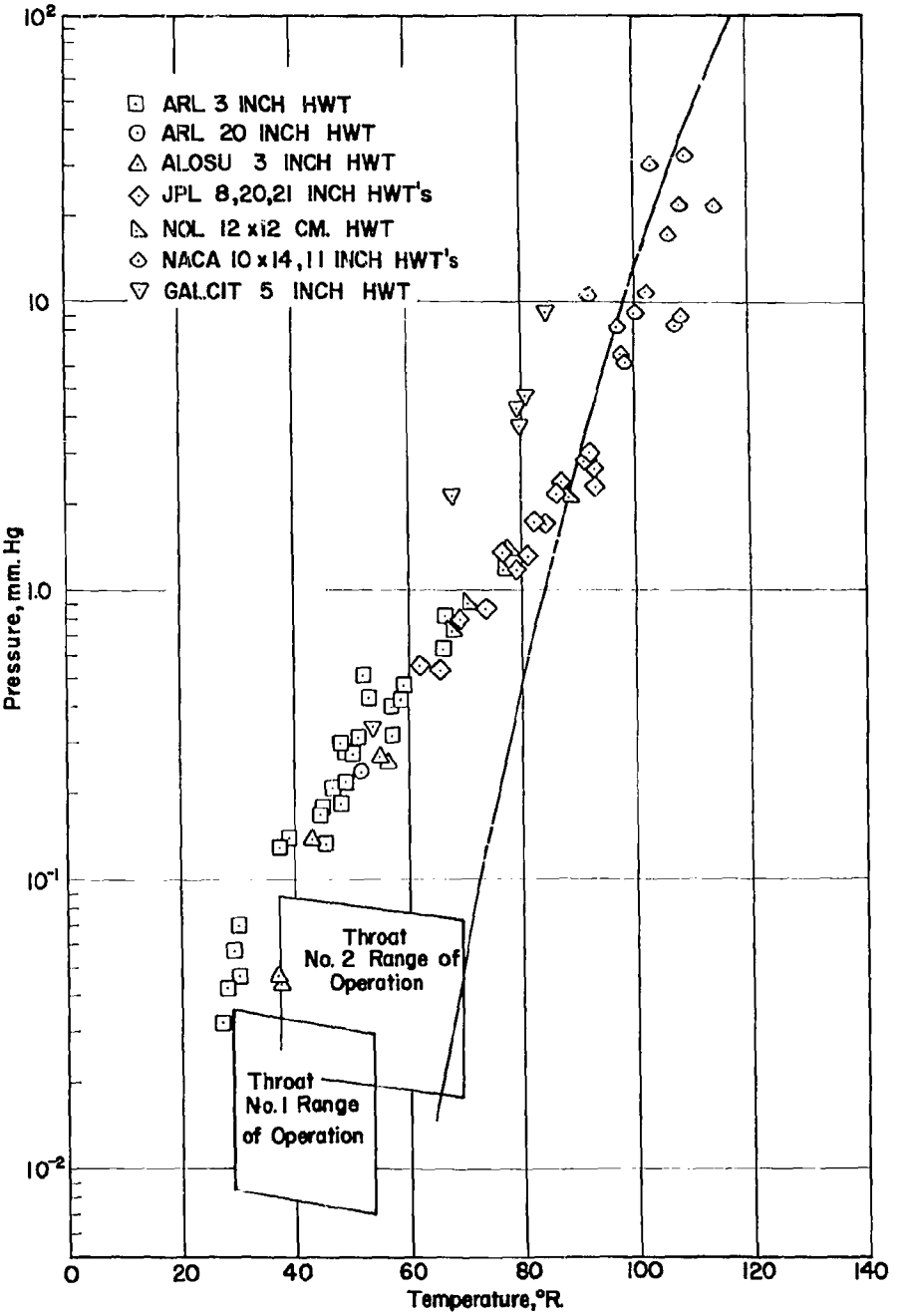

FIGURE 23 - OBSERVED CONDENSATION OF AIR IN HYPERSONIC WIND TUNNELS

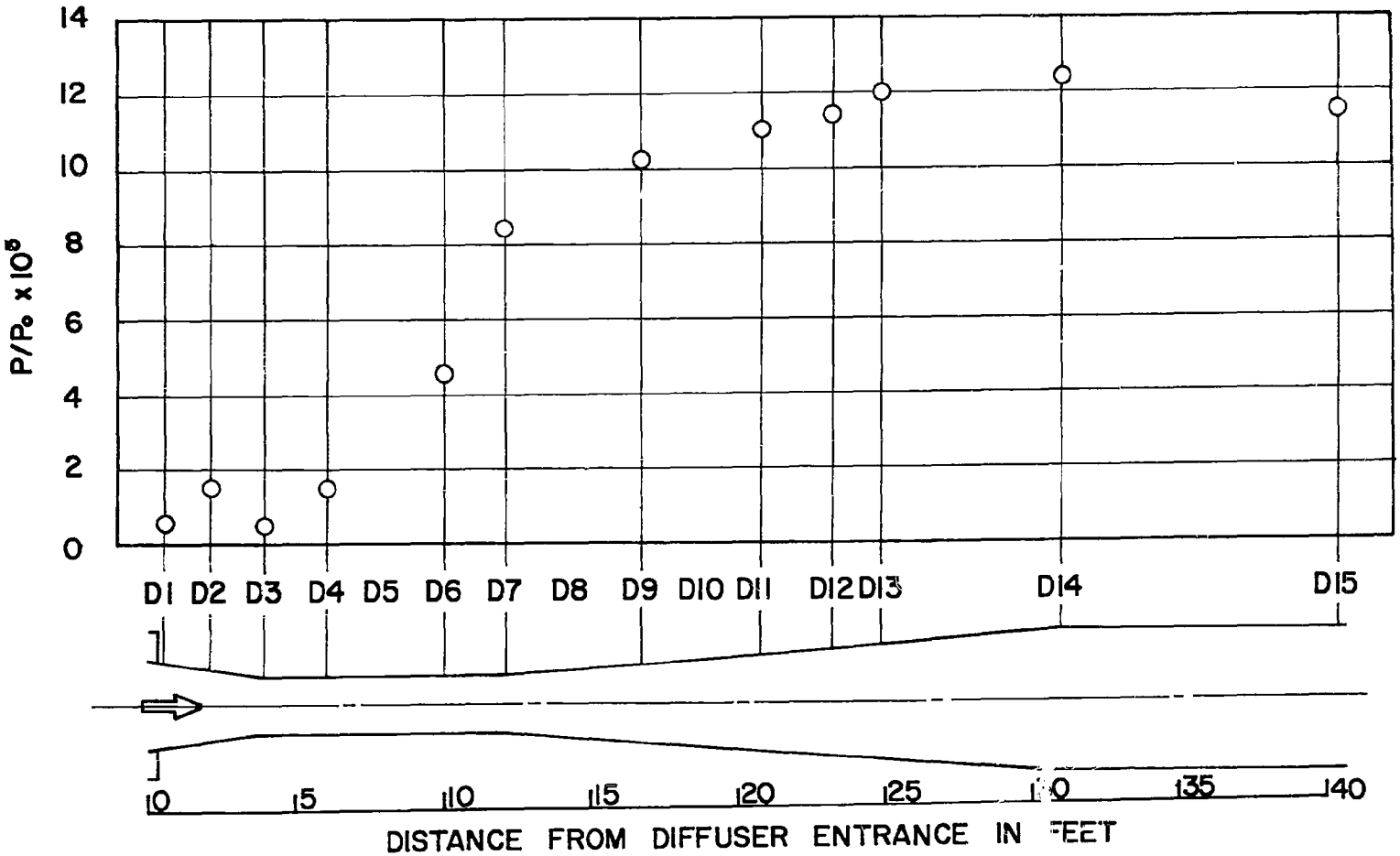

FIGURE 24 - DIFFUSER PRESSURE DISTRIBUTION

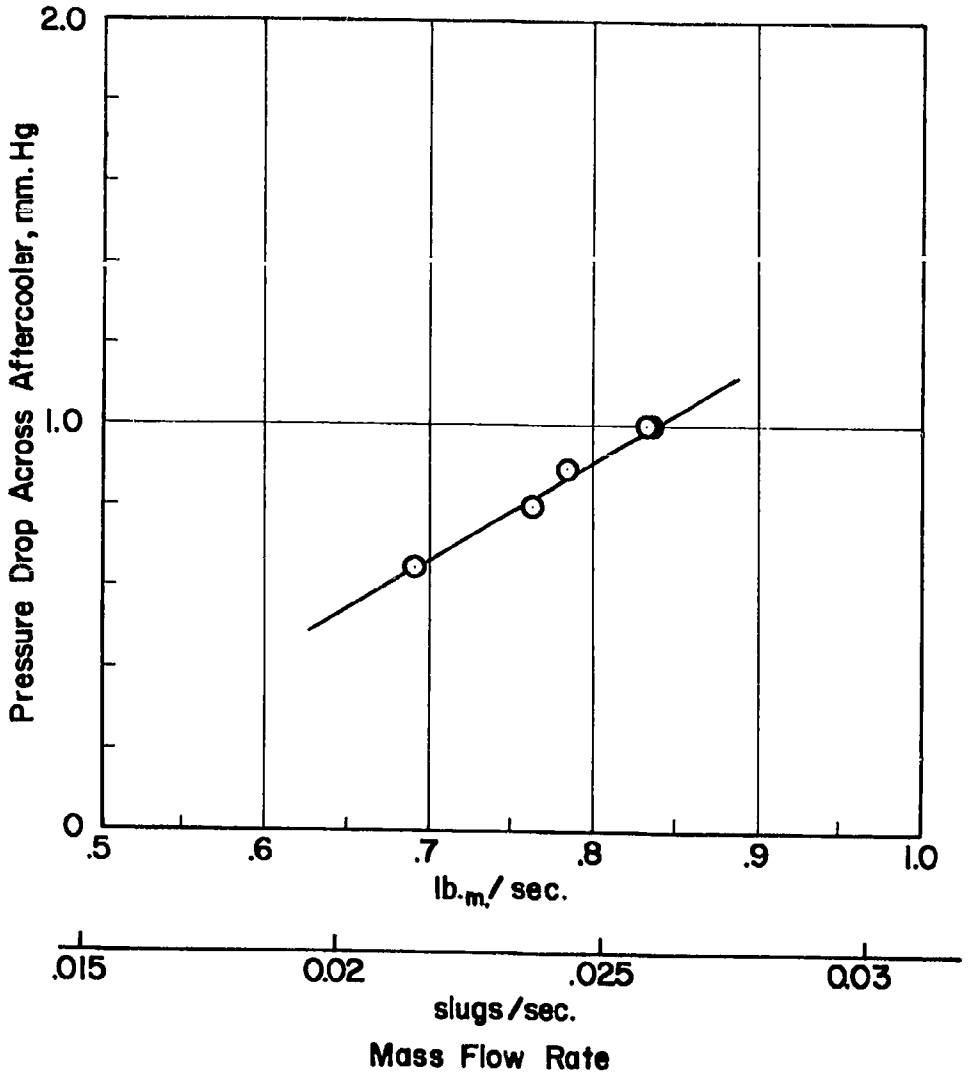

FIGURE 25-PRESSURE DROP ACROSS THE AFTERCOOLER

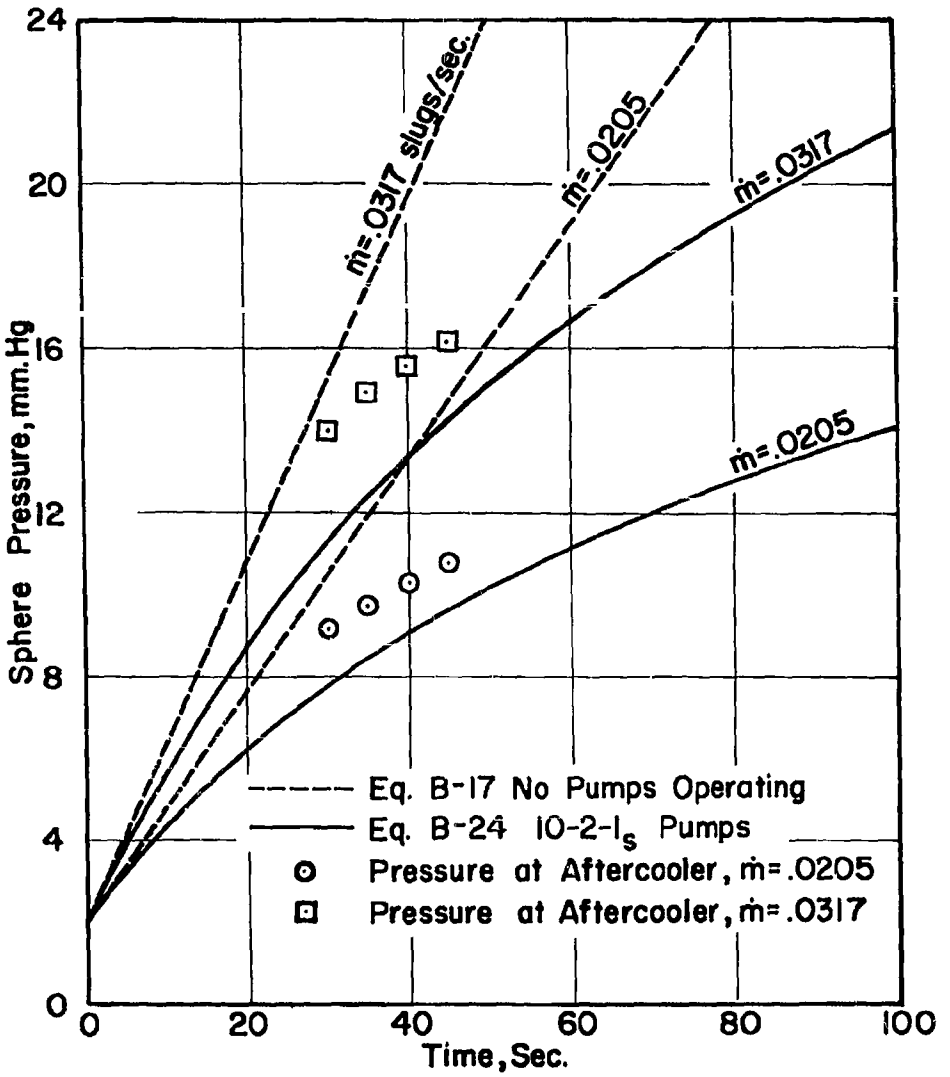

FIGURE 26-SPHERE PRESSURE vs. TIME DURING TUNNEL OPERATION

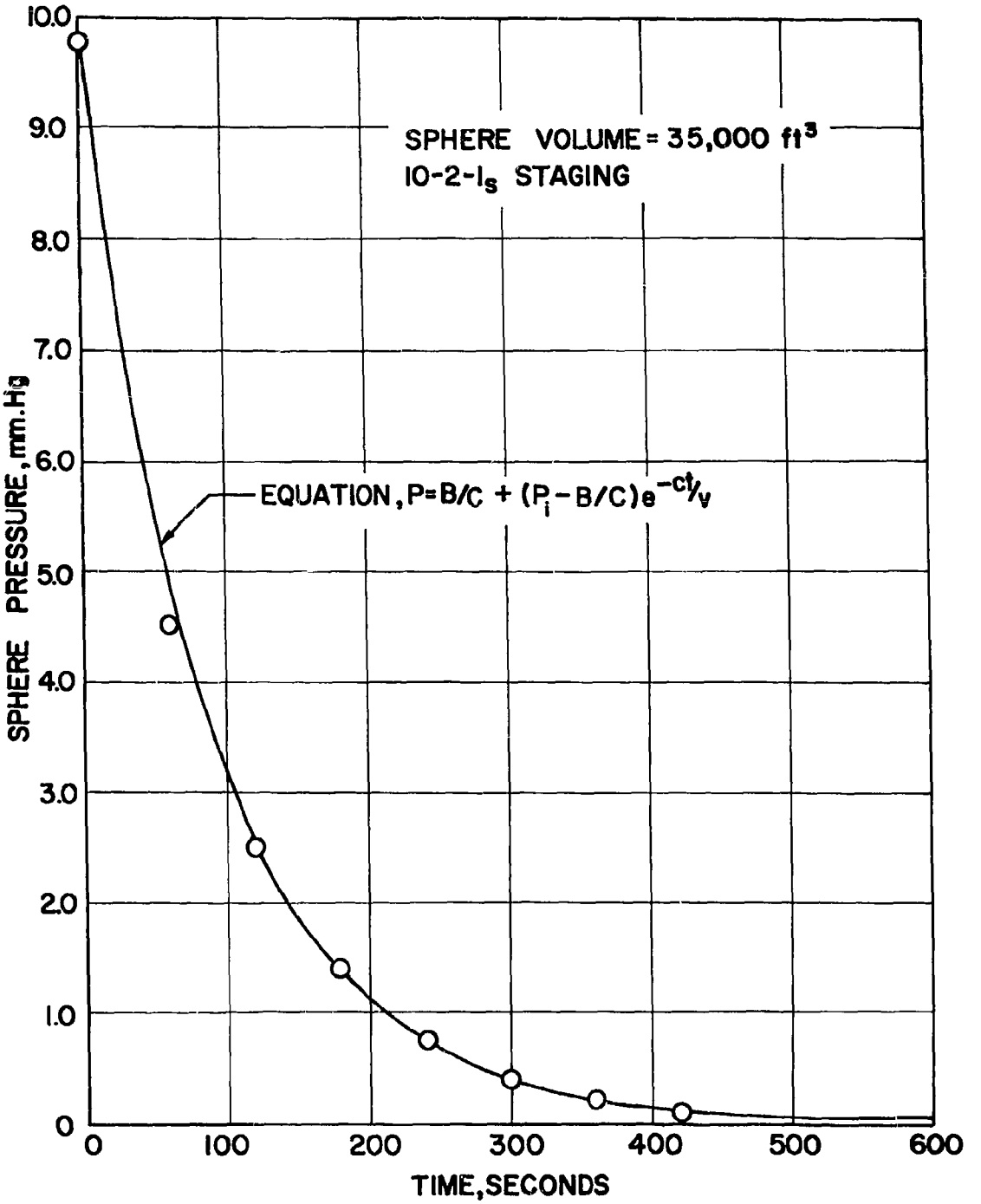

FIGURE 27 - EXPERIMENTAL EVACUATION RATE OF SPHERE

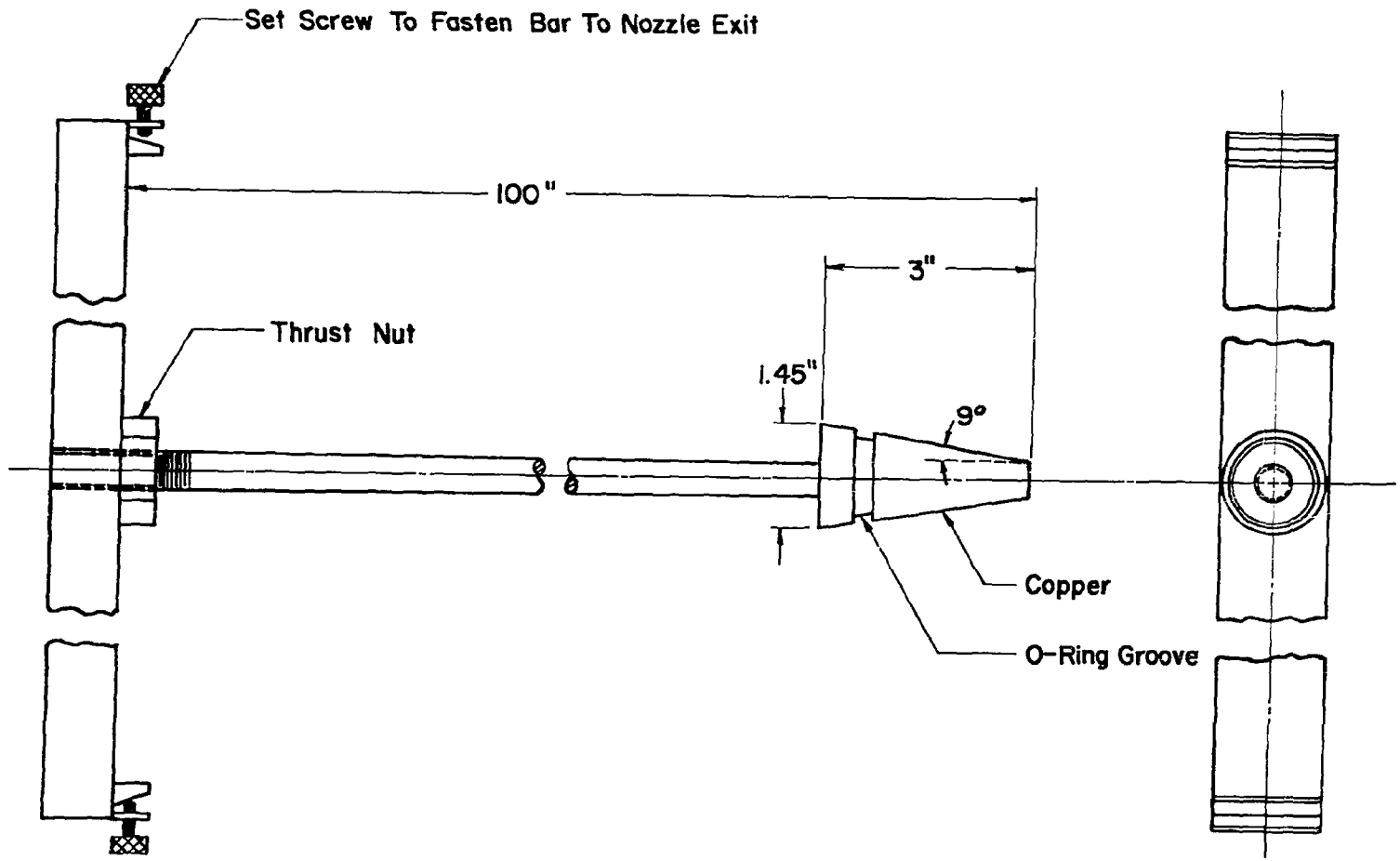

FIGURE 28 - NOZZLE PLUG DIMENSIONS

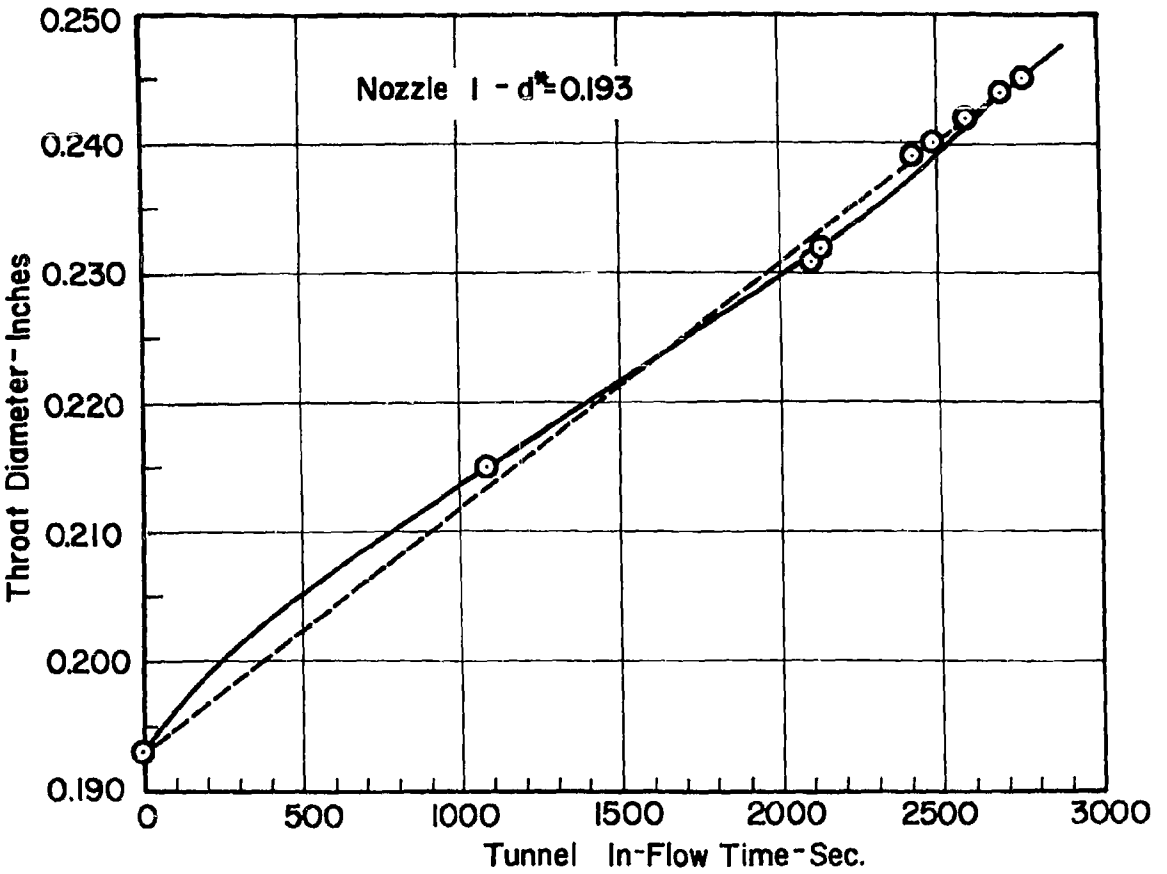

FIGURE 29 - NOZZLE THROAT GROWTH WITH ACCUMULATED TIME

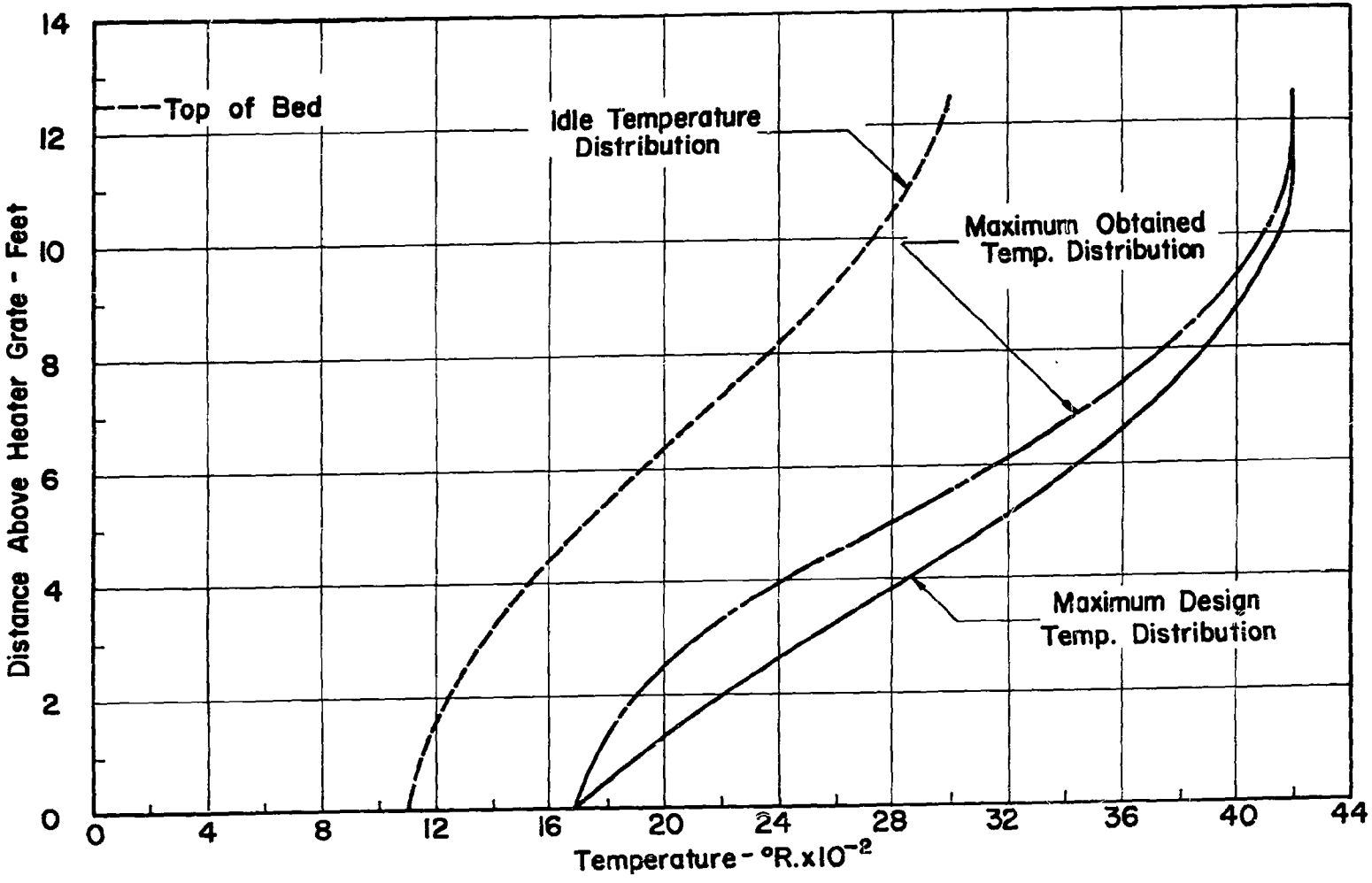

FIGURE 30 - BED TEMPERATURE DISTRIBUTION

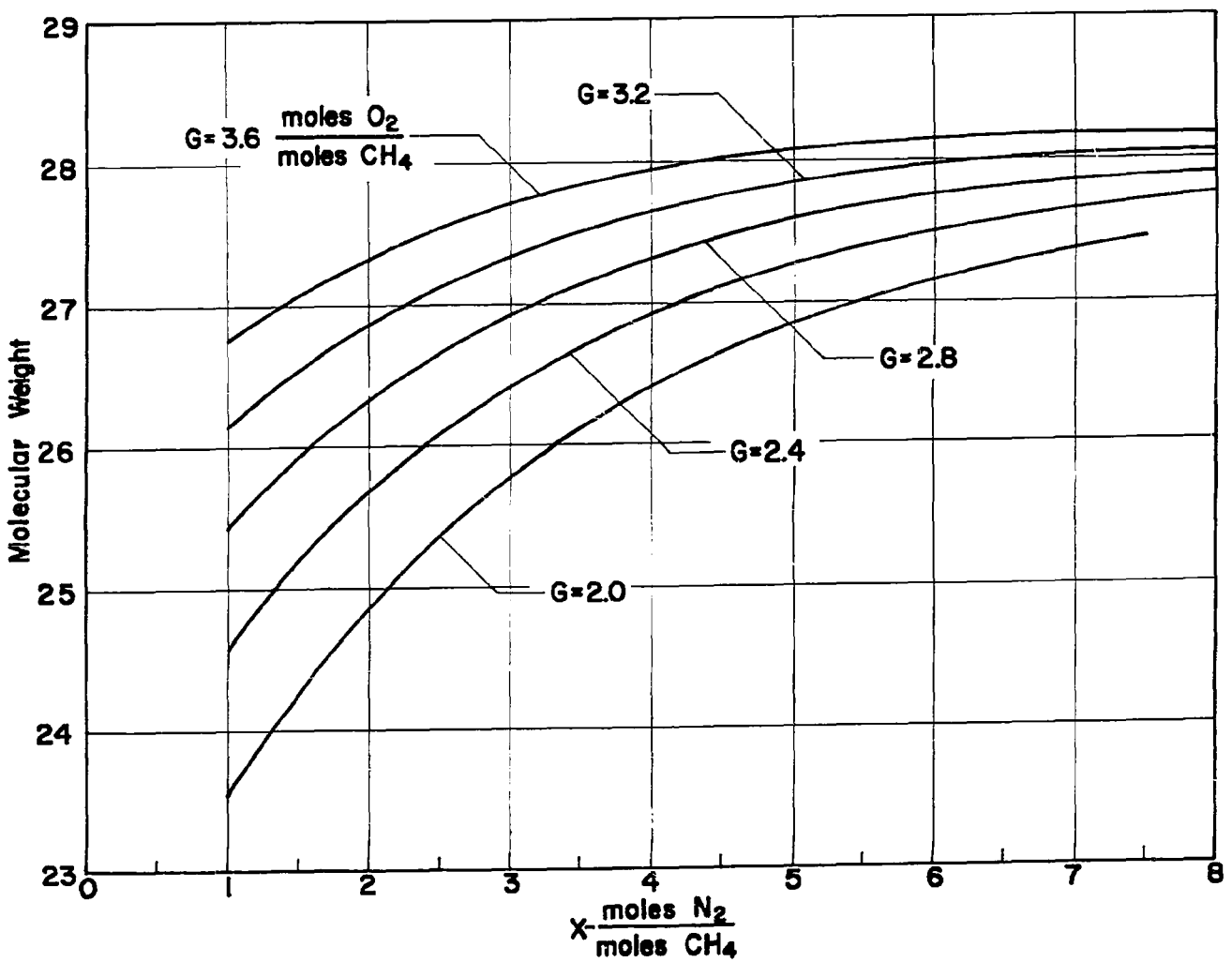

FIGURE 31 - MOLECULAR WEIGHT vs. $\frac{\text{moles } N_2}{\text{moles } CH_4}$

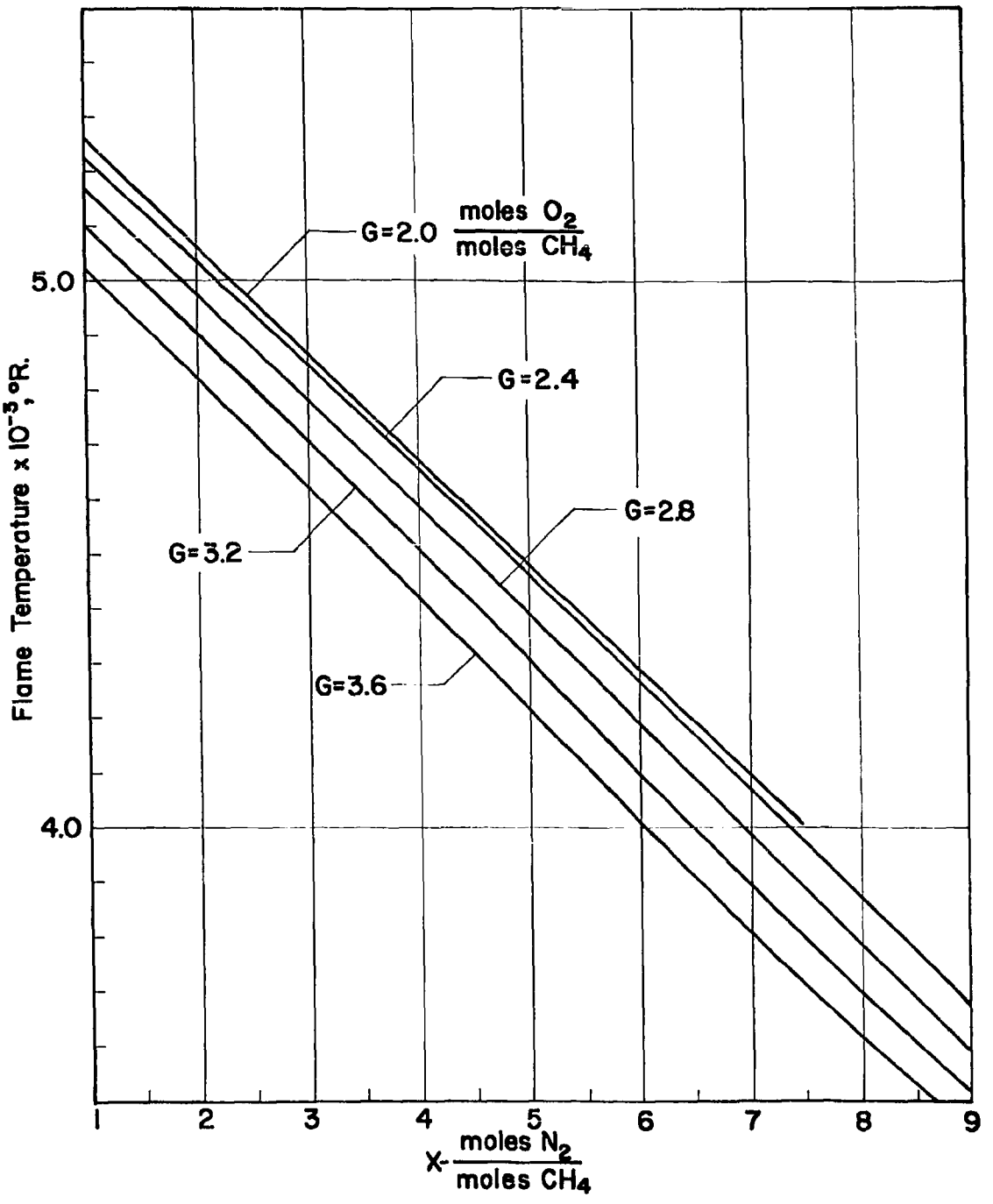

FIGURE 32-FLAME TEMPERATURE vs. $\frac{\text{moles } N_2}{\text{moles } CH_4}$

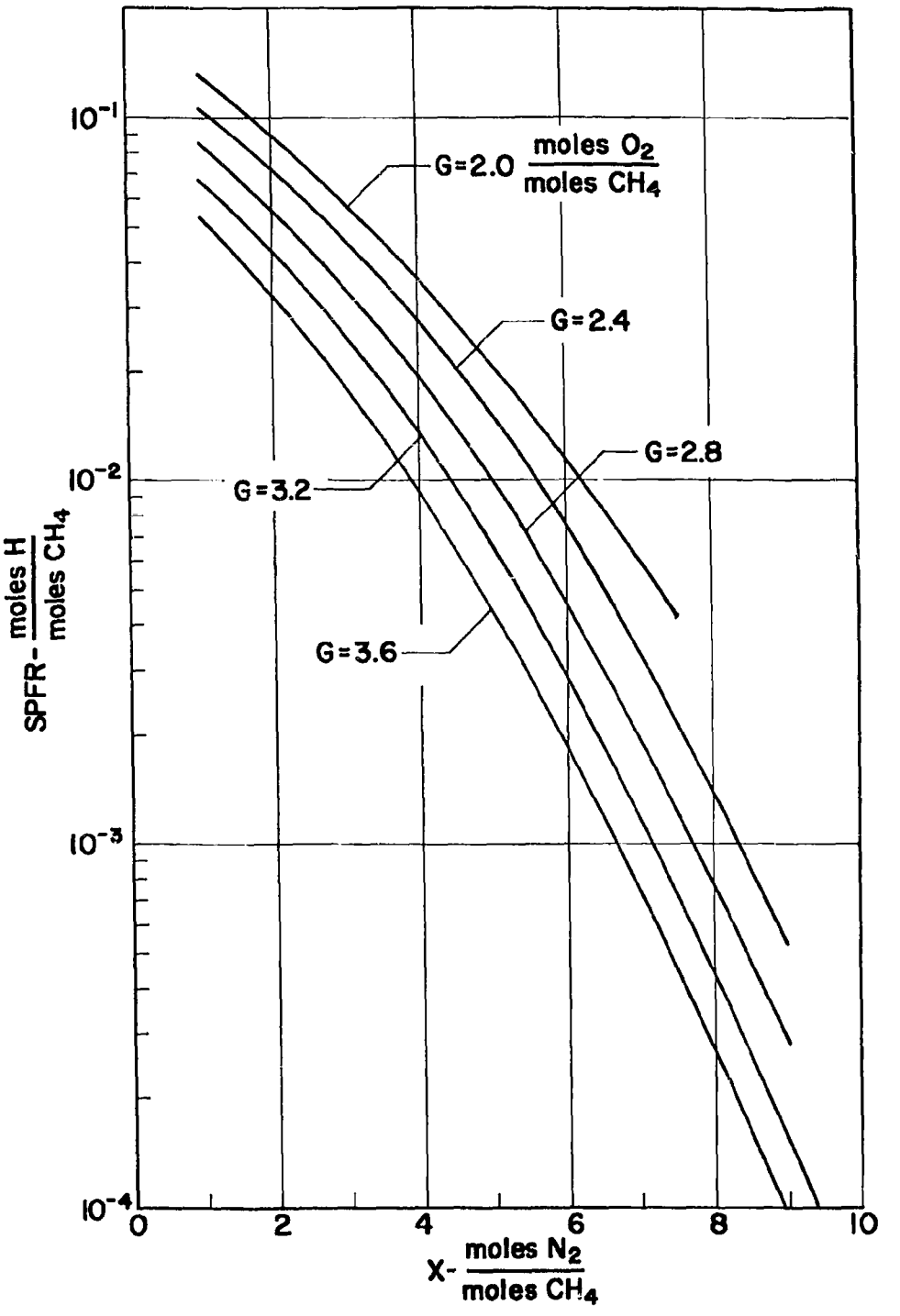

FIGURE 33 - SPFR OF H vs. $\frac{\text{moles } N_2}{\text{moles } CH_4}$

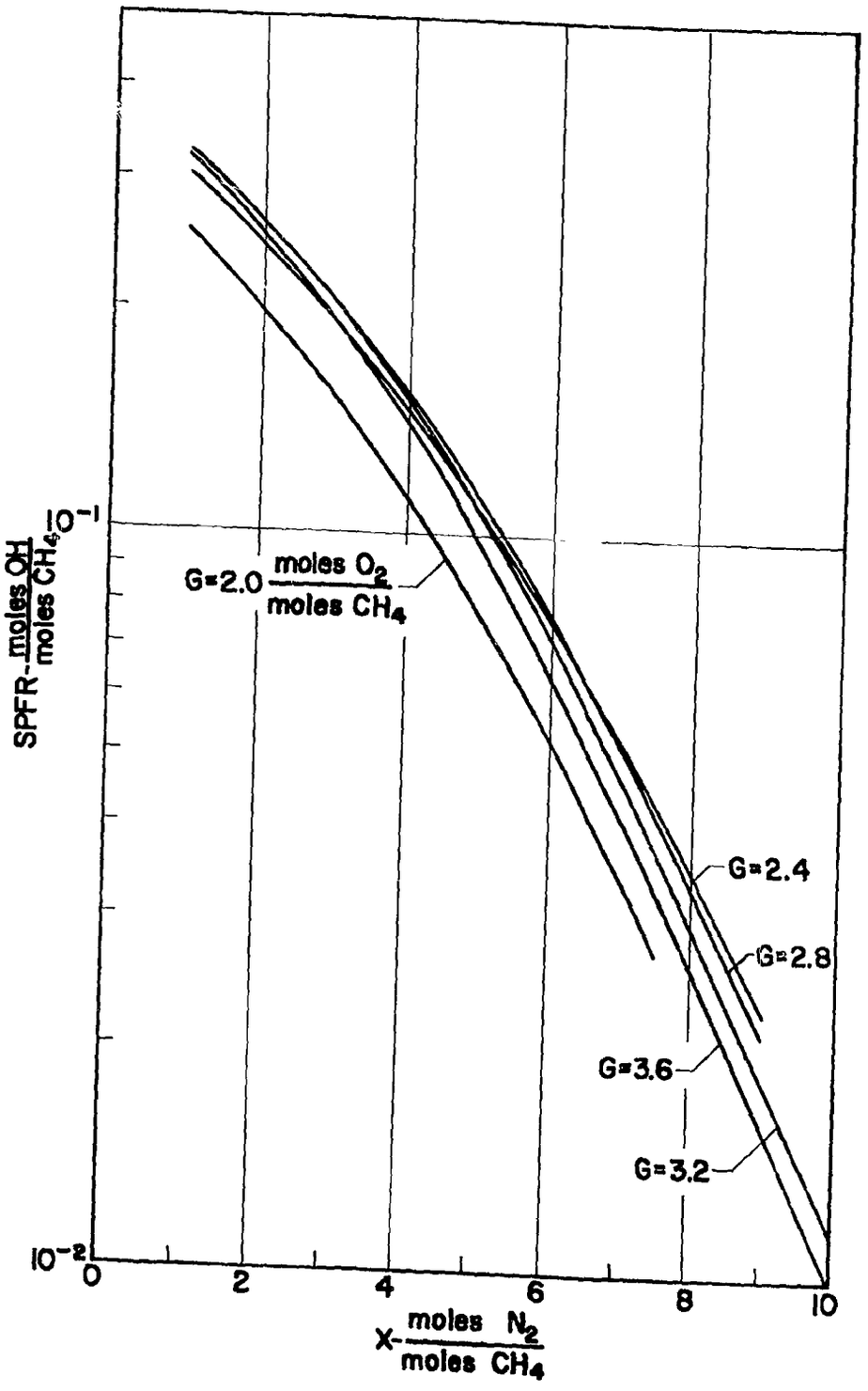

FIGURE 34-SPFR OF OH vs. $\frac{\text{moles } N_2}{\text{moles } CH_4}$

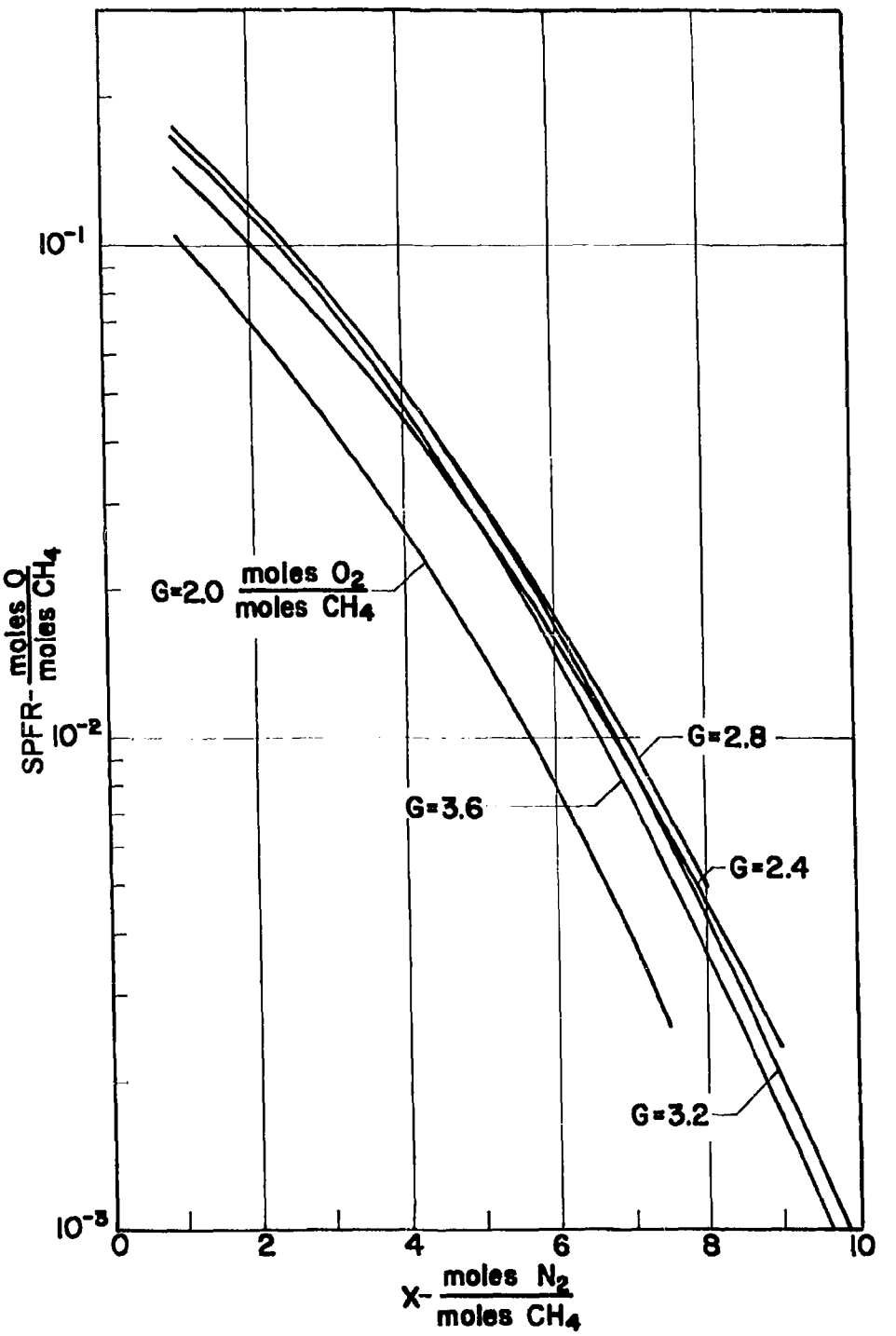

FIGURE 35-SPFR OF O vs. $\frac{\text{moles } N_2}{\text{moles } CH_4}$

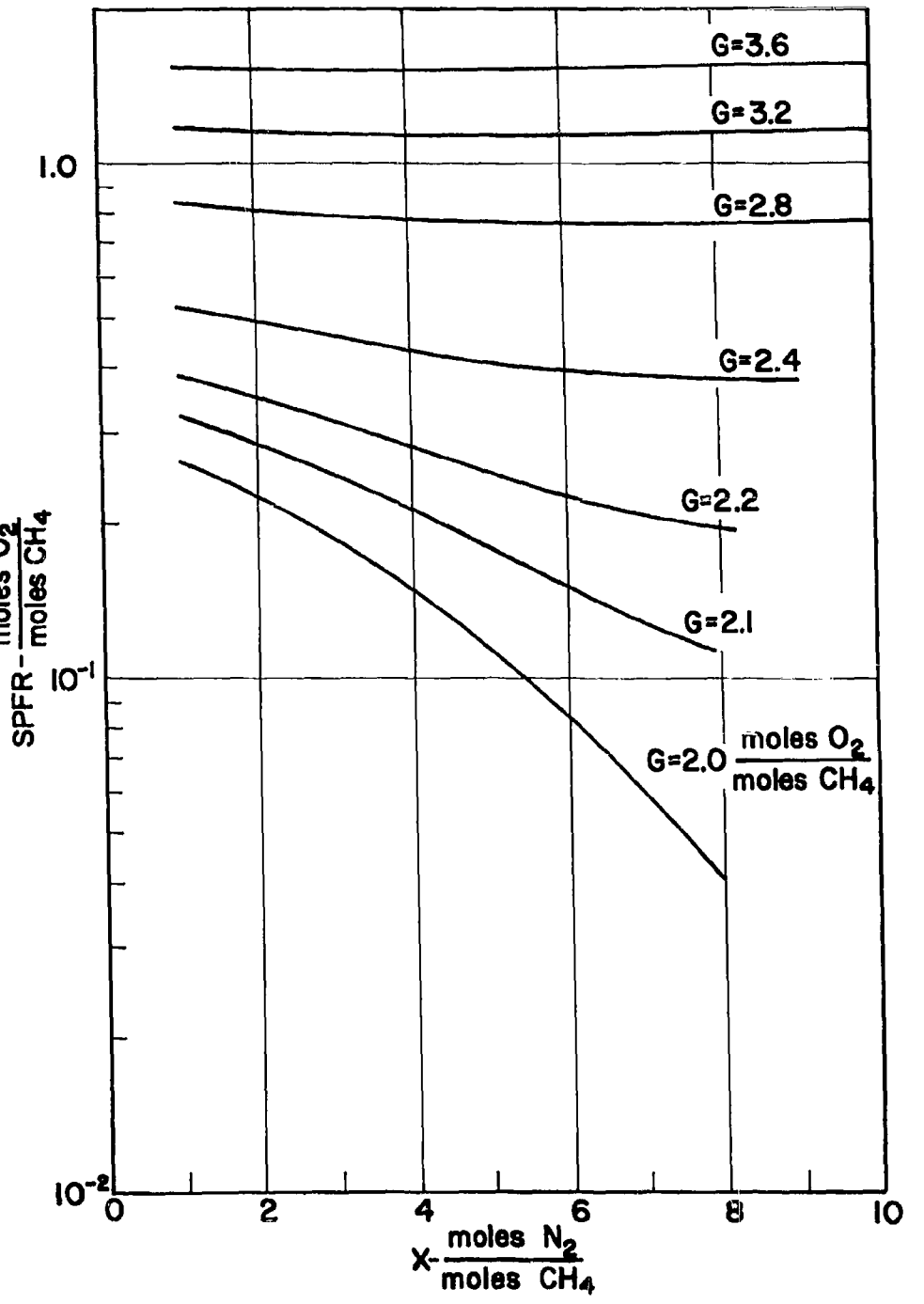

FIGURE 36-SPFR OF O_2 vs. $\frac{\text{moles } N_2}{\text{moles } CH_4}$

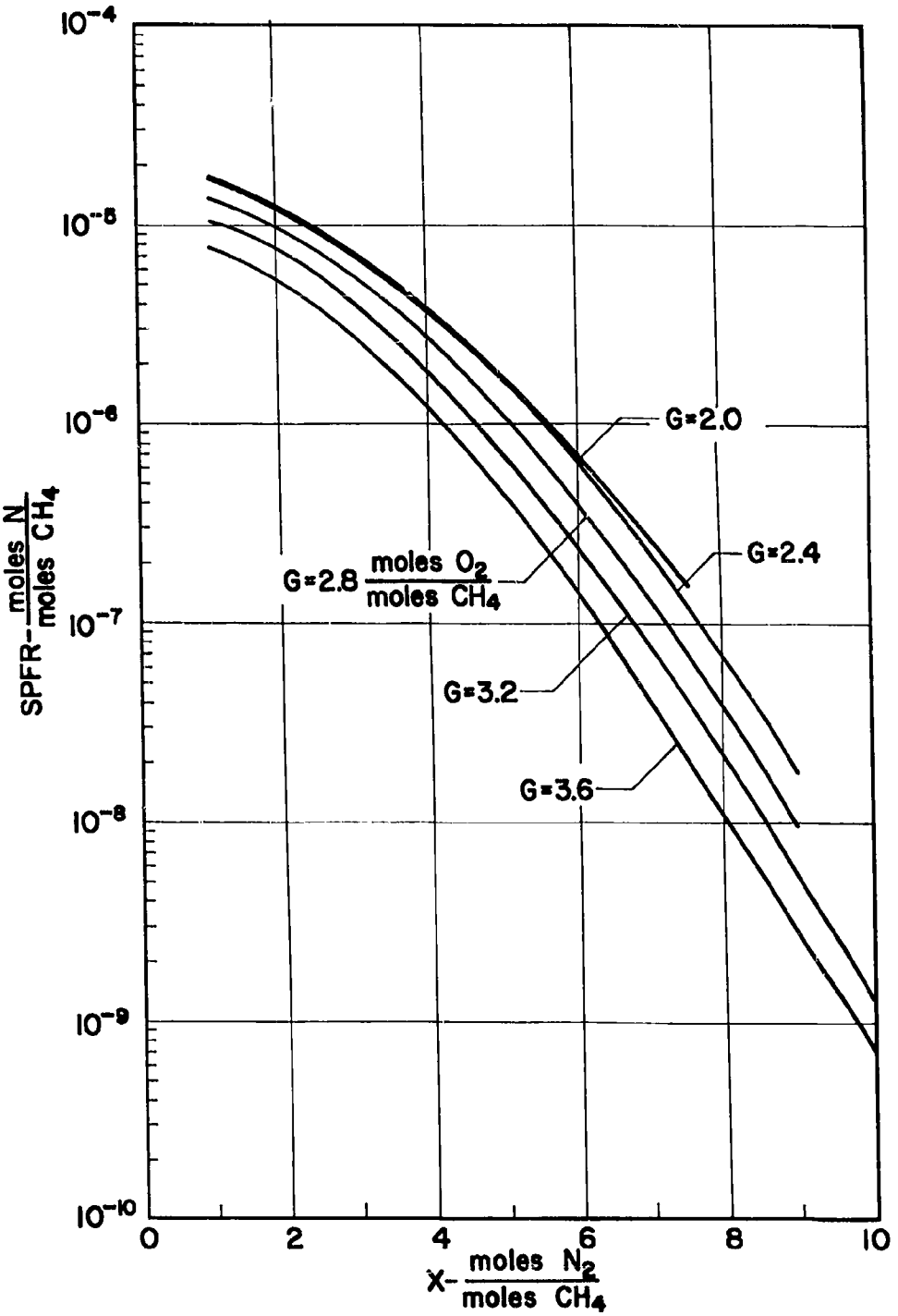

FIGURE 37 - SPFR OF N vs. $\frac{\text{moles } N_2}{\text{moles } CH_4}$

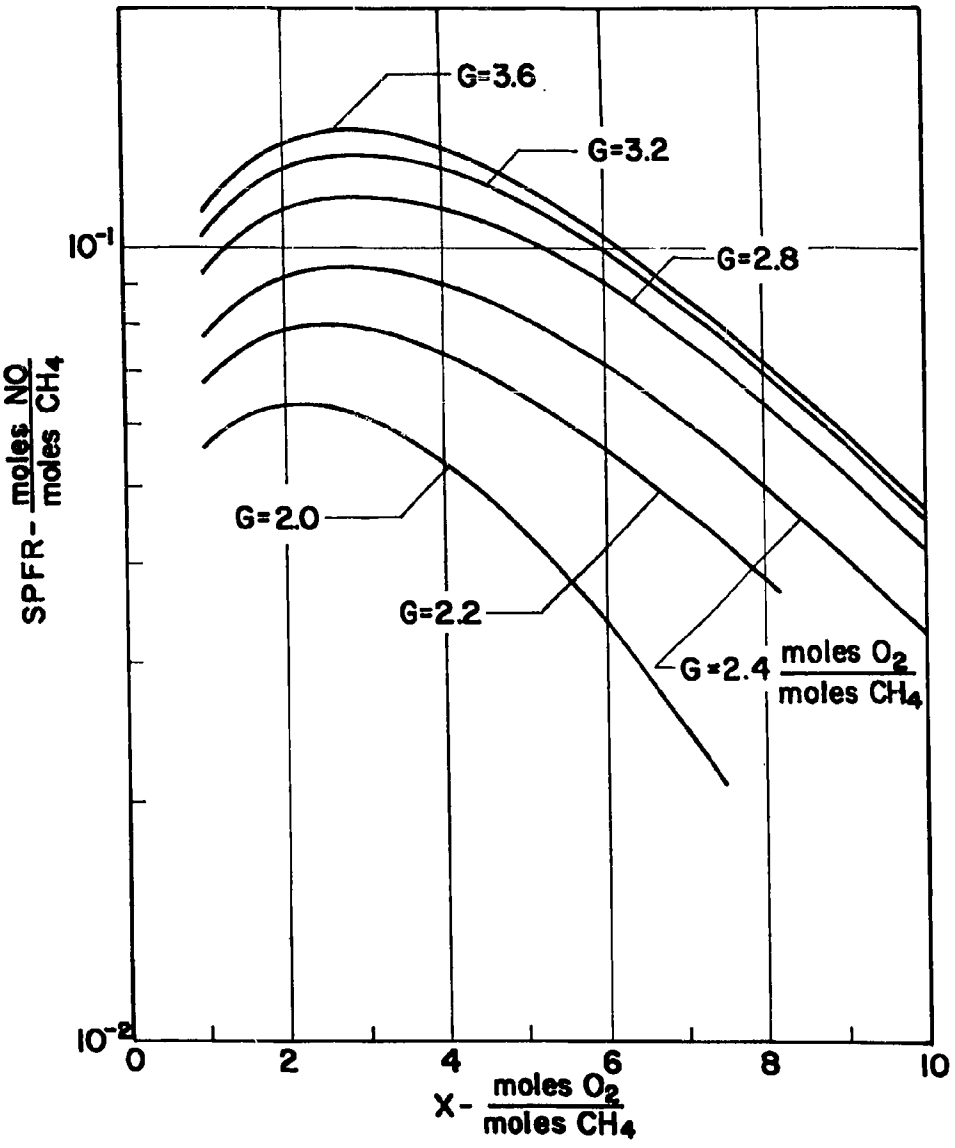

FIGURE 38 - SPFR OF NO vs. $\frac{\text{moles } N_2}{\text{moles } CH_4}$

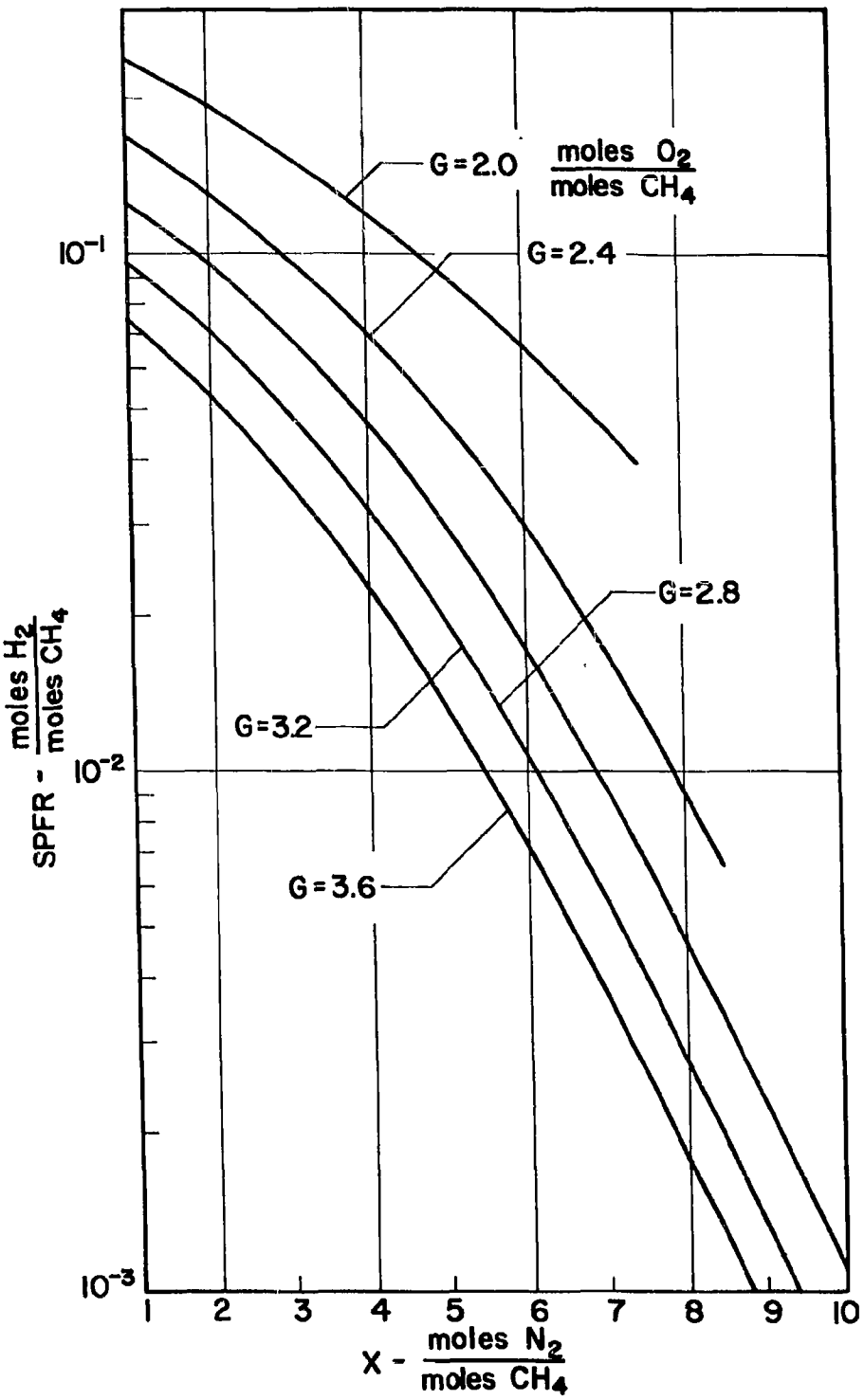

FIGURE 39- SPFR OF H_2 vs. $\frac{\text{moles } N_2}{\text{moles } CH_4}$

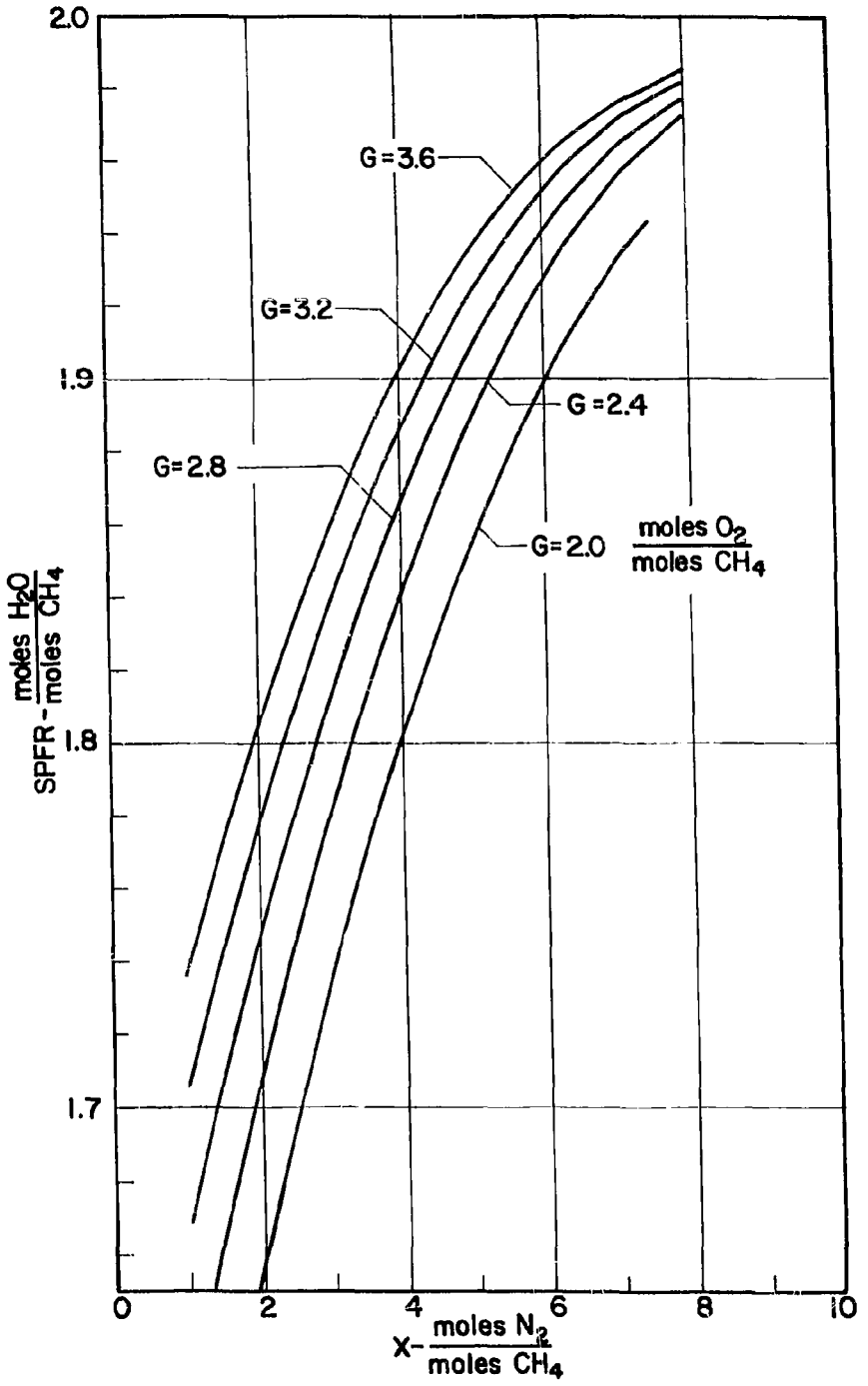

FIGURE 40-SPFR OF H_2O vs. $\frac{\text{moles } N_2}{\text{moles } CH_4}$

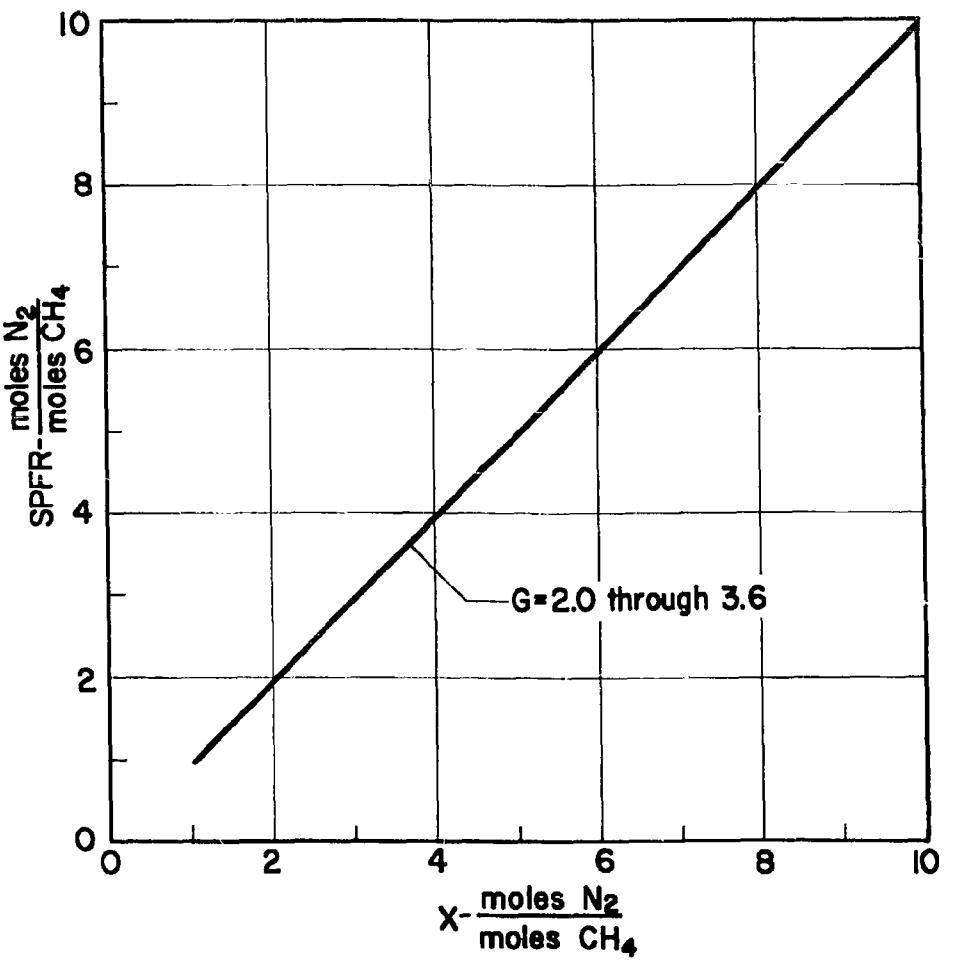

FIGURE 41 - SPFR OF N_2 vs. $\frac{\text{moles } N_2}{\text{moles } CH_4}$

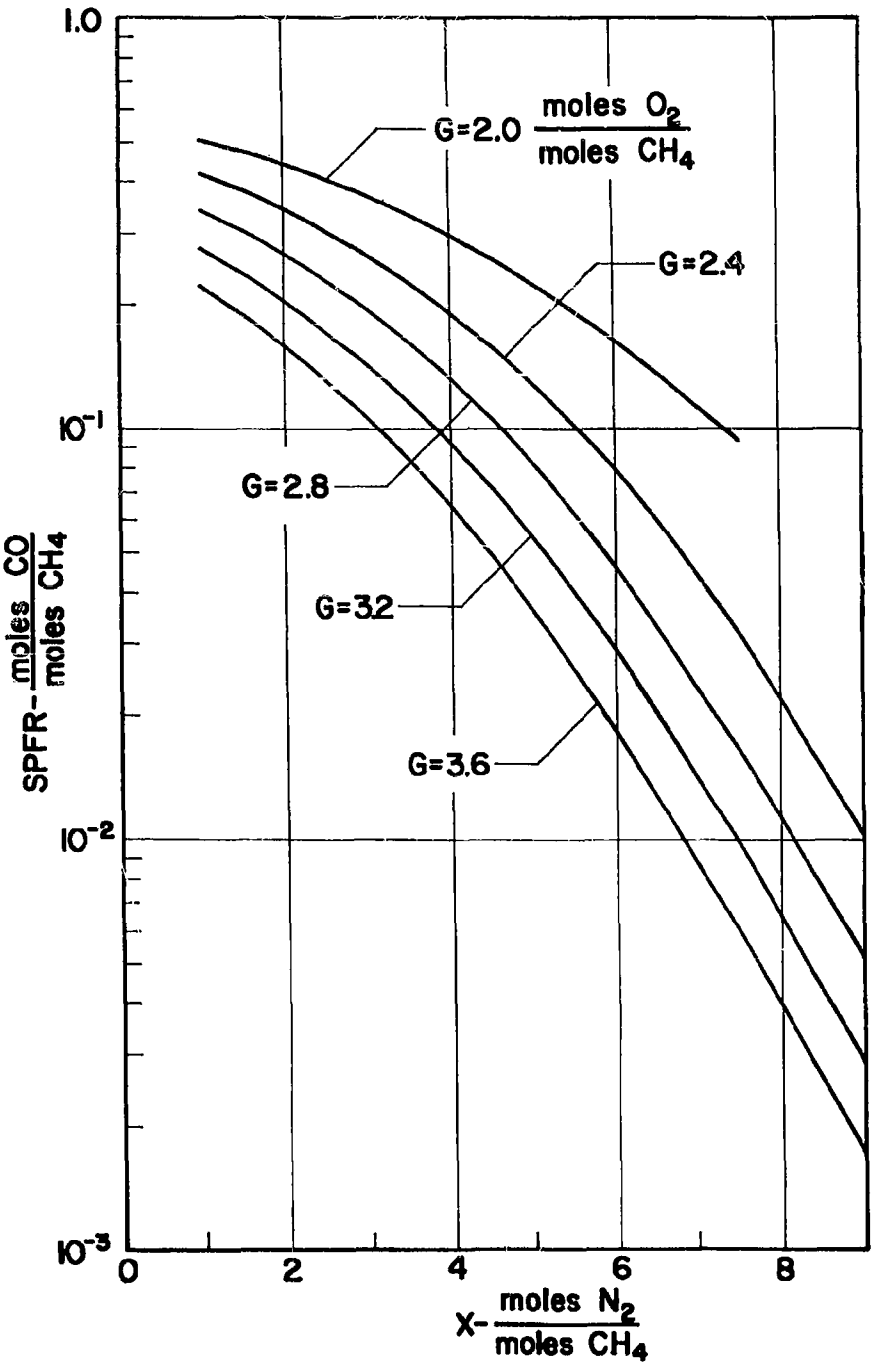

FIGURE 42-SPFR OF CO vs. $\frac{\text{moles } N_2}{\text{moles } CH_4}$

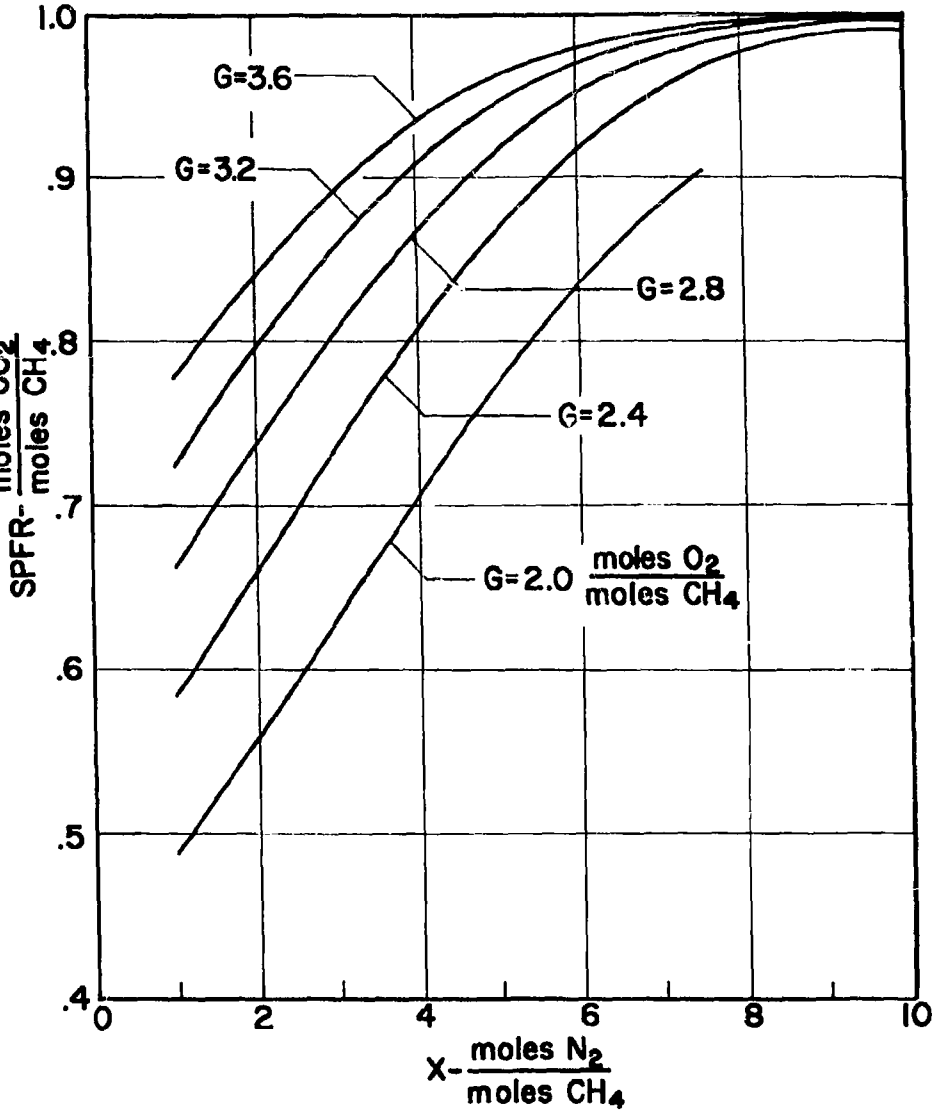

FIGURE 43-SPFR OF CO_2 vs. $\frac{\text{moles } N_2}{\text{moles } CH_4}$

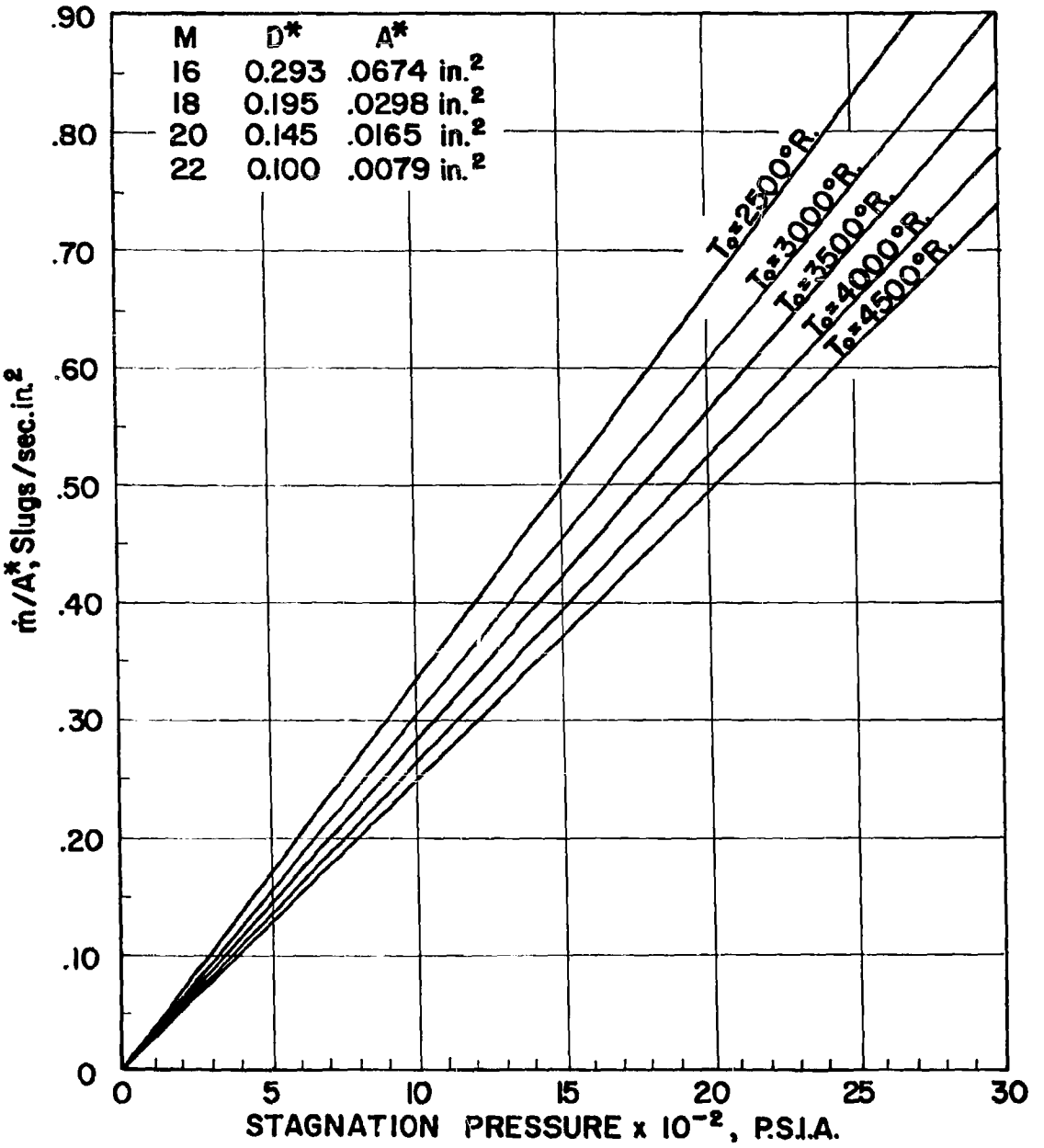

FIGURE 44-MASS FLOW RATE OF 30" HYPERSONIC WIND TUNNEL

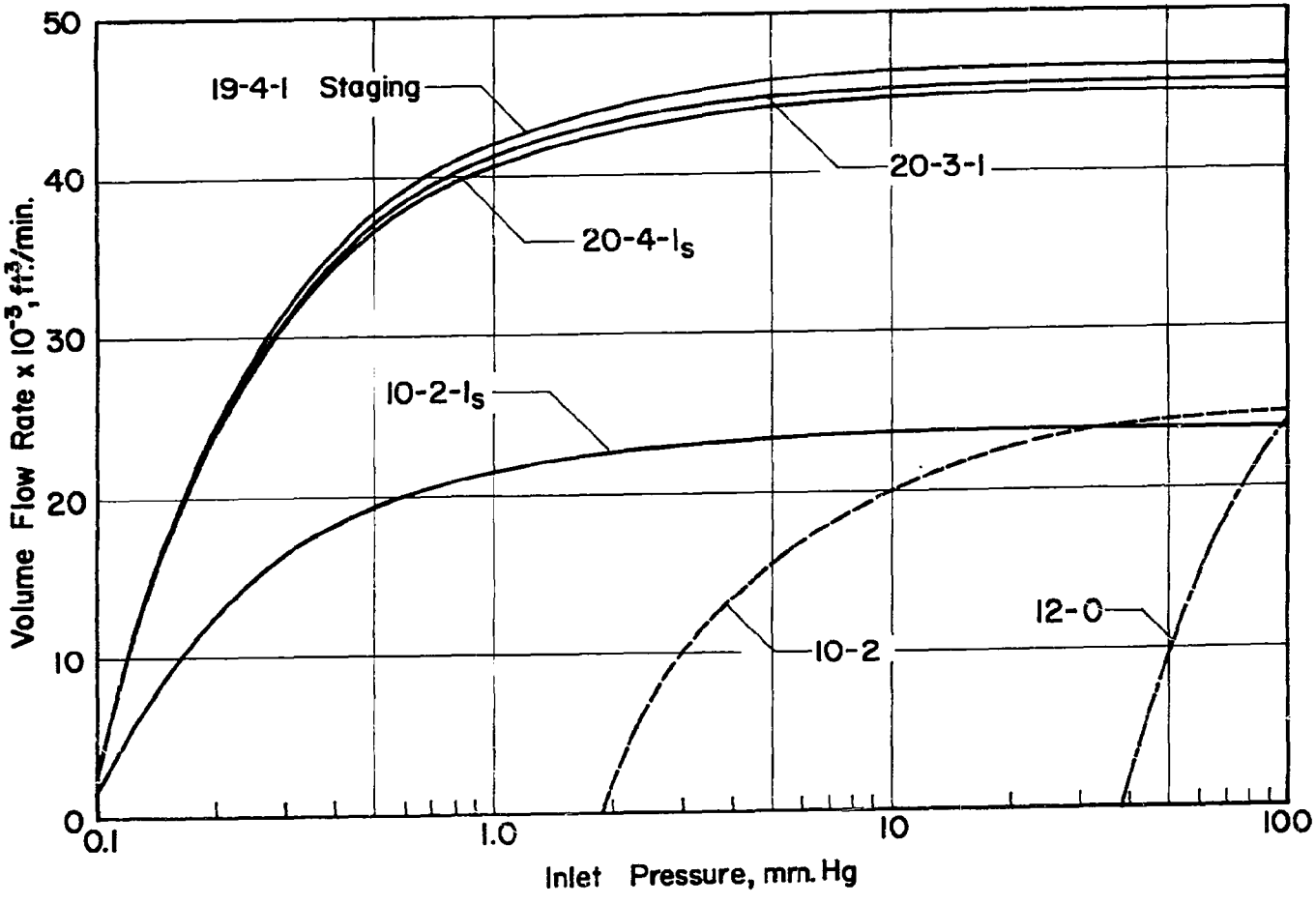

FIGURE 45 - VOLUME FLOW RATE FOR VARIOUS STAGING COMBINATIONS

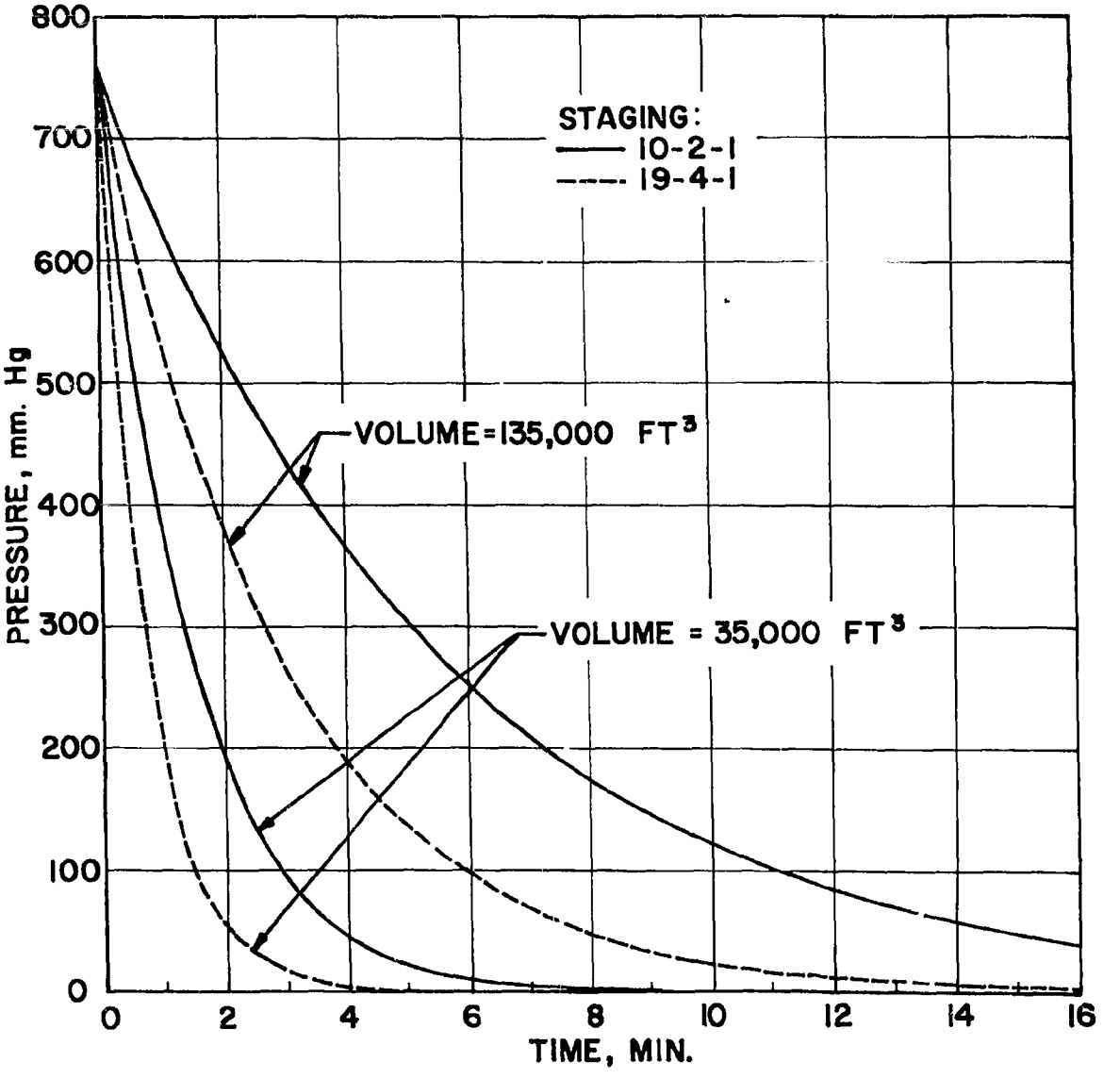

FIGURE 46-EVACUATION RATE FROM ATMOSPHERE FOR SPHERES AT VARIOUS STAGINGS.

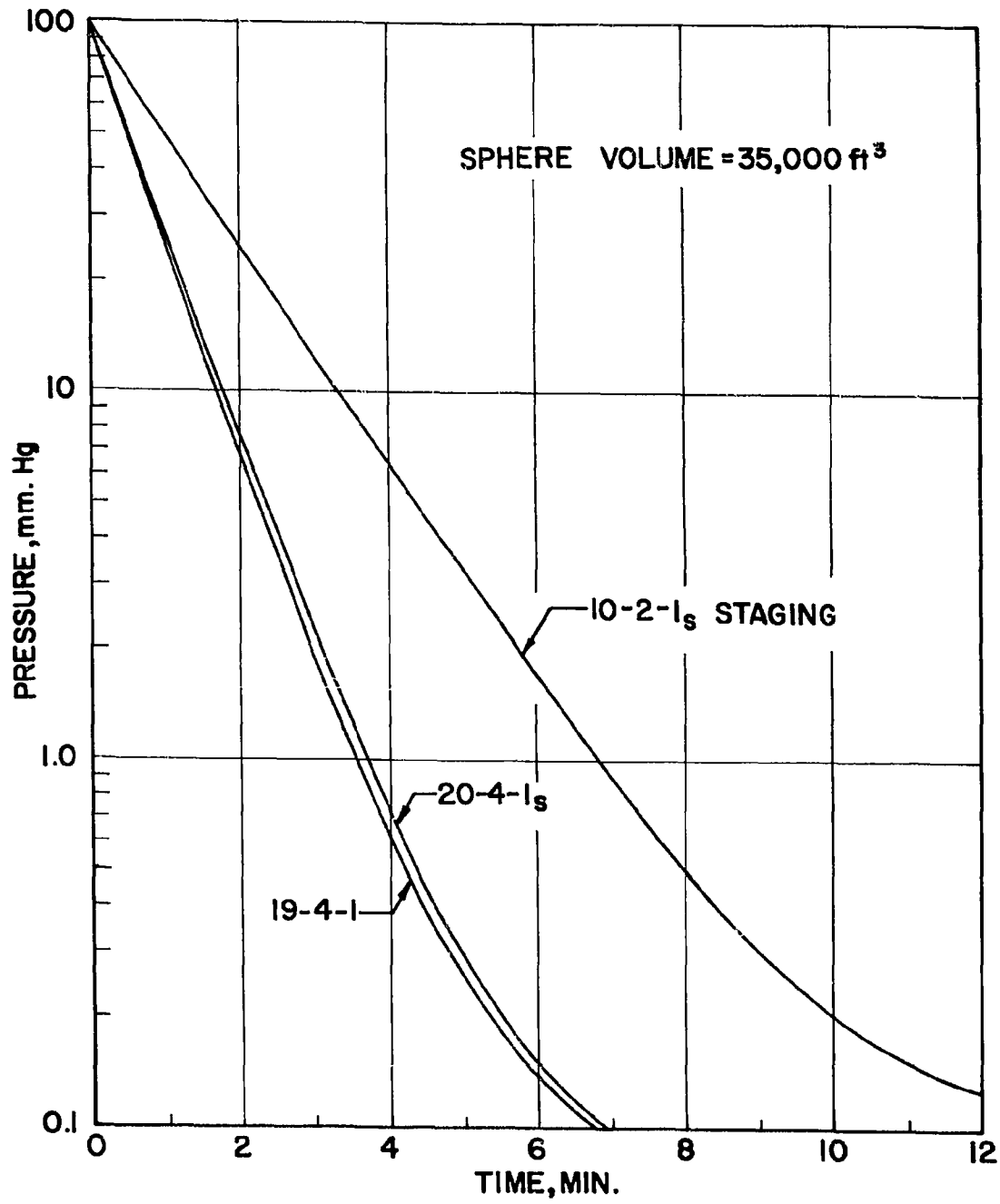

FIGURE 47-EVACUATION RATE OF 35,000 FT³ SPHERE

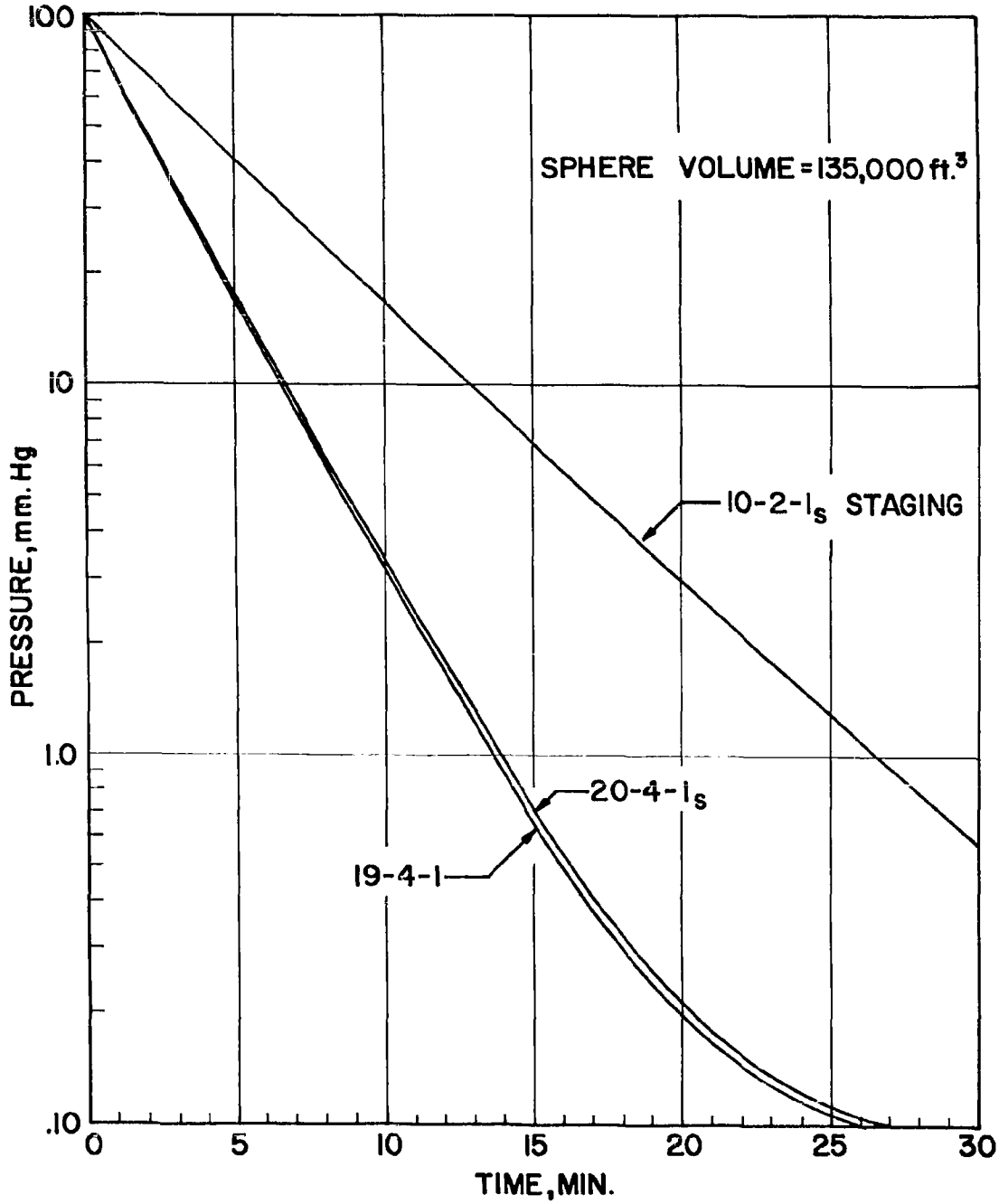

FIGURE 48-EVACUATION RATE FOR 135,000 FT³ SPHERE

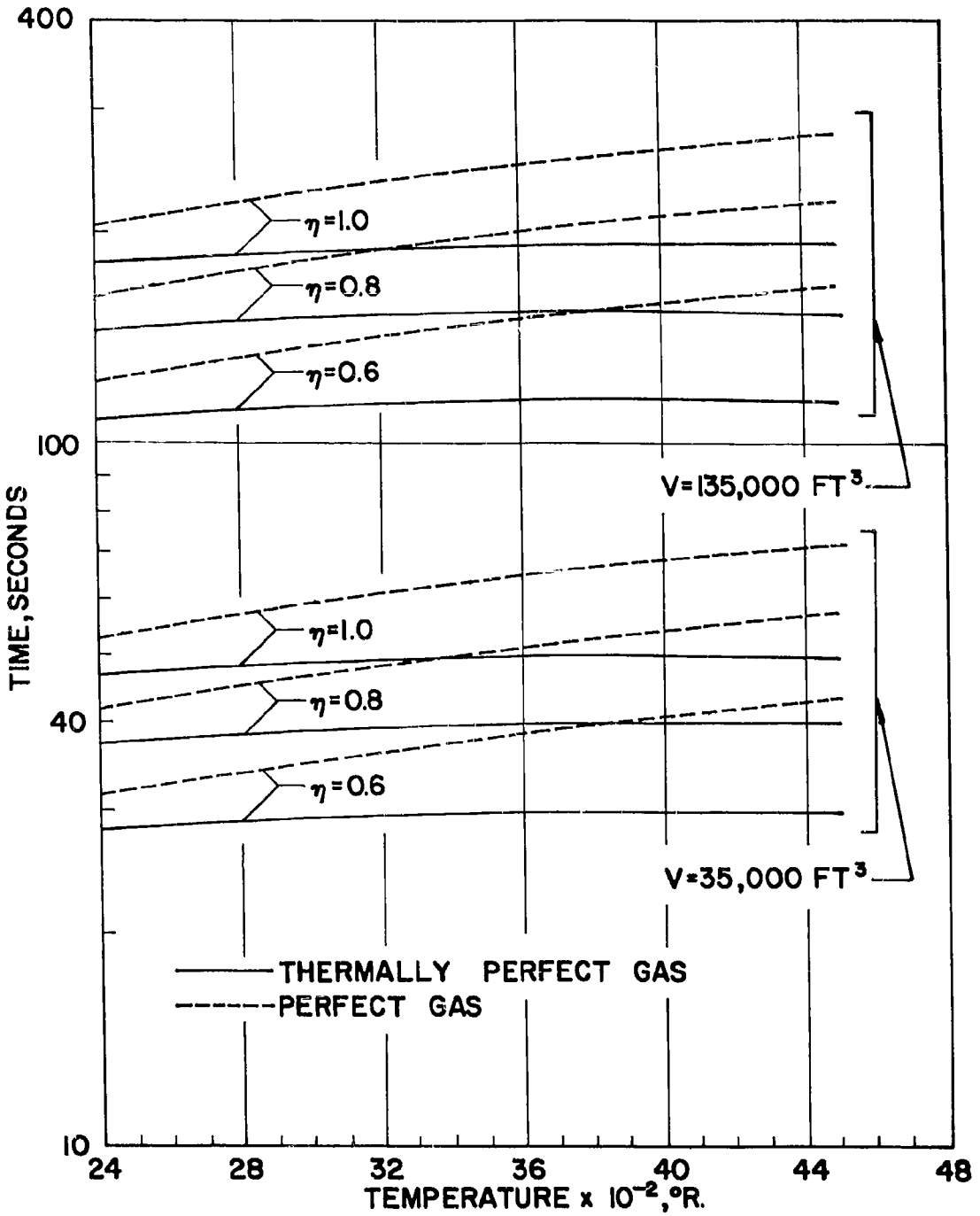

FIGURE 49-RUN TIME vs. STAGNATION TEMPERATURE FOR M=16

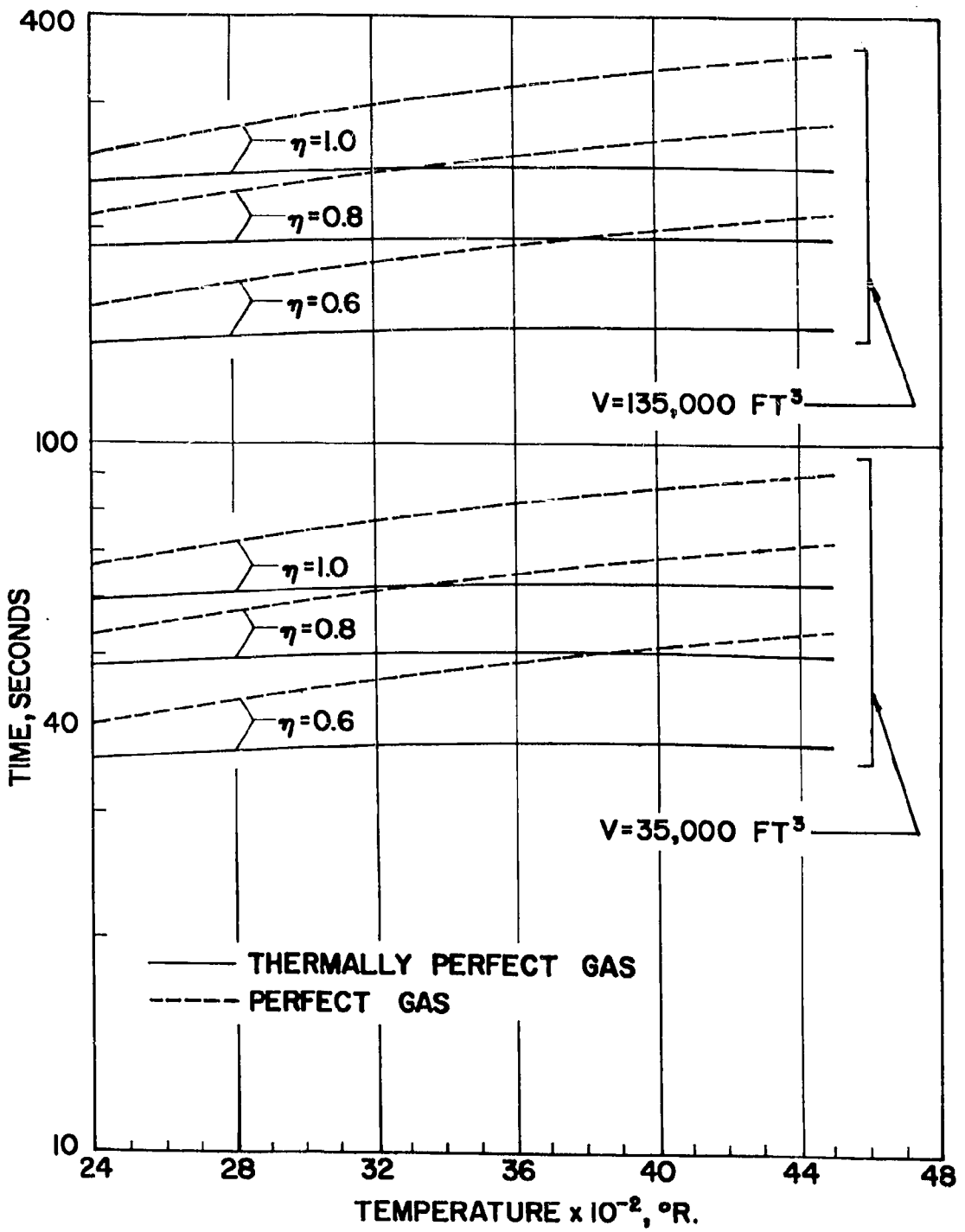

FIGURE 50 - RUN TIME vs. STAGNATION TEMPERATURE FOR M=18

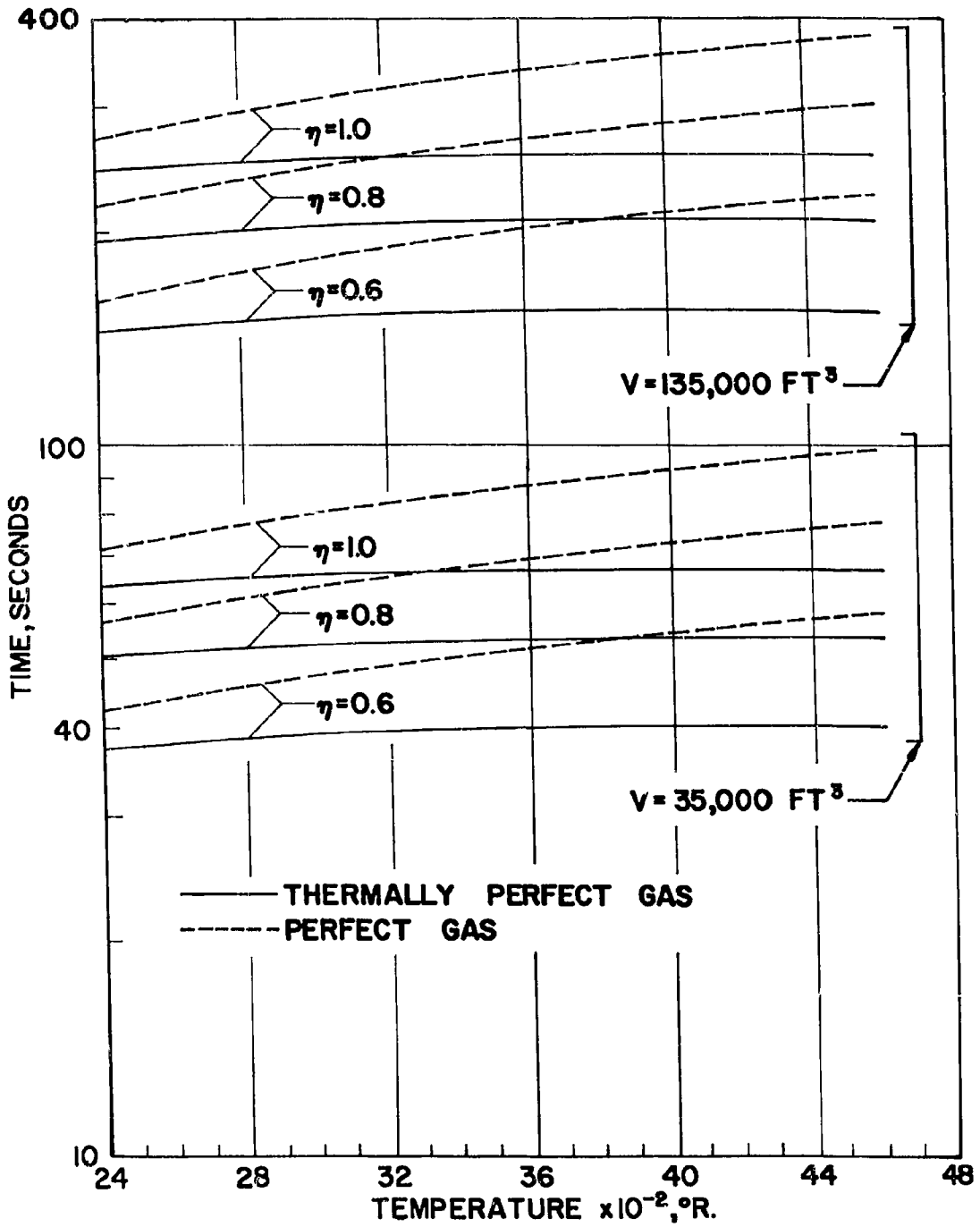

FIGURE 51-RUN TIME vs. STAGNATION TEMPERATURE FOR M=20

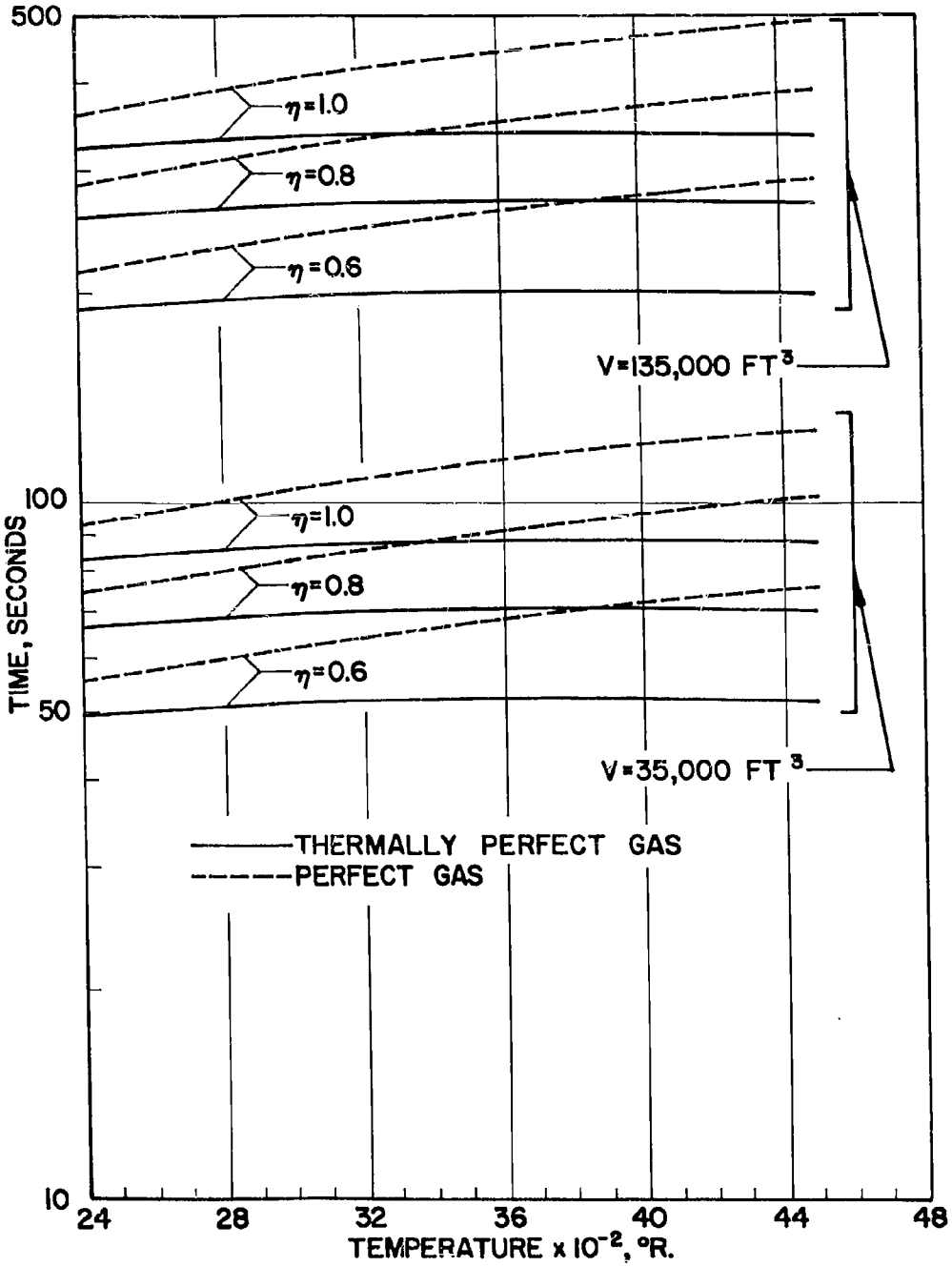

FIGURE 52 - RUN TIME vs. STAGNATION TEMPERATURE FOR M=22

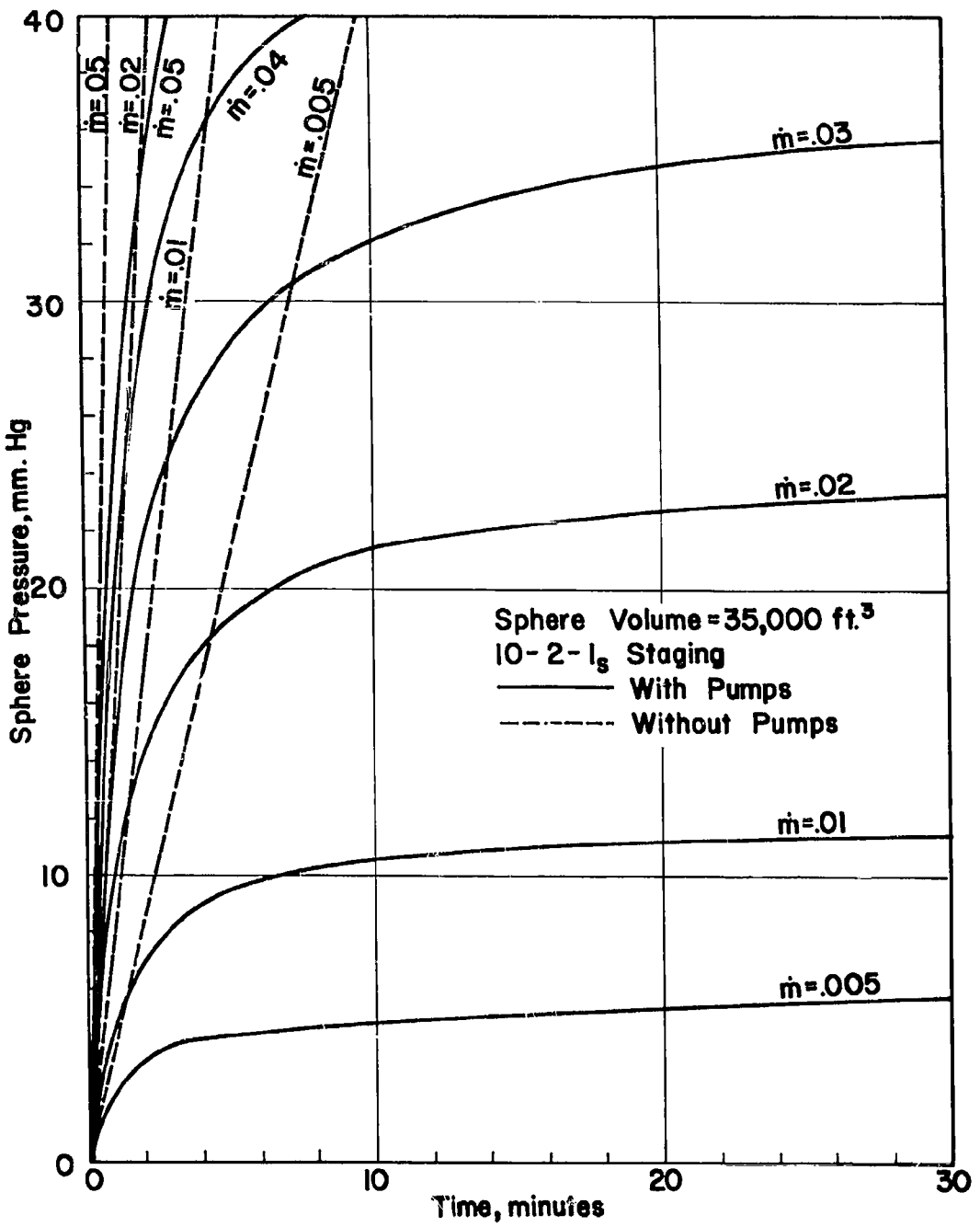

FIGURE 53a - EFFECT OF VACUUM PUMP OPERATION ON SPHERE PRESSURE RISE WITH TIME

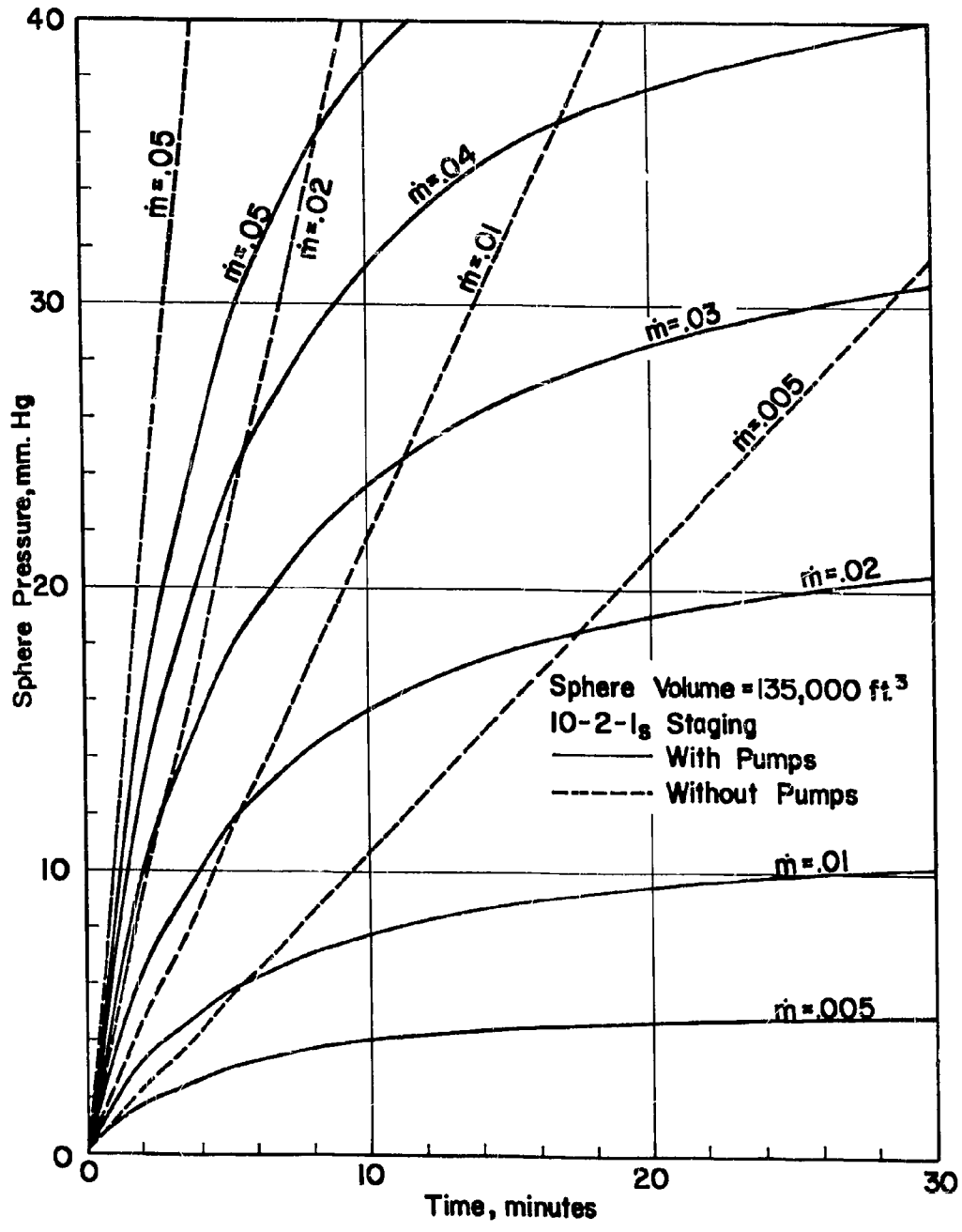

FIGURE 53b - EFFECT OF VACUUM PUMP OPERATION ON SPHERE PRESSURE RISE WITH TIME

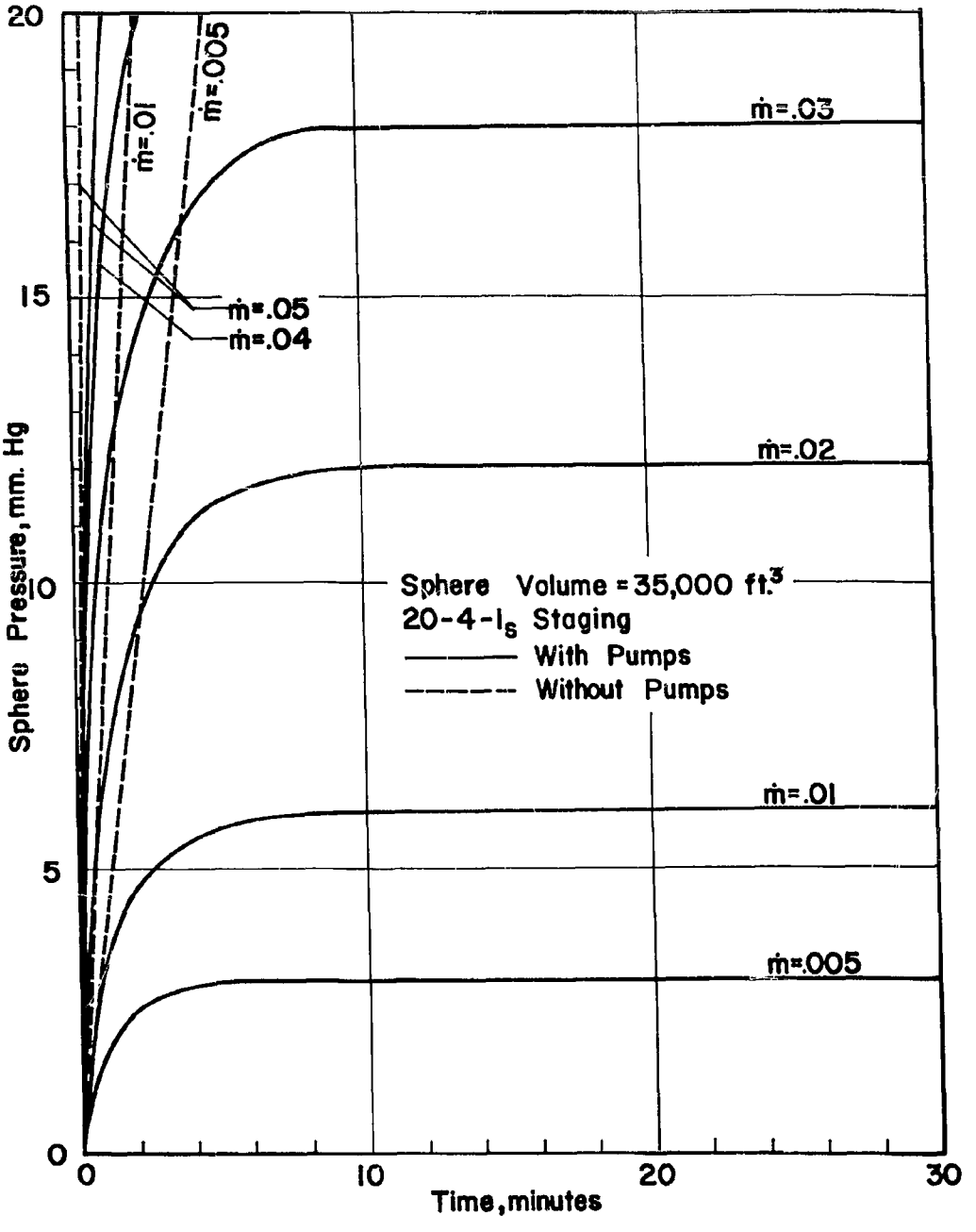

FIGURE 53c-EFFECT OF VACUUM PUMP OPERATION ON SPHERE PRESSURE RISE WITH TIME

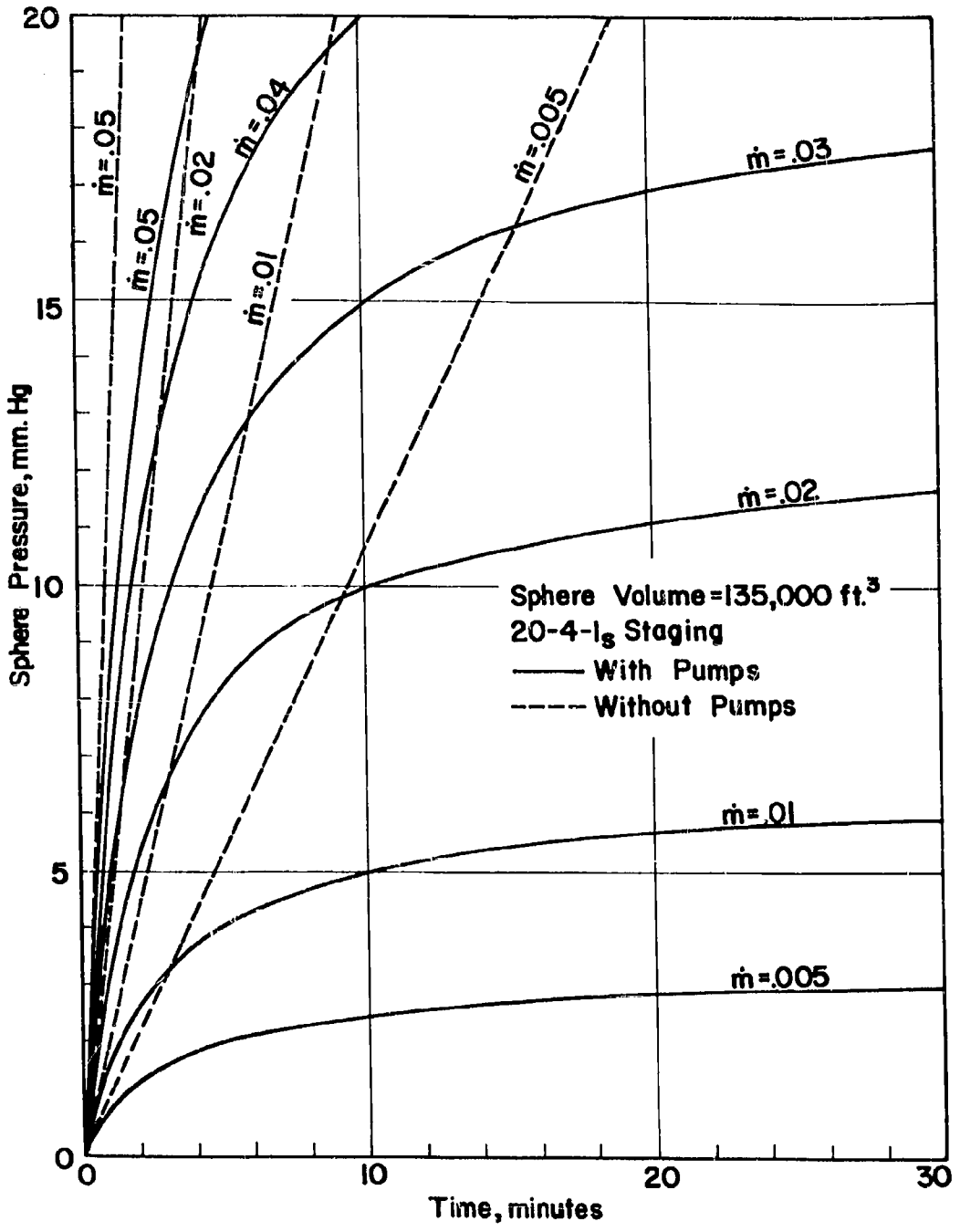

FIGURE 53d-EFFECT OF VACUUM PUMP OPERATION ON SPHERE PRESSURE RISE WITH TIME

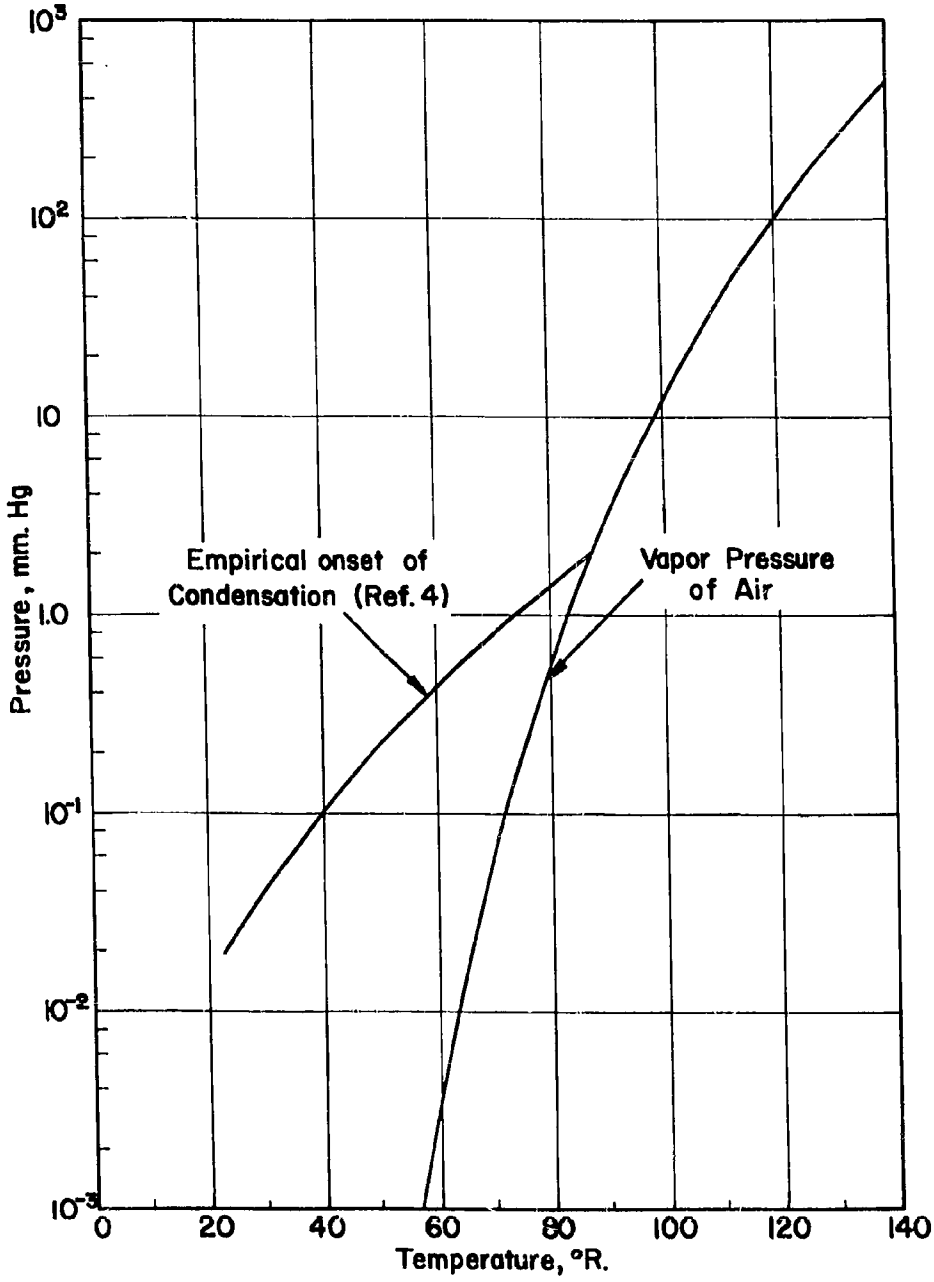

FIGURE 54-AIR PROPERTIES FOR ESTIMATING LIQUEFACTION LIMITS

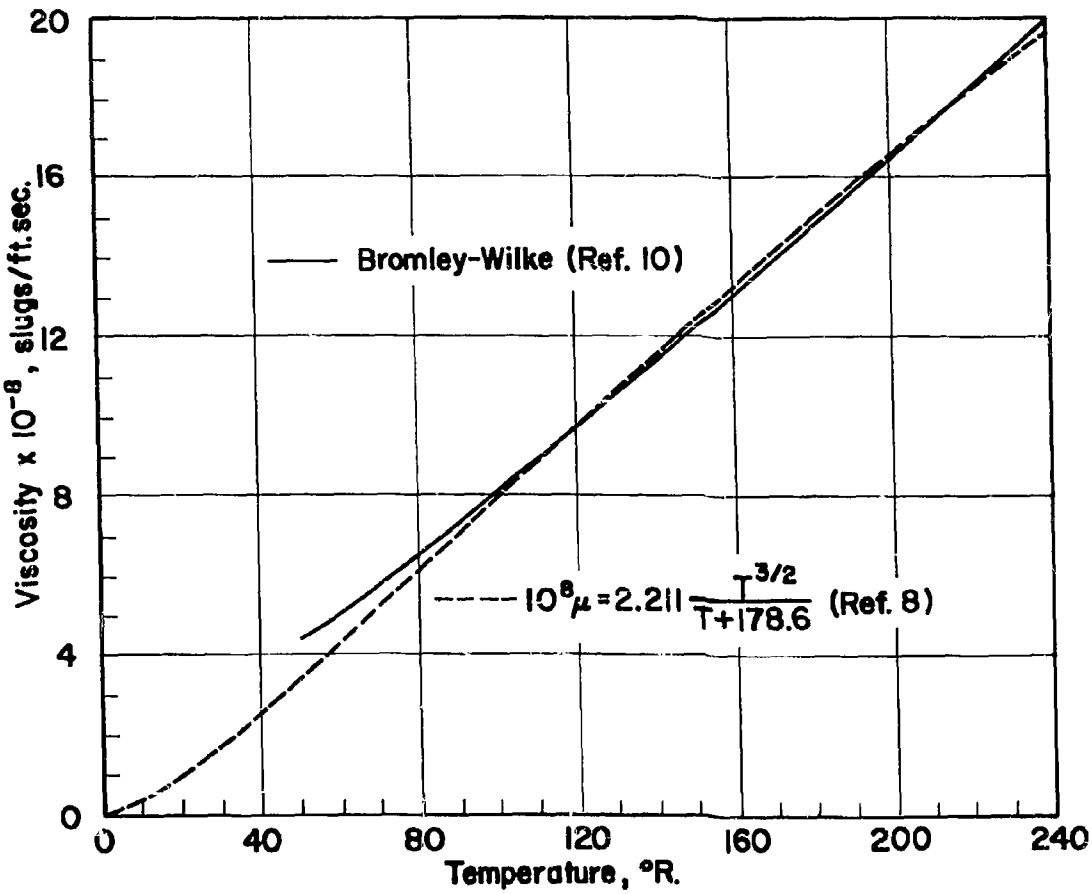

FIGURE 55-VISCOSITY OF AIR AT LOW TEMPERATURES

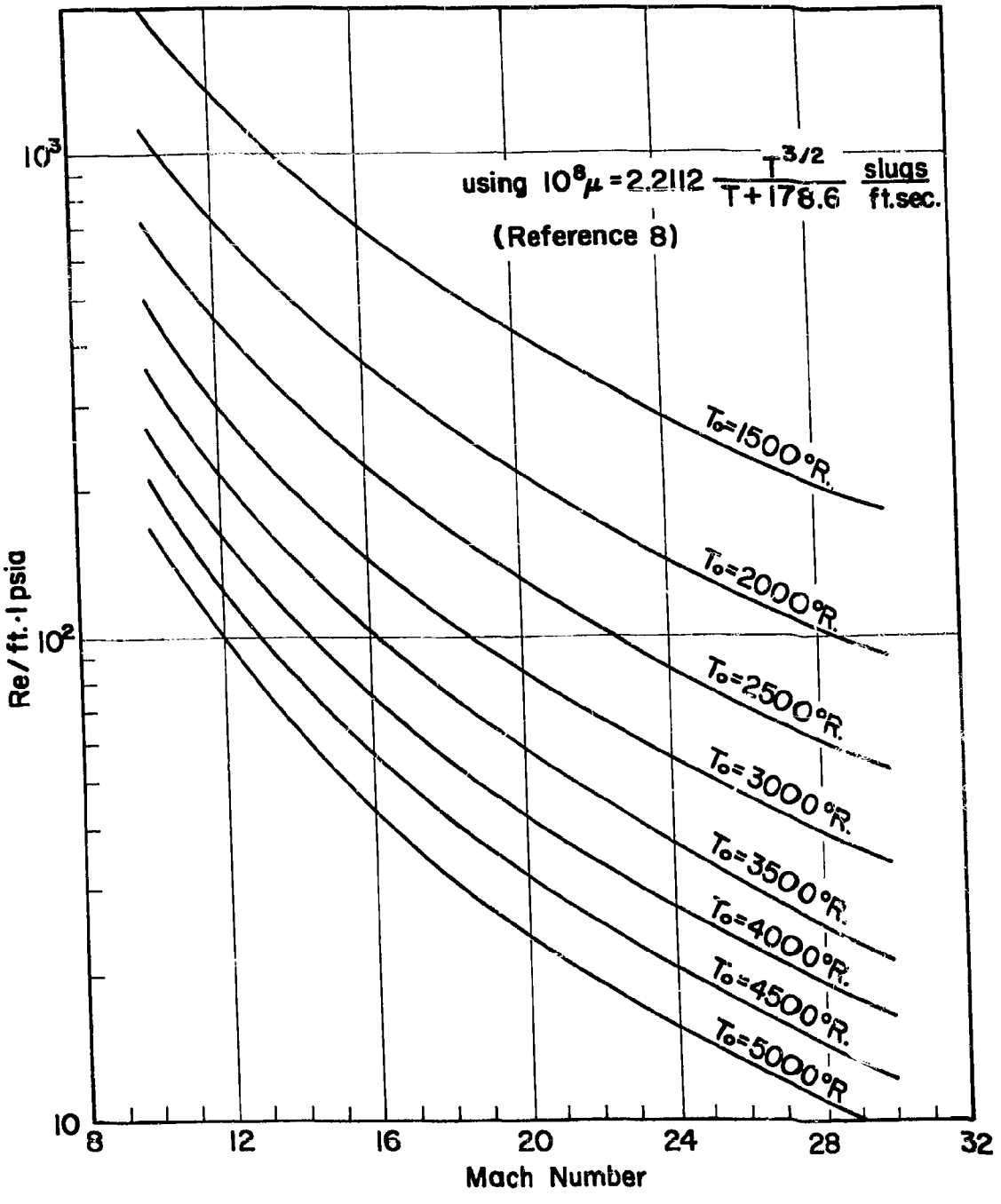

FIGURE 56-REYNOLDS NUMBER PER FOOT vs. MACH NUMBER